

72248

NASA CR-54694
4429-6013-R0000



PROGRAM OF ANALYTICAL AND EXPERIMENTAL
STUDY OF POROUS METAL IONIZERS

VOLUME I

by
HAYWOOD SHELTON AND DAVID F. HALL

FACILITY FORM 802

N67 16572
(ACCESSION NUMBER)
132
(PAGES)
4429-6013-R0000
(NASA CR OR TMX OR AD NUMBER)
CR-72248

(THRU)
1
(CODE)
17
(CATEGORY)

Prepared for
NATIONAL AERONAUTICS AND SPACE ADMINISTRATION
CONTRACT NAS 3-7109

GPO PRICE \$ _____

CFSTI PRICE(S) \$ _____

Hard copy (HC) 2.00

Microfiche (MF) 1.30

TRW SYSTEMS
AN OPERATING GROUP OF TRW INC.

NOTICE

This report was prepared as an account of Government sponsored work. Neither the United States, nor the National Aeronautics and Space Administration (NASA), nor any person acting on behalf of NASA:

- A.) Makes any warranty or representation, expressed or implied, with respect to the accuracy, completeness, or usefulness of the information contained in this report, or that the use of any information, apparatus, method, or process disclosed in this report may not infringe privately owned rights; or
- B.) Assumes any liabilities with respect to the use of, or for damages resulting from the use of any information, apparatus, method or process disclosed in this report.

As used above, "person acting on behalf of NASA" includes any employee or contractor of NASA, or employee of such contractor, to the extent that such employee or contractor of NASA, or employee of such contractor prepares, disseminates, or provides access to, any information pursuant to his employment or contract with NASA, or his employment with such contractor.

Requests for copies of this report should be referred to

National Aeronautics and Space Administration
Office of Scientific and Technical Information
Attention: AFSS-A
Washington, D.C. 20546

SUMMARY REPORT

PROGRAM OF ANALYTICAL AND EXPERIMENTAL STUDY
OF POROUS METAL IONIZERS

by

David F. Hall, and Haywood Shelton

Prepared for:

NATIONAL AERONAUTICS AND SPACE ADMINISTRATION

22 January 1967

Contract No. NAS3-7109

Technical Management
NASA Lewis Research Center
Cleveland, Ohio
Spacecraft Technology Division

ELECTRIC PROPULSION TECHNOLOGY DEPARTMENT
Power Systems Division
TRW Systems
One Space Park
Redondo Beach, California

PROGRAM OF ANALYTICAL AND EXPERIMENTAL STUDY
OF POROUS METAL IONIZERS

by

Haywood Shelton and David F. Hall

ABSTRACT

Cesium ion and neutral emission were measured from pure and alloyed porous metal ionizers at current densities up to 50 ma/cm^2 . The neutral emission was measured as a function of the angle from the normal and found not to be distributed as the cosine. Iridium, iridium-tungsten alloy, rhenium-tungsten alloy, and pure tungsten emitters were studied. In addition, the effects of Ta, Nb, Mo, Rh, Pt, C, Si and Al on the surface of porous W emitting cesium ions were studied.

TABLE OF CONTENTS

	<u>PAGE</u>
ABSTRACT	iii
SUMMARY	1
INTRODUCTION	2
EXPERIMENTAL CONFIGURATION AND TECHNIQUES	3
Porous Metal Ionizer Tests	3
Vacuum	
Samples	
Accelerator Design	
Detector and Collector	
Neutral Detector	
Neutral Detector Collimation	
Sputtering and Evaporation	
Method of Taking Data	
Absorption Lifetime Measurements	17
Experimental Apparatus	
Experimental Procedures	
EXPERIMENTAL RESULTS	19
Sample Preparation	19
Neutral Efflux vs Angle	26
Significance of Noncosine Distribution	
Effect of Other Elements on Tungsten Surfaces	36
Oxygen	
Carbon	
Aluminum	
Iridium	
Rhenium	
Tantalum	
Niobium	
Molybdenum	
Rhodium	
Platinum	
Silicon	
Tabulation of the Properties of Studied Contaminents On Porous Tungsten	52-54
Ionizer Test Results	55
Test 0 - Confirmatory Test of Astromet 10-1	
Test 1 - Hughes 324-S 3.9 μ W	
Test 2a - Light Ir Coating on Hughes 324-S	
Test 2b - After Oxygen	
Test 3 - Heavy Ir Coating on Hughes 324-S	
Test 4 - Union Carbide ORGPD 4848-82-1 4.1 μ W	

TABLE OF CONTENTS (Cont'd.)

	<u>PAGE</u>
Test 5 - Hughes 324-S 3.9 μ W	
Test 6 - TRW W-5% Re Spherical Prealloyed	
Test 7 - Hughes 276 W-50% Ir Prealloy	
Test 8 - Hughes 225 W-50% Ir Mixture	
Test 9 - Hughes 280 100% Ir	
Test 10 - TRW ST 1-9 3.9 μ W	
Test 11 - TRW 57-3 Dendritic W-Re	
Test 12 - EOS 788 Low Density, Shaped Pore W	
Tabulated Test Parameters and Evaluation Sheets	102
Metallurgical Studies	119
Enhanced Sintering By Rhodium Diffusion From the Braze	
Evidence of Enhanced Sintering Related to Vacuum Environment	
Or Hot Molten Copper	
CONCLUSIONS	119
REFERENCES	124

PROGRAM OF ANALYTICAL AND EXPERIMENTAL STUDY
OF POROUS METAL IONIZERS

by Haywood Shelton and David F. Hall

TRW Systems

SUMMARY

A number of porous metal ionizer materials were tested, particularly with respect to their emission of neutral cesium at high current densities. This neutral emission has a noncosine angular distribution. Iridium and iridium alloys have higher work functions but appear to sinter more rapidly than tungsten. All pure tungsten ionizers have essentially the same neutral fraction and critical temperature at low current densities (approximately 5 ma/cm^2), but their high-current-density operation depends on the porous structure at the surface. Rhenium and molybdenum readily alloy with tungsten, Re improves and Mo impairs the operation, the degree depending on their concentration in the tungsten. The major effects of tantalum and niobium alloyed with tungsten arise from their strong affinity for oxygen -- with traces of oxygen these alloys show generally low neutrals and high, rounded critical temperatures. Rhodium and platinum on tungsten raise the work function slightly, but they diffuse rapidly and cause rapid sintering. Silicon on tungsten is an excellent ion emitter: it results in low neutrals and critical temperature, but it cannot be reevaporated and eventually causes the porous emitter to solidify. Carbon on tungsten as a carbide is an excellent ion emitter, giving low neutrals and low critical temperature, but it cannot be evaporated and if deposition continues, bulk carbon that plugs pores is formed; also, it has a low work function (approximately 4.45 volts), although a very low critical temperature. Aluminum adsorbed to clean tungsten has a lifetime given by $\tau = \tau_0 \times 10^{+5040 E/T}$, where $\tau_0 = 10^{-16}$ sec and $E = 5.3$ volts.

INTRODUCTION

This report covers in final form the work performed by TRW Systems from April 5, 1965, to May 5, 1966, under Contract NAS3-7109 for Lewis Research Center of the National Aeronautics and Space Administration. This contract called for the testing of 12 samples of porous metals manufactured with improved techniques designed to produce high-quality ionizers for use in cesium ion engines. The primary objectives of these tests were (1) to conduct the measurements in an exacting manner so as not to obscure the results by the presence of foreign contaminants or by use of unknown processes, (2) to extend the measurements where practical to high current densities (50 ma/cm^2), and (3) to make cesium neutral fraction measurements at various angles, including normal to the ionizer surface. The samples tested included pure porous tungsten sintered from small spherical particles of tungsten, iridium-coated porous tungsten; porous pure iridium, iridium-tungsten alloys, and a rhenium-tungsten alloy; low-density porous tungsten; and a porous rhenium-tungsten alloy of dendritic structure that was made by melting.

The contract also called for the experimental testing of the effects of depositing other metals on the surface of porous tungsten emitting cesium ions. Information was to be obtained on the adsorption lifetime of these materials on the tungsten, the diffusion or alloying of these materials into the porous tungsten, and the effects of these materials on the work function and cesium binding energy, which would in turn affect the cesium neutral fraction and the critical temperature. The materials studied were iridium, rhenium, tantalum, molybdenum, niobium, rhodium, platinum, silicon, carbon, and aluminum. Only with aluminum was it possible to obtain quantitative adsorption lifetime data.

EXPERIMENTAL CONFIGURATION AND TECHNIQUES

Porous Metal Ionizer Tests

Vacuum. - The experiment made use of an 18 x 23 inch Pyrex bell jar sealed with a Viton A "L" gasket to a stainless steel baseplate, which in turn was mounted with bakable metal gaskets to a 140 liter/sec Welch Turbomolecular Pump. This pump has no diffusion pump oil or "headgate"; it consists of cascaded turbine blades rotating at 16,000 rpm, through which heavy organic molecules have no change of back-diffusing from the mechanical roughing pump or oil-lubricated bearings. To open the vacuum system, air, argon, or nitrogen is first admitted directly into the bell jar, and then the turbine is stopped. Thus oil vapors are barred from entering the experimental region by the long path of air through which they must diffuse.

A quadrupole mass spectrometer located in the area of the porous tungsten measured the partial pressure of gases. These pressures varied somewhat with the time after exposure to air, the degree of cleaning and the power of the ion beam. During operation oxygen and hydrocarbons were below the instrument sensitivity of 1×10^{-9} torr. Water vapor was reduced below 1×10^{-8} torr by the large area of copper at liquid nitrogen surrounding the experiment. Carbon dioxide produced by decomposing cesium carbonates reduced to below 1×10^{-8} torr soon after initial warm up. Nitrogen liberated from the collector was the main gas present at about 5×10^{-7} torr at high ion power levels.

Samples. - Impregnated samples were machined into discs 0.157 inch in diameter and 0.020 inch thick. This size is small enough that current densities of up to 50 ma/cm^2 can be obtained with acceleration potentials of 20 KV or less without the use of grids, yet large enough that braze penetration and geometrical variations due to thermal expansion do not usually present problems. When allowance is made for the plenum shoulder on which the sample sits and the usual braze penetration, the effective area of the sample is $0.10 \pm 0.01 \text{ cm}^2$.

Figure 1 shows a sample resting in a molybdenum plenum ready for brazing. Pure rhodium powder is mixed with turpentine to form a paste, which is placed in a groove around the emitter and at the joint between the plenum chamber and the tube. A minimum of the paste is used in the latter joint, because it gets hotter during the braze and the moly-rhodium alloying might seriously weaken the thin tube. The brazing is carried out in one step by carefully observing the braze material while electron-bombarding it with about 50 ma

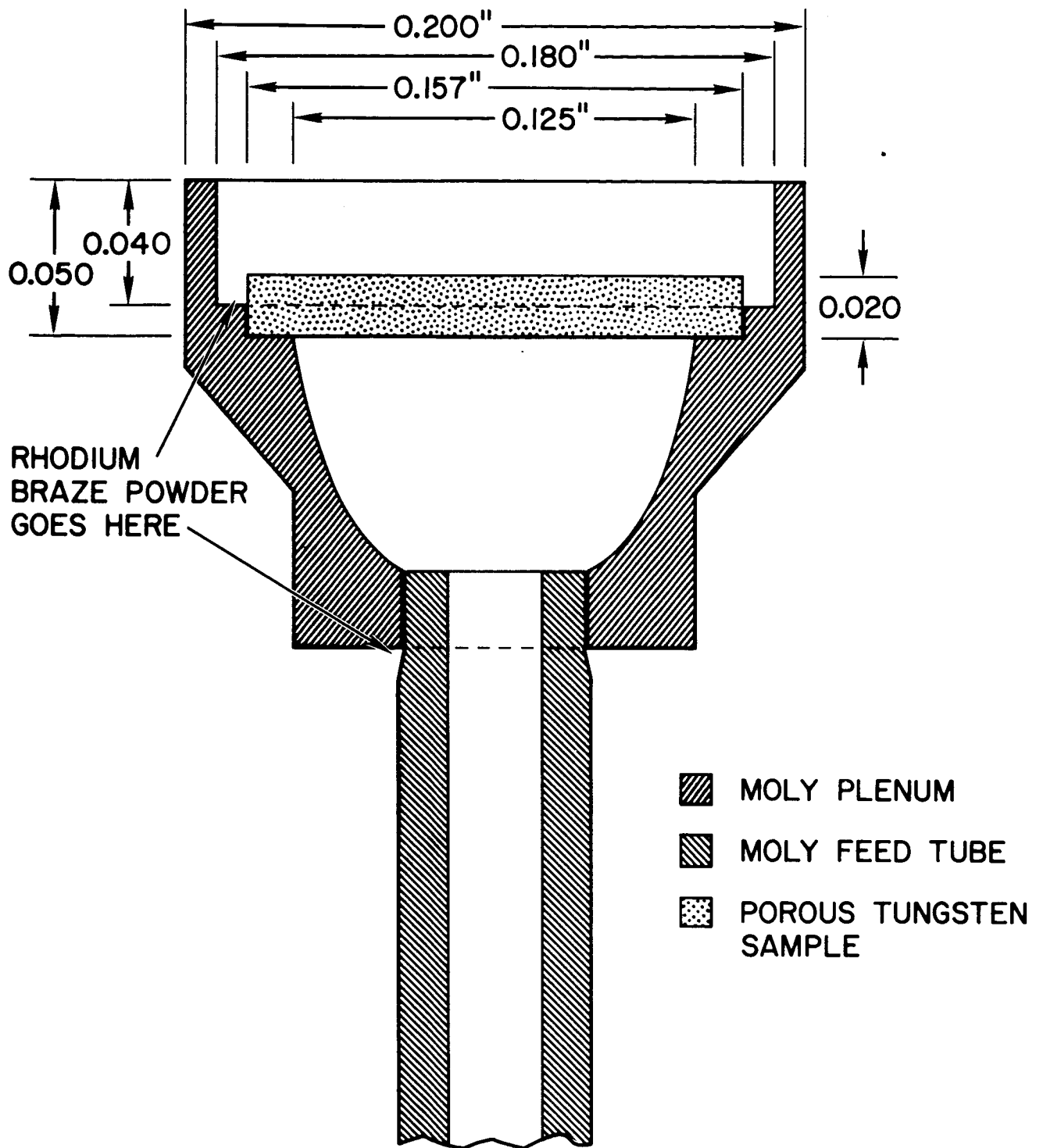


Figure 1. Cross section of sample sitting in a molybdenum plenum ready for brazing.

of 2000-volt electrons from slightly below the plane of the emitter. At the first sign of rhodium melting (2240°K), the temperature is dropped.

Following the brazing operation the sample receives its first transmittivity measurement. A second measurement is made after etching, if it receives etching, and a final measurement is made following testing. Each of these measurements is made by pumping on one side of the sample and noting the time required for 30 cm³ of air at 20 torr on the other side to drop to 4/5 its initial pressure. This pressure provides Knudsen flow.

Ignoring the change in volume that takes place during the time measurement, the equation of the system is $p = p_0 \exp(-t/\tau)$. Here p is the pressure in the high pressure side of the system and $1/\tau = \bar{v} T A / (4V)$. Substitution of $\bar{v}/4 = 11,600$ and $\tau = 5 t_m$ gives the transmittivity as

$$T = \frac{30 \text{ cm}^3}{0.1 \text{ cm}^2 \cdot 11,600 \text{ cm}^3/\text{sec} \cdot 5 t_m} = 5.2 \times 10^{-3} t_m.$$

Although this measurement does not yield very accurate absolute values, it is quite suitable for obtaining the comparative values we seek. Typically samples range in transmittivity from 1×10^{-5} to 5×10^{-4} .

The next assembly process is to install the filament and thermocouples. A 0.001-inch-wall tantalum tube (with a spotwelded seam), of 0.200 inch o.d. and about 1/2 inch long, is spotwelded to the outside of the plenum below the rim. The other end is then spotwelded to a nickel bushing, which is kept from touching the feed tube by a ceramic tube. Next, 0.003 inch thermocouple wires (6 and 26-percent rhenium-tungsten) are sandwiched into a small bend in a 0.001-inch niobium tab and spotwelded to the side of the plenum chamber. Two thermocouples are used to provide extra reliability through redundancy. At various times during the experiment when the bell jar is clean, the calibration of these thermocouples is checked by sighting a Leeds and Northrup Model 8622-C optical pyrometer, corrected for the Pyrex glass of the bell jar and the emissivity of tantalum, in the vicinity of the thermocouples. In Figure 2 is pictured a sample at this stage of the assembly.

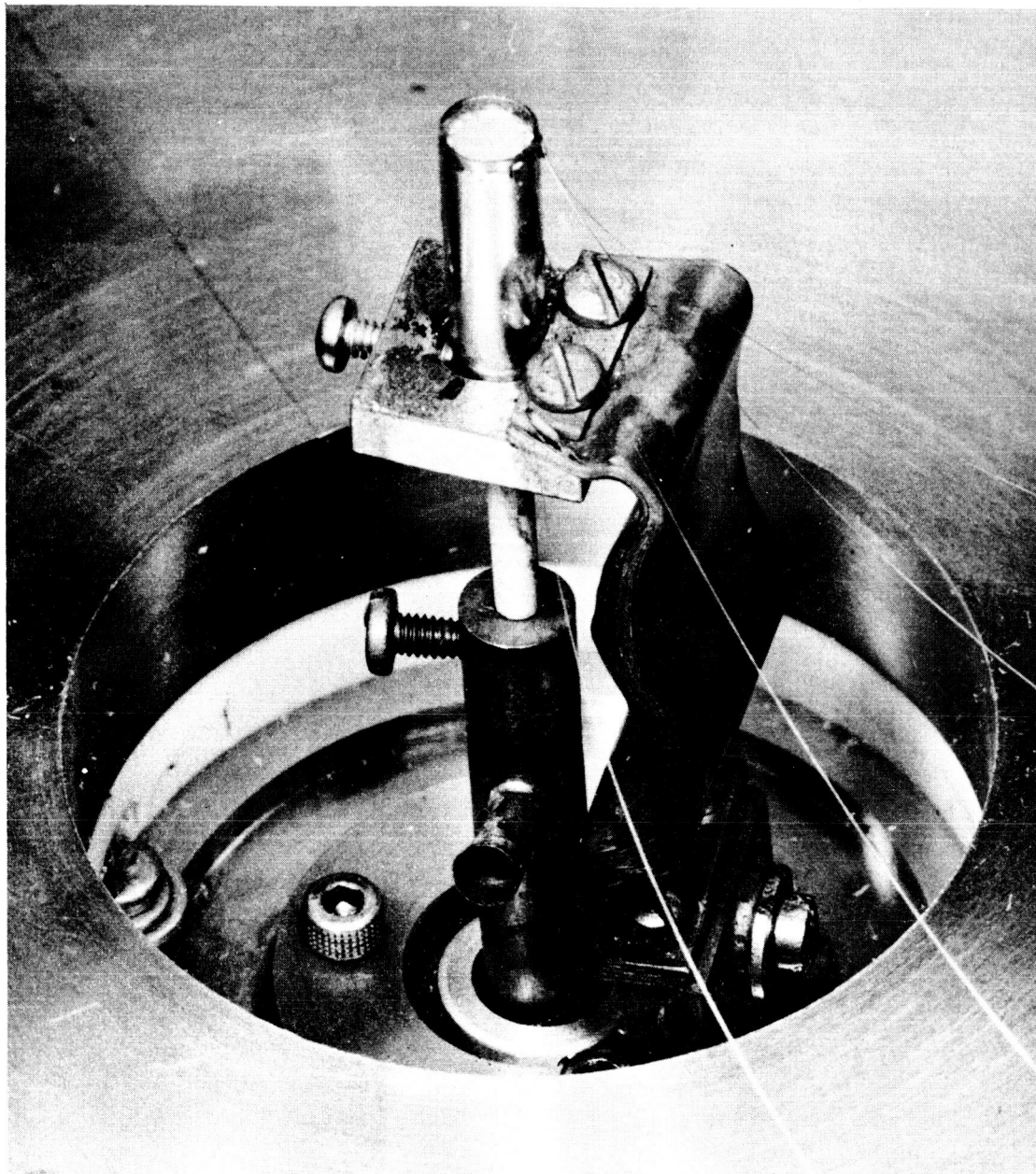


Figure 2. Photograph of sample brazed into plenum with heater and thermocouple leads attached. It is mounted in the test fixture. Prominent are the copper straps that carry heater current.

Figure 3 shows the assembly of the experiment schematically and can be referred to during the following discussion. The 2-inch-long, 1/16-inch-diameter molybdenum feed tube slides for about 1 inch into the thick-wall molybdenum tube and is secured with a set screw. This narrow diameter molybdenum feed tube was chosen to minimize conduction of heat from the plenum; in fact, heat is actually generated in the feed tube. Cesium leakage from the joint between the tubes is handled by cascade differential pumping of the cesium to an area where it is completely trapped. Also, as a further insurance against leakage, a small drop of aqueous solution of CsCl is placed in the tight-fitting joint. The nickel bushing to which the filament is spotwelded is held by a stainless steel screw in a stainless steel clamp; copper strips leading from the screw and clamp by keeping them cool. These strips carry the ~50 amperes required to heat the ionizer and are used for flexibility. At the other end they are joined to a block that is cooled across thin Teflon to the water-cooled base. (The cooling water is isolated from ground by two glass drip columns.) By this means the current-carrying capacity of the hermetic feed-through is considerably enhanced, since both the heat conducted down the filament lead and that generated in the feed-through are conducted into the base.

The heavy molybdenum rod into which the 1/16-inch o.d. molybdenum feed tube is fixed was chosen for its high thermal conductivity and low thermal expansion. This tube is brazed to a stainless steel fitting that seals into a flared 1/2-inch o.d. copper tubing about 4-inches long that forms the oven. This OFHC copper tube is sealed at its bottom end by pinching and then heating it until the copper melts and is wrapped with nichrome wire coated with glass thread, which forms the heater for the oven. A glass ampoule of cesium is placed in the oven, and the flare seal is then tightened. After the chamber is evacuated, the glass ampoule is broken by squeezing the copper, a thermometer is attached, and the whole oven is wrapped with glass wool for thermal insulation. This oven and seal assembly has successfully withstood temperatures greater than 400°C, at which level sufficient cesium pressure to achieve 50 ma/cm² ion current density is usually obtained unless the sample transmittivity is quite low.

The whole emitter assembly is sealed with Teflon between two stainless steel knife edges and projects through the bottom of the baseplate, as shown in Fig. 3.

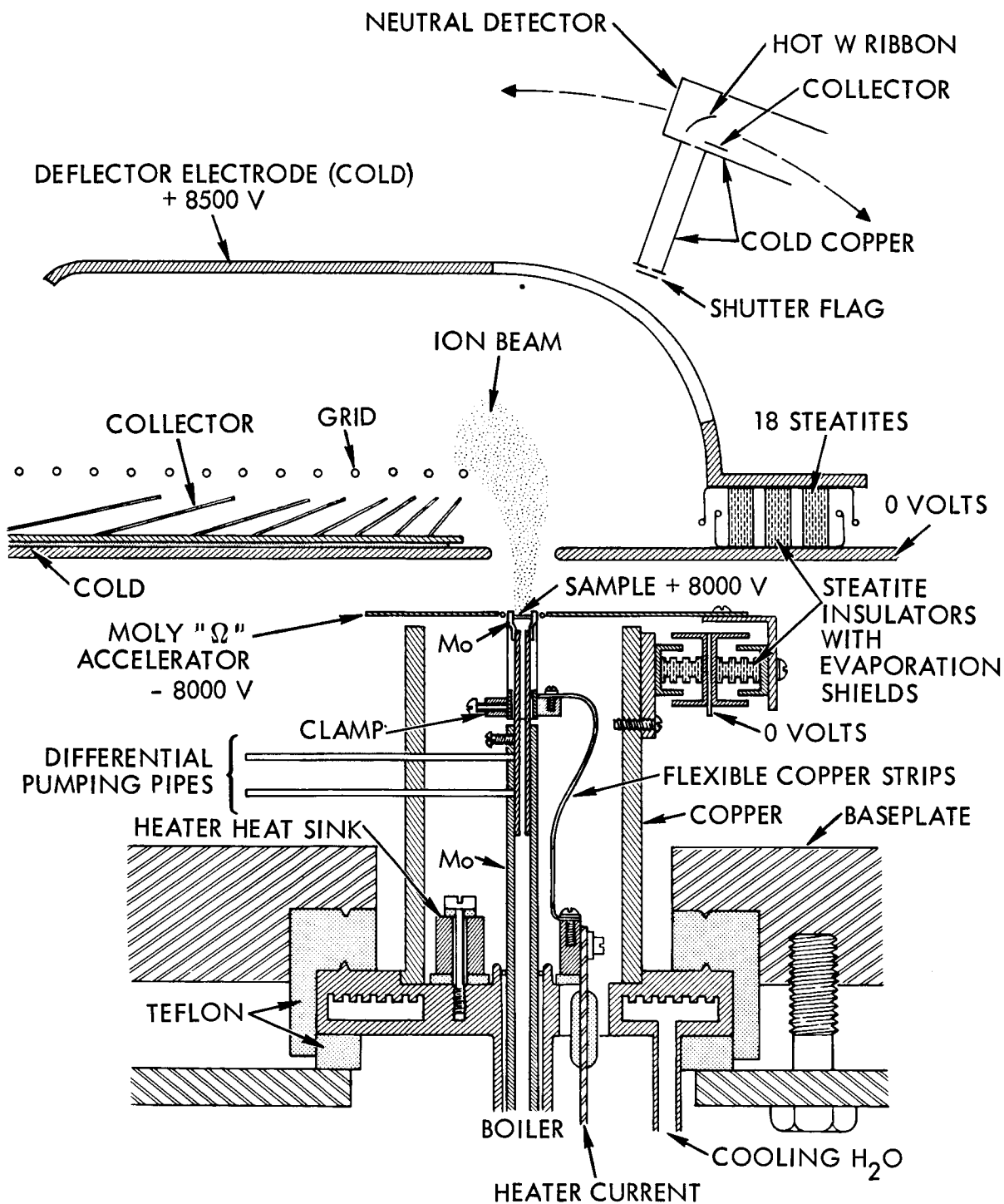


Figure 3. Schematic diagram of complete experimental configuration in cross section.

The Teflon makes a good vacuum seal and provides adequate voltage insulation. On a copper jacket surrounding the emitter and filament are mounted the insulators that support the accelerator electrode. The copper, which is attached to the water-cooled base, shields and cools the insulators and their evaporation shields. These insulators are standard 1/2-inch steatite standoff insulators with 6-32 threads with grooves machined on their outside surfaces to inhibit sliding sparks.

Accelerator design. - The position of the sample with respect to the accelerator results in an Ω -shaped accelerating field. This arrangement has several attractive features: no cesium is directly incident on the accelerator, thus minimizing drain currents across the small, ~ 16 Kv gap between the accelerator and plenum; no material from the accelerator can strike the sample under test and contaminate it; no scattering structure exists to alter the interpretation of the measured neutral fraction; a hot ionizing surface can be placed above and close to the sample to clean it by sputtering with cesium ions (by reversing accelerating-potential polarities); and various contaminants may be sputtered or evaporated onto the sample surface in situ.

The lip of the plenum protrudes through an aperture in a 0.040 inch thick molybdenum plate. The contour of this lip, shown clearly in Figure 1, is crucial in focusing the ions inward against space charge repulsive forces to make the electric field and current density uniform across the emitter surface. A computer program has been employed to assure this uniformity and calculate ion trajectories.

In the most recent accelerator design a loop of 0.020-inch tungsten wire is placed in a large aperture in the molybdenum plate. This loop may be heated by passing a current through it and usually is maintained at a temperature just below thermionic emission level. Consequently, the equilibrium coverage of cesium on this negative electrode is reduced and the wire can be periodically flashed.

Figure 4 is a picture of the accelerator electrode in place. The molybdenum plate is electropolished every time the sample is removed to remove any field-emitting whiskers and rough edges that might have developed in the previous

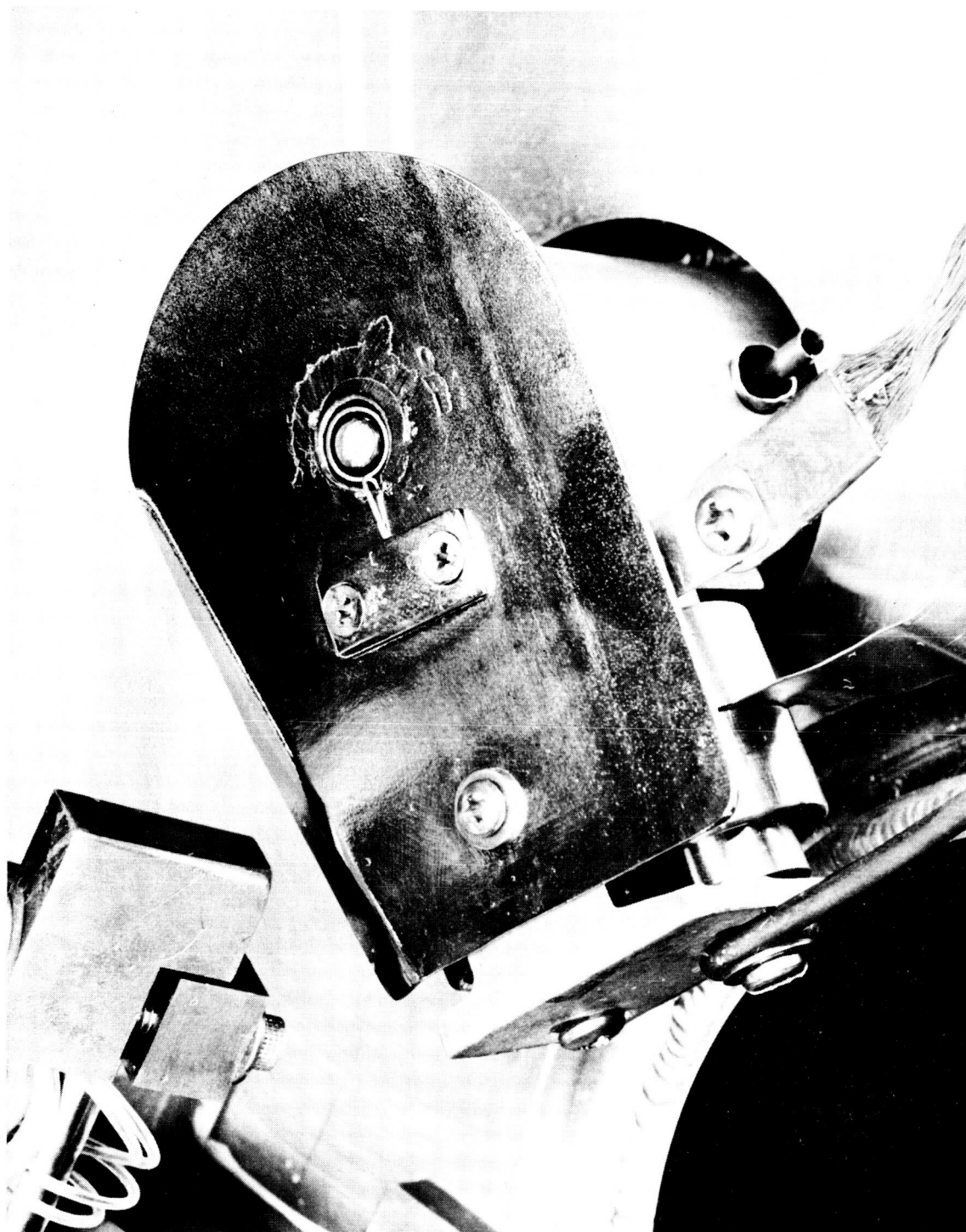


Figure 4. Photograph of accelerator electrode in place. Note ring of tungsten wire surrounding plenum which may be heated by current leads shown at bottom.

operation. Also, the plate has a thin sheet of mica sandwiched between it and its supporting bracket to increase its operating temperature. The bend in one side of the plate reduces drain currents from cold, cesium-covered parts below the cold plate.

Deflector and Collector. - After leaving the acceleration region, the ion beam passes through a 3/4-inch aperture in the liquid-nitrogen-cooled cold plate $\sim 1/4$ inch above the accelerator. This aperture is seen in both Figures 3 and 5. The ions are decelerated through this aperture from a negative potential that measurements assured us is more than adequate to prevent electron backstreaming to the sample.

Since measurements of the neutral efflux normal to the surface of the sample as well as at various angles were desired, and since the neutral detector does not distinguish between neutral atoms and ions, it was necessary to deflect the ion beam. This deflection is provided by the curved copper electrode shown in Figures 3 and 6. The electrode is maintained at a potential a few hundred volts above that of the ionizer and therefore curves the beam into the slatted collector shown in these figures. A slot in the electrode center allows neutral atoms to pass undisturbed to the neutral detector. The deflector is electrically insulated from the 0-volt cold plate by 18 1/2-inch steatite insulators, which also serve as heat conductors. The deflector, which is subjected to up to 50 watts of power from the collection of secondaries, must be cooled to prevent the evaporation of the cesium incident upon it; cesium evaporating from the deflector would result in a higher density of cesium above the source, and the consequent increase in charge exchange with ions directed toward the neutral detector would result in erroneously high neutral detector readings.

The collector is also constructed to avoid contributing to the neutral cesium density above the cold plate aperture. It consists of a number of slats at angles which shadow this region from sputtered and evaporated cesium. Much of the cesium incident on the collector is trapped by its bottom plate, which is kept cold by heat conduction across a thin Teflon sheet between it and the cold plate. The grid placed above the collector suppresses secondary electrons from the collector; the 50 watts incident on the deflector arise from ion collection by this grid.

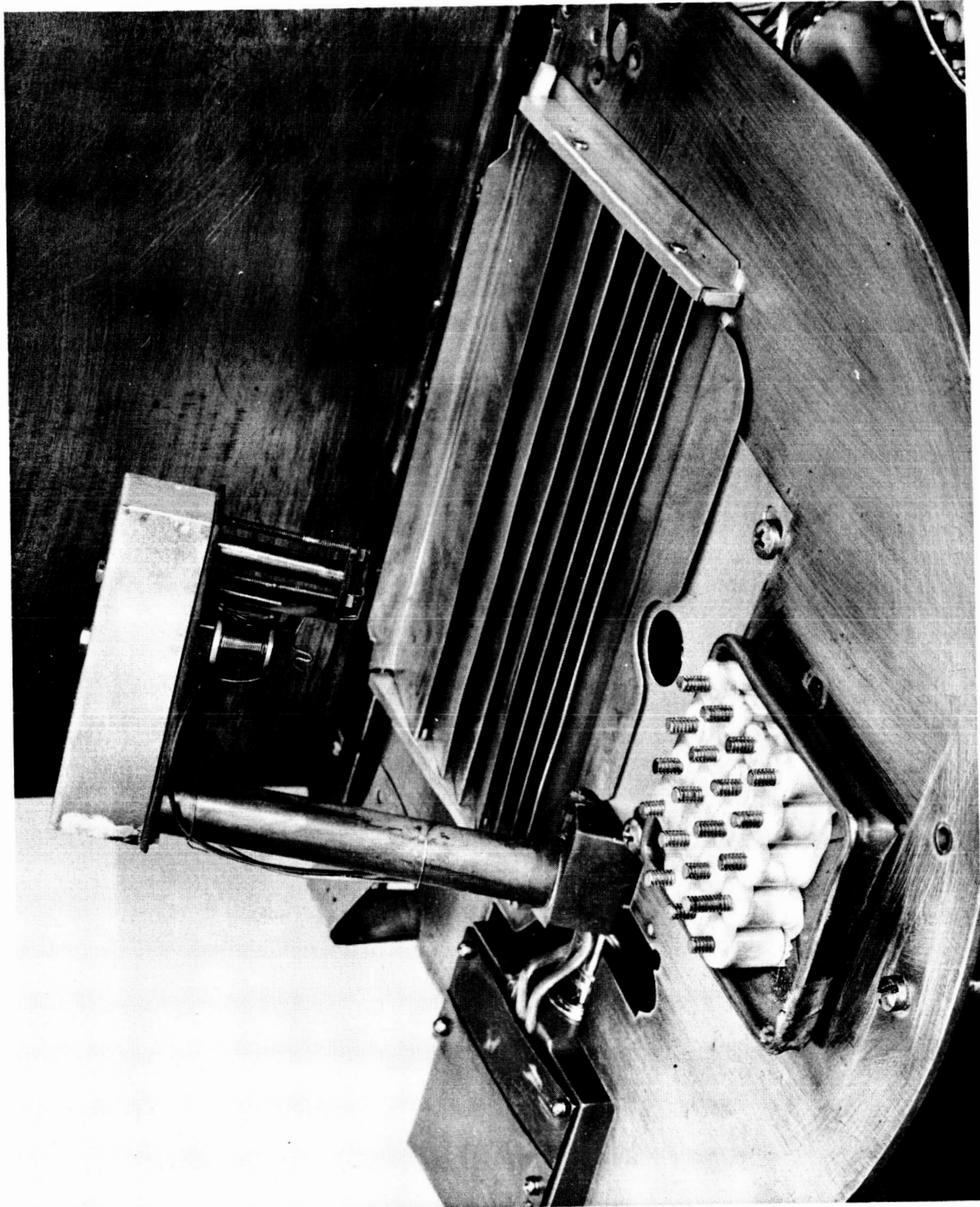


Figure 5. Photograph showing movable neutral detector and cold plate in place. Ion beam terminators on slatted collector. Exposed are the 18 steatite insulators which mount the deflector electrode.

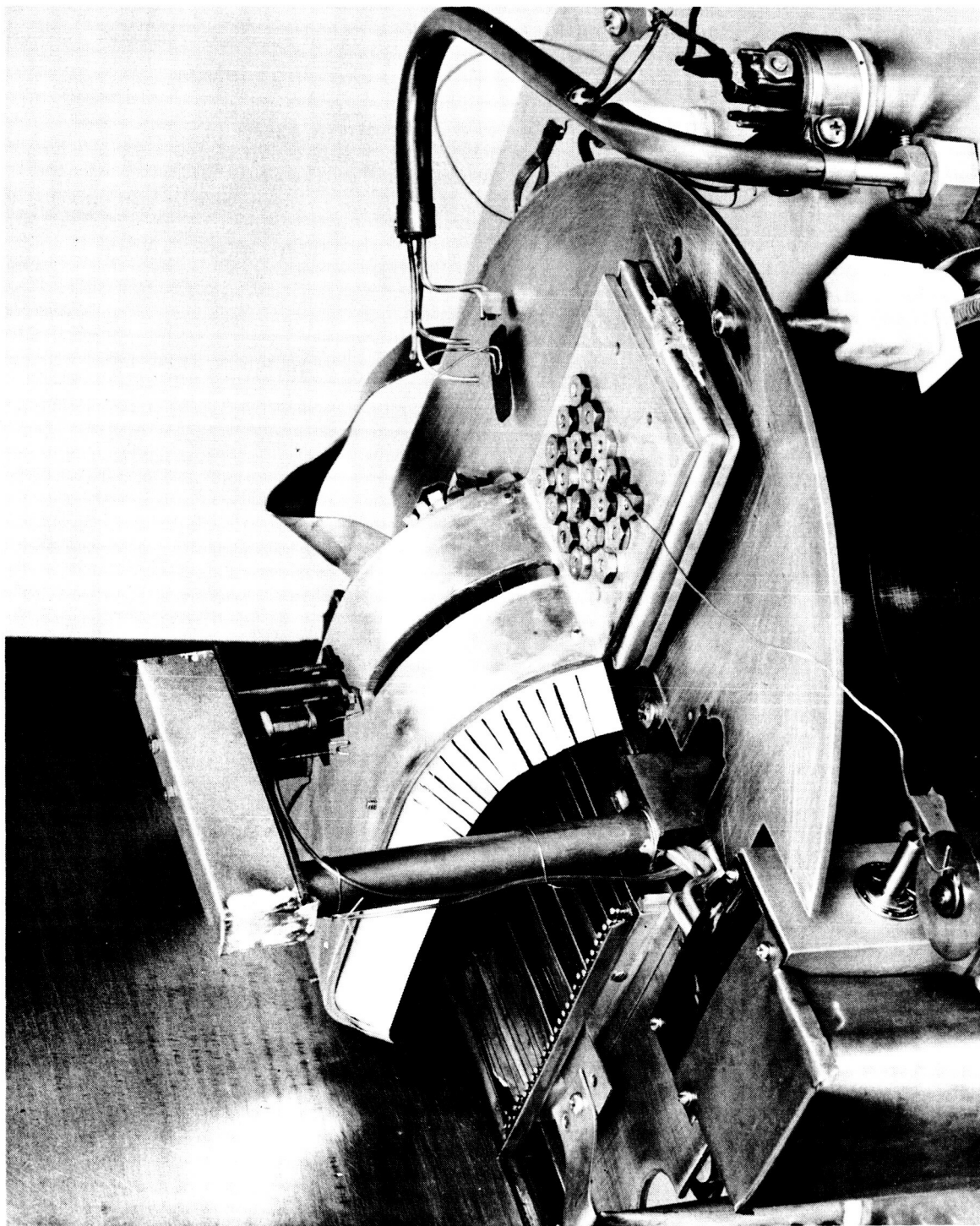
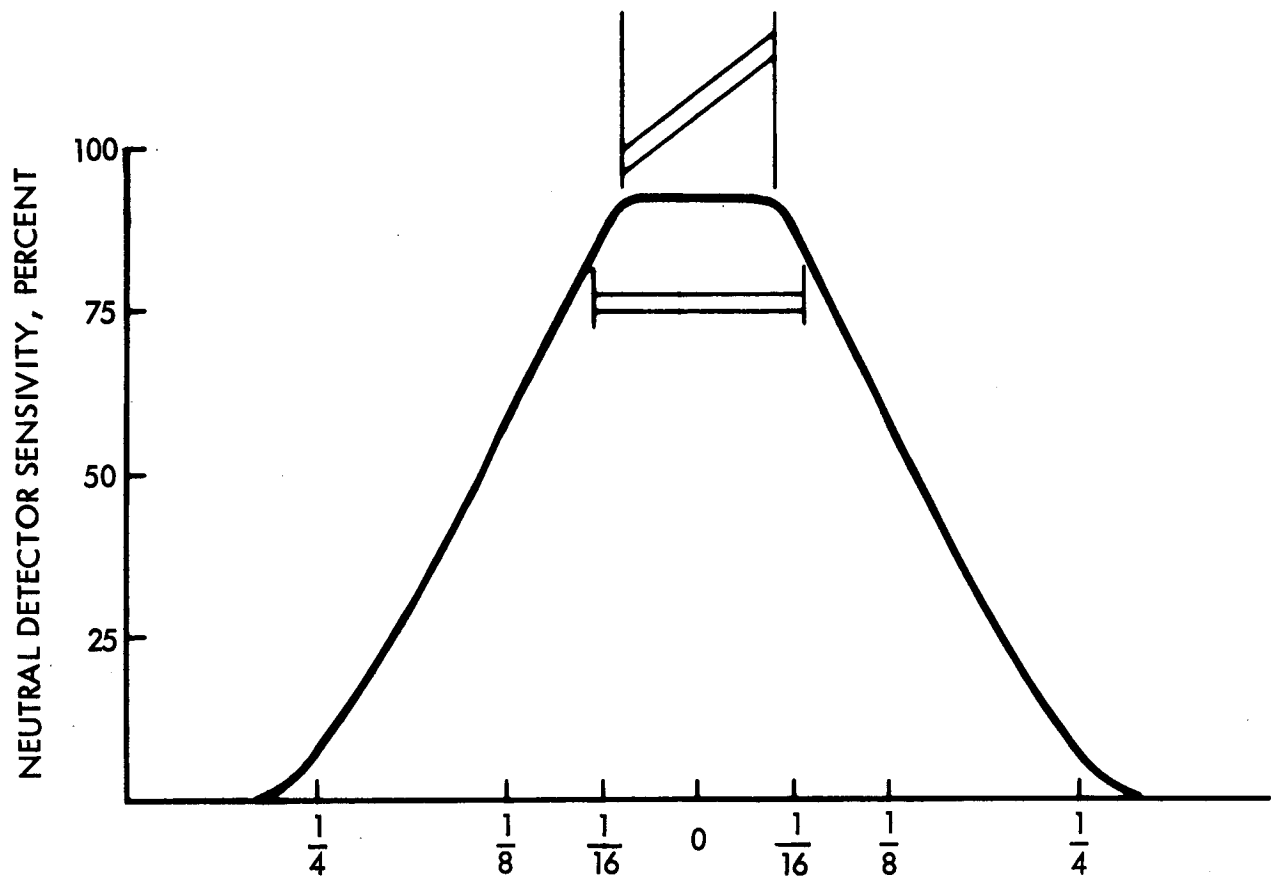


Figure 6. Photograph of completely assembled experiment showing curved deflector electrode, collector grid, and movable arm used for back sputtering sample and applying contaminants.

Neutral Detector. - The neutral detector consists basically of a flag shutter, two collimation apertures, a tungsten ionizing ribbon, and a collector, all at 0 volts and LN_2 temperature with the exception of the ionizing ribbon, which is hot and typically adjusted to +125 volts. The current incident on the collector, which is measured by a Hewlett Packard 425A Micro-Micro Ammeter, ranges between 0.001 and 100 nanoamps. The design of the collimation system is such that the solid angle of acceptance is much greater than that subtended by the sample. Cesium build-up on the collector and adjacent parts is periodically removed by reversing the polarity of the ribbon and raising its temperature above that of thermionic emission.

Neutral Detector Collimation. - To obtain the true distribution of neutrals when a collimated neutral detector is employed, a correction must be applied to the measured distribution. If the collimation is accomplished by using a pin-hole-sized, neutral-cesium-sensitive "eye" in conjunction with a small circular aperture much closer to the sample, then only neutrals from a small circular area of the sample surface can reach the sensitive "eye" when the sensor is normal to the sample axis. However, as the sensor angle deviates from the normal the viewed area increases as $1/\cos \theta$ and becomes elliptical. Therefore a collimated sensor sees a cosine distribution as a constant distribution out to small angles, where the ellipse becomes larger than the diameter of the porous surface. Any cylindrically symmetric collimation system employing a pair of apertures, such as is used in our detector, with any distribution of umbra and penumbra would require the same $1/\cos \theta$ correction as long as only a small portion of the emitter surface is viewed. However, no correction is needed if collimation provides a constant sensitivity to the entire sample surface. Our collimation system approximates this latter case, as will be shown.

Figure 7 shows the sensitivity of our neutral detector collimation system (which has 1/16-inch-diameter apertures at 3 and 4 inches) to neutral cesium coming from points on the emitter surface when the axes of the detector and emitter coincide, i.e. at 0° viewing angle. The size of the sample is indicated. Notice that the sensitivity is constant over most of the surface area of the sample. Also indicated is the apparent size of the sample when viewed from a neutral detector position of 45° , at which angle the entire surface falls within the constant portion of the sensitivity



PERPENDICULAR DISTANCE FROM THE NEUTRAL DETECTOR AXIS AT SOURCE

Figure 7. Neutral detector sensitivity in percent at the emitter surface as a function of perpendicular distance in inches from the detector axis. The effective diameter of the emitter at 0 and 45 degree viewing angles is indicated.

curve. This increase in sensitivity up to 45° is a maximum in the direction shown; we are observing the result of increasing the major axis of the ellipse while its minor axis remains constant. When this small change of sensitivity is averaged over the entire emitter area, the estimated correction is less than 2 percent... a value we are neglecting. If the correction were applied to the measured values of neutral efflux vs angle, the resulting distribution would be less cosine in form than that indicated by the uncorrected data.

Sputtering and evaporation. - Back sputtering the sample surface with cesium ions has repeatedly removed various surface contaminants and, in the absence of the arrival of further contamination, produced a stable, clean surface. Back sputtering may also be used to open a surface that has been closed by surface sintering or machining. The process is carried out by swinging the tungsten ribbon mounted on the arm shown in Figure 6 over the sample, heating the ribbon to above critical temperature, and rearranging potentials.

Contained in the sputtering arm are extra current leads for evaporating contaminants onto the sample. For instance, aluminum was evaporated onto the surface by wrapping aluminum wire around a tungsten filament. This process may be carried out while the ionizer is in normal operation.

Many of the contaminants studied were most conveniently applied to the surface by swinging a sheet of material over the operating ionizer. Such a sheet is seen attached to the sputtering arm (at the left of the tungsten ribbon) in Figure 6. In this method, the impinging cesium ions sputter the contaminant onto the sample. From a knowledge of the sputtering yield, ion current density, and the geometry, the arrival rate of the contaminant at the sample can be estimated.

Method of taking data. - When a sample is first put into operation its performance is often poor, owing to surface or bulk contamination. Various techniques are employed to improve its performance, the choice depending on the suspected contamination and the requirements of the test (such as high-temperature operation, sputtering, high-current operation, or exposure to C_2H_2). A "clean" surface is recognized by the repeatability of its performance between

1850°K and critical temperature as measured on successive temperature runs between cleaning operations, after operation at other current densities, and on successive days of operation. In the case of pure tungsten, its cleanliness is also determined by the similarity of its performance at low current densities to that of previously tested samples, and by its response to oxygen and acetylene.

After the cleaning operation, data are taken at current densities from 1 to 50 ma/cm², the runs often being interspersed with additional cleanings to verify that they have no effect. Next, neutral efflux vs angle is measured at one or more current densities. Then data are obtained in the presence of 5×10^{-6} torr of oxygen, the data-taking operations often being interspersed with returns to the clean surface. Finally, any contaminants currently under study are applied and their effects recorded.

ADSORPTION LIFETIME MEASUREMENTS

Experimental apparatus. - The experiment was conducted in an Ultek Model TNB high vacuum system with a Viton-sealed bell jar. The combined pumping of its ion pumps and titanium sublimator produced a background pressure of 5×10^{-9} torr. The apparatus is shown schematically in Figure 8. The oven was made of massive tungsten to minimize any alloying of the material being studied and to maintain a constant temperature. A high-speed shutter mechanism above the oven was used to abruptly start and stop the molecular beam, which was directed to a hot, 0.001-inch-thick, polycrystalline tungsten ribbon. The desorbed molecules from the tungsten ribbon were ionized by an energetic electron beam and launched into a high-resolution quadrupole mass spectrometer, the sensitivity and time response of which were increased by use of a Bendix 306 magnetic electron multiplier. The output was displayed on an oscilloscope.

The arrival rate of each metal was controlled by the oven temperature. An optical pyrometer was used to measure the ribbon temperature, the proper emissivity and glass corrections being made. The mass spectrometer was tuned to the isotope of the metal that had the lowest background reading.

Experimental apparatus is treated in great detail in Reference 1.

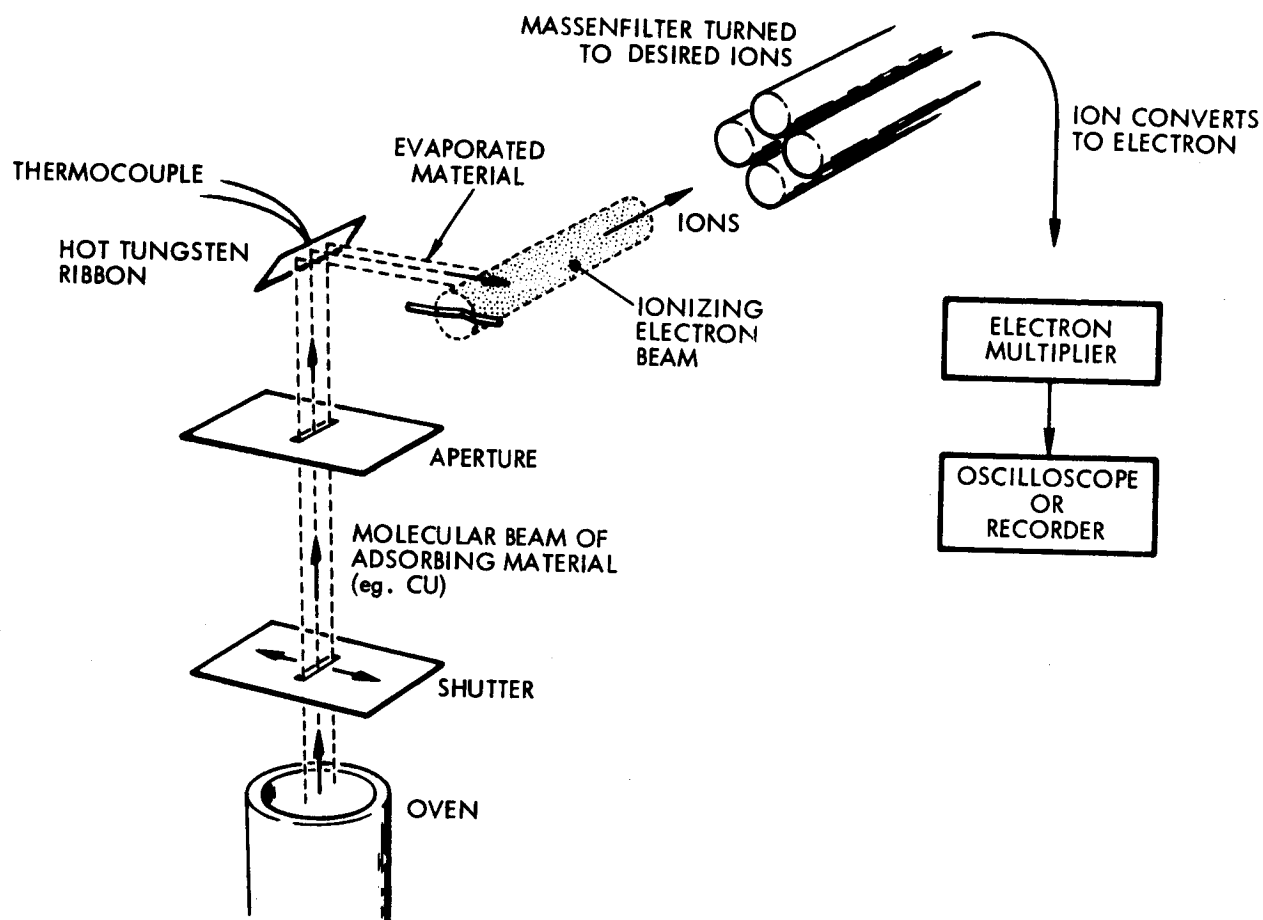


Figure 8. Schematic of experiment to measure the desorption time of various metals on polycrystalline tungsten.

Experimental procedure. - To assure a clean surface, the tungsten ribbon was flashed to high temperatures before the shutter was opened to start the beam. The oscilloscope was triggered at the opening and closing of the shutter, which started and stopped the beam in a much shorter period of time than the lifetime being measured.

When the low-coverage measurements were made under conditions of unity sticking coefficient, the traces were exponential curves of the forms $\Gamma_0 [1 - \exp(-t/\tau)]$ and $\Gamma_0 \exp(-t/\tau)$ for opening and closing of the shutter, respectively, Γ_0 being the equilibrium evaporation rate (equal to the arrival rate) and t the time after the shutter was actuated. In this type of measurement the evaporative lifetime was easily obtained from the initial slope of the oscilloscope trace. Deviations from unity sticking coefficient would have appeared as an initial step in the output.

In the case of higher-coverage measurements in which the lifetime was dependent upon coverage, the traces were not exponential and the lifetimes and corresponding coverages were determined by graphical analysis. The curve shown in Figure 9 aids understanding of the technique that was used. By definition, the evaporation rate is equal to the surface coverage divided by the lifetime. Since the evaporation rate was the property measured and the coverage at the point P is the area designated A, the lifetime is the area A divided by the height of the curve at this point. The accuracy of the calculation depends only on the accuracy of the time base and not on the vertical scale.

Experimental procedure is discussed in more detail in Reference 1.

EXPERIMENTAL RESULTS

Sample Preparation

As was to be expected, the techniques employed in sample preparation considerably influenced the measured performance of samples. Therefore, a discussion of the areas of importance follows.

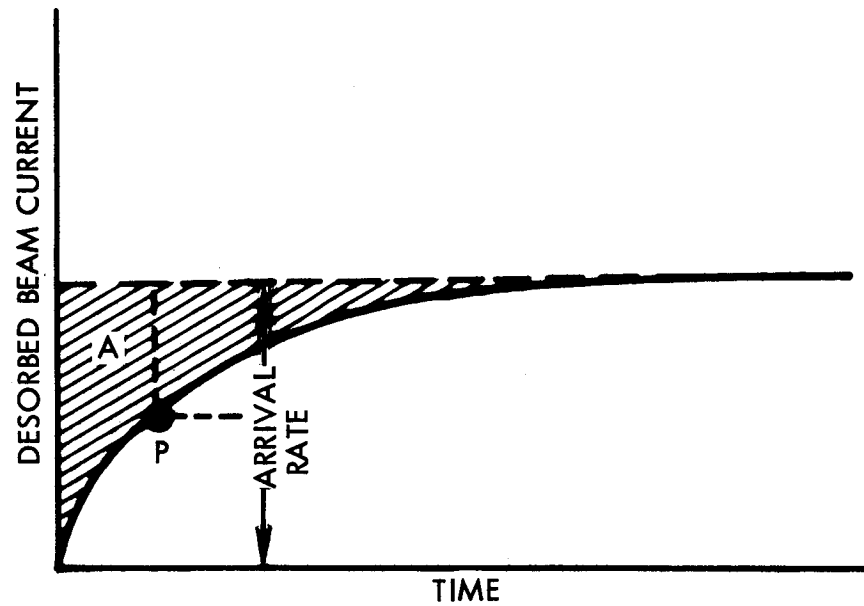


Figure 9. Typical waveform of desorption current. The method of deriving desorption lifetimes at a specific surface coverage from this waveform is discussed in the text.

When tested samples were sectioned, braze run on the rear surface and/or significant further sintering of the porous tungsten were occasionally discovered. The probable explanation for the braze runs is drawn from the phase diagrams of rhodium with tungsten and rhodium with molybdenum. In brazing rhodium and tungsten, holding the temperature just above the melting point of rhodium causes the tungsten to begin to dissolve into the rhodium. After only a few percent of tungsten is dissolved, the alloy solidifies at this temperature, halting braze flow before either sufficient time or increased liquid volume allows it to leave the desired area. Unfortunately, the molybdenum-rhodium phase diagram is not nearly so attractive; a eutectic of 60-weight-percent molybdenum exists below the melting point of rhodium. Thus, this system is not self-terminating and there is a substantial increase in liquid volume. Probably more important still is the possibility that this molybdenum-rhodium eutectic can dissolve large amounts of tungsten. Phase diagrams of the tertiary system are not available.

As causes of the extended regions of further sintering adjacent to the braze, two possibilities have been entertained: (1) that the molybdenum transported by the eutectic liquid to the tungsten diffuses into the porous tungsten, and (2) that the rhodium itself diffuses into the tungsten during extended high-temperature operation. Experiments in which these contaminants were sputtered onto the surface of a sample and the observed correlation of further sintering with histories of extended high-temperature operation both indicate that the rhodium is responsible. Furthermore, on at least one occasion we observed sintering of porous tungsten adjacent to a rhodium braze when no molybdenum was present. Nonetheless, experimenters planning further work should consider the possibility of hot-machining the plenums from solid tungsten; we believe that this would at least eliminate the possibility of braze runs across the rear surface of samples while relaxing the need for the close tolerance between sample and plenum. Another alternative would be to electron-beam weld the samples to the plenum. However, this weld is difficult to make and requires a very skilled operator with considerable practice.

The surfaces of samples after machining and deinfiltration are rough and burnished, as shown at 1000X in Figure 10. Probably these surfaces are cold-worked and that surface sintering occurs upon the first high-temperature operation. Many of the samples we have tested have therefore been etched prior to testing. Anodic electroetching in concentrated sodium hydroxide was used on the front surface after brazing. Although the electroetch probably does not preferentially enlarge big pores, as would a chemical etch, the resulting surface roughness makes verification with the microscope difficult. (See Figure 11 of Hughes 324-S at 750X). We also suppose that high work function facets of the grains of tungsten are preferentially exposed and that contaminants from the vacuum system deposited on the surface during brazing and other handling are removed. The rear surface has often been chemically etched to improve transmittivity by filling the plenum with Purex and 5-percent sodium hydroxide for 2 minutes while the plenum is immersed in boiling distilled water. The porous tungsten is then force-flushed with hot distilled water until the flush water no longer shows any basic reaction. These treatments have repeatedly increased measured transmittivity and improved ionizer performance. Occasionally they have been used to rejuvenate a surface sintered closed by excessive high-temperature operation.

A second technique for controlling the mechanical condition of the surface is extended sputtering with cesium ions. This method produces a surface very similar in appearance to that obtained by anodic etch, as Figure 12 shows.

When we became more interested in metallographic examination of samples, another possible technique for treating the front surface became apparent. The surface was metallographically polished for high-magnification viewing while it was still infiltrated and then was deinfiltrated in the usual way. As shown in the photograph of Hughes 324-S (Figure 13), the resulting surface is quite smooth with no apparent burnishing. To compare its performance with that of a heavily sputtered surface, first the data were taken with the polished surface and then this sample was heavily sputtered. As shown in Figure 14, the polished surface (solid curves) was superior to the sputtered surface (dashed curves). At 5 ma/cm^2 the polished- and sputtered-surface curves

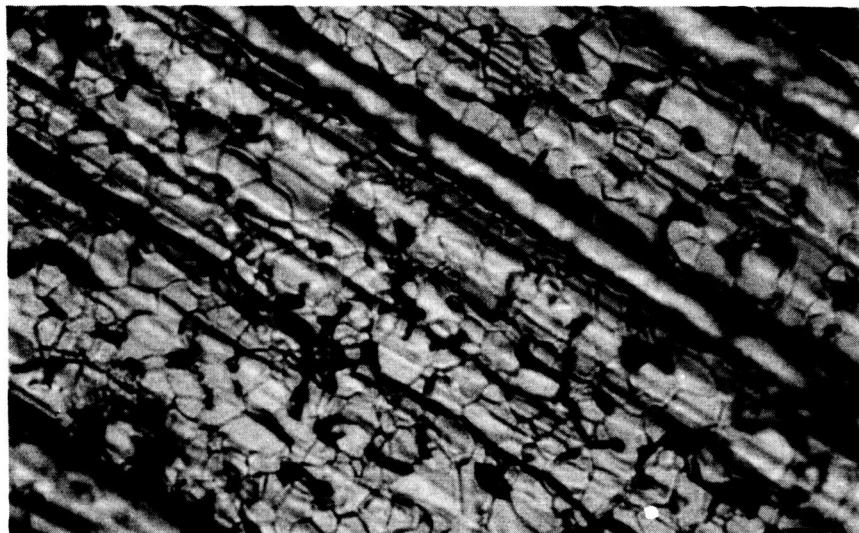


Figure 10. Photomicrograph at 1000X of Union Carbide sample as received from machinist. Sample is still infiltrated with copper.

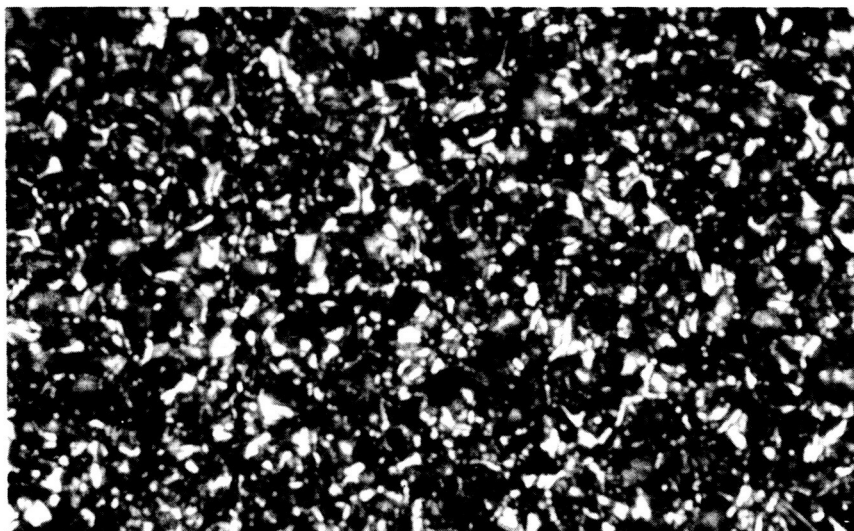


Figure 11. Photomicrograph at 750X of Hughes 324-S sample after electrolytic etch.

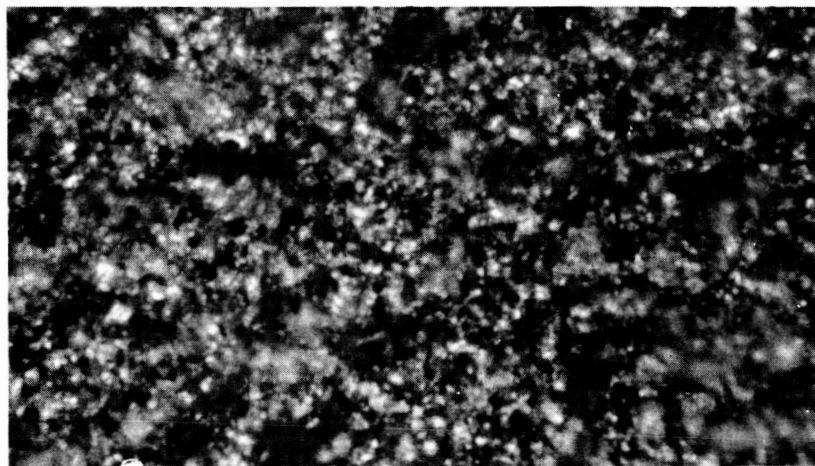


Figure 12. Photomicrograph at 700X of Hughes 324-S
after sputtering surface with cesium ions.

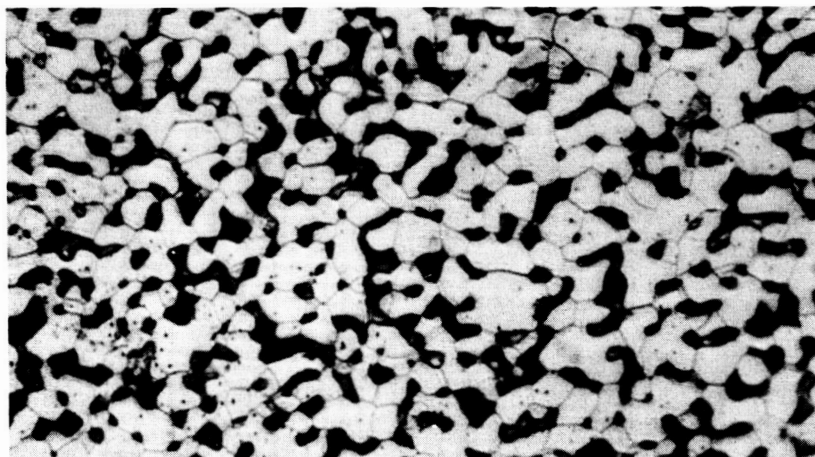


Figure 13. Photomicrograph at 1000X of Hughes 324-S

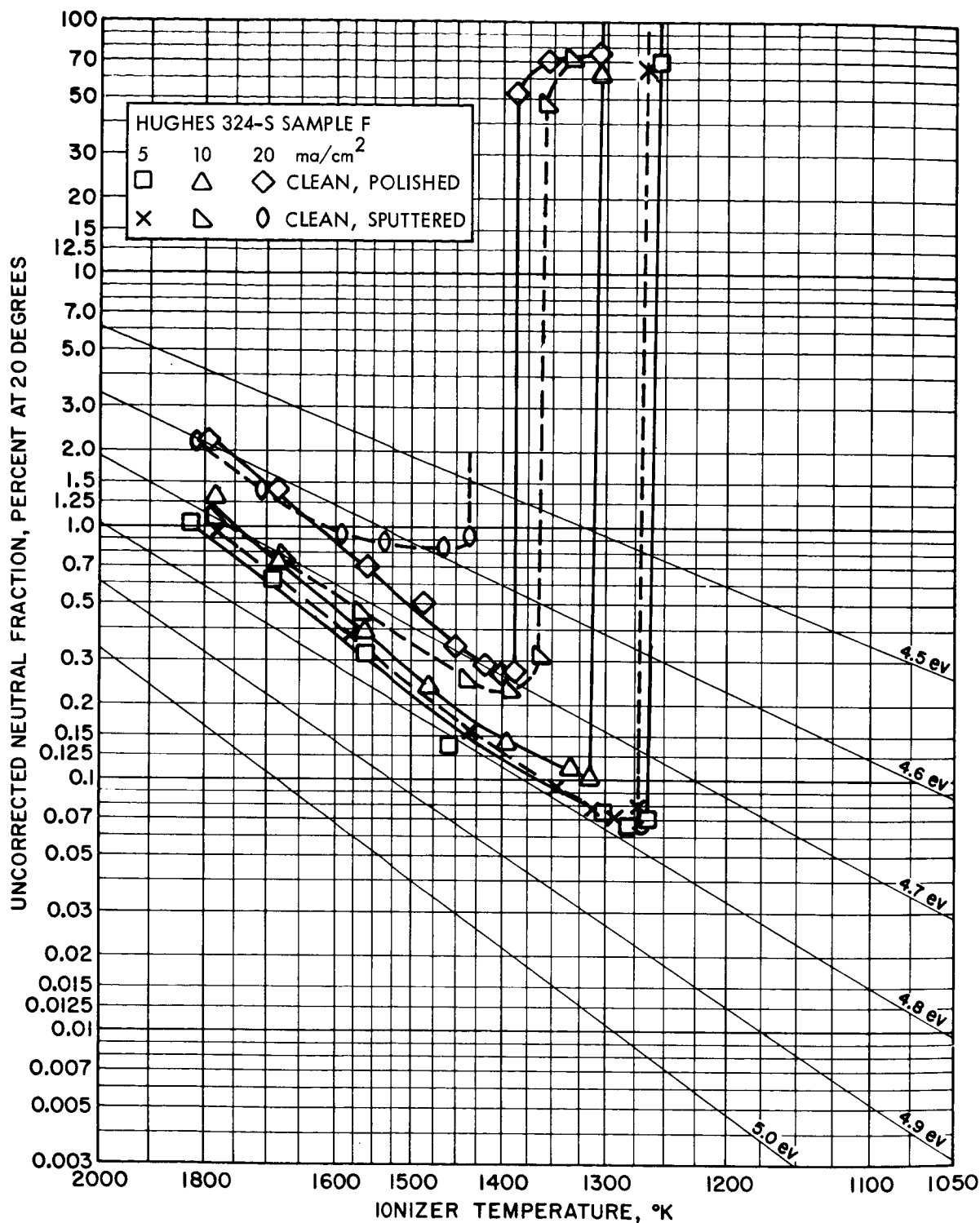


Figure 14. Uncorrected neutral fraction from heavily sputtered Hughes 324-S Sample F at 20 degrees from normal vs temperature compared to polished surface of Sample F at several ion current densities.

are identical, but at 10 and 20 ma/cm² the critical temperature is ~50° higher and the neutral efflux is increasingly higher in the sputter case.

As will be discussed under Test 5, later attempts to reproduce this result failed; little change in performance was observed when a polished surface was sputtered. However, the polishing process is attractive even in the absence of a direct performance improvement because it eliminates the need for etching the deinfiltreated sample. Etching is an uncertain process with potential for contaminating the ionizer. Furthermore, polished ionizers probably have a lower emissivity than conventional surfaces, leading to a reduction in the required heater power.

Neutral Efflux vs Angle

In the past most experimenters, including ourselves, have measured the current in a neutral detector at some fixed angle both during ion production and with acceleration potentials suddenly removed. In our earlier experiments we interpreted the ratio of these two currents as the true neutral cesium fraction leaving the surface. This interpretation is correct only if the angular distribution of cesium neutrals is the same for both conditions. (None of our experiments are made with the scattering structures above the ionizer typical of high-current-density ion engines; hence the usual corrections for such structures are not required and the measured neutral efflux distribution of the sample is not perturbed.) The present experiment measures these two distributions and indicates that the total integrated neutral fraction is approximately a factor of 2 smaller than that given by the simple ratio of the current readings. In the following discussions, the interpretation of neutral detector readings for a constant distribution is first discussed, and then a correction factor to account for nonconstant distribution is derived. Next, a typical example of the

measured portion of a distribution is presented and numerical values for the correction factor obtained by making reasonable guesses at the form of the unmeasured portion of the distribution are given. Finally, some ramifications of this result for contact thruster development are noted.

Derivation of correction factor for neutral detector measurements. - If the distribution of neutrals were the same in the operating and nonoperating conditions, then the percent of neutrals would be given by

$$\% N = \left[I_{ND_1} / I_{ND_2} \right] \times 10^2 \quad (1)$$

where the subscripts 1 and 2 refer to the accelerating potentials being on and off, respectively. Because removing the acceleration potentials from an ionizer operating near the critical temperature will prematurely drive it past the critical condition, the following equivalent expression has usually been employed. It also allows the data to be taken more rapidly:

$$\% N = \frac{K I_{ND_1}}{I_+ + K I_{ND_1}} \times 10^2 \quad (2)$$

In this expression $K = I_+ / (I_{ND_2} - I_{ND_1})$, is the "calibration constant" of the neutral detector. The second term in the denominator of Eq. (2) may be ignored for neutral fractions of less than approximately 5 percent, permitting more rapid data reduction.

This simple interpretation of neutral detector readings was used until a year ago, although we had long suspected that the angular distribution of neutral efflux did change between the conditions of ion production and nonproduction. In particular, we expect that whereas the neutral efflux would have a cosine distribution when the acceleration potentials were removed, the neutral efflux with acceleration potentials applied would contain far fewer neutrals at large angles to the normal. The reasoning behind our assumption was that in the 100-percent-neutrals case the entire ionizer surface is believed to be covered with cesium by virtue of surface migration, which implies the cosine distribution. On the

other hand, it is believed that during ion production, emission occurs from within the pores and the tungsten surface itself is free of cesium. Thus, the only way a neutral atom can take a direction significantly different from normal is by scattering off the high-work-function outer rim of its pore. Of course, such a scattering process is very likely to ionize the atom.

These expectations about the angular distribution of the neutral efflux were borne out by experiment. A cosine distribution of the 100-percent neutral fraction was obtained from every sample on which angular data were taken, whereas the distributions from these samples during normal ion production were never cosine. We are faced, therefore, with the problem of applying a correlation factor to the values of neutral fraction given by Eq. (1) or Eq. (2), since the fundamental assumption underlying these equations is false.

The form of such a correction may be easily derived without a knowledge of the distributions themselves. If the measured neutral density is given as a function of angle by

$$j(\theta) = j(0) f(\theta) \quad (3)$$

where $f(\theta)$ is the normalized distribution [$f(0) = 1$] and $j(0)$ is the measured neutral current density at $\theta = 0$, then the total neutral efflux is given by

$$I_n = 2\pi r^2 j(0) \int_0^{\pi/2} f(\theta) \sin \theta d\theta. \quad (4)$$

Here r is the radius of the neutral detector arc with subscripts 1 and 2 again denoting ion production and nonproduction modes, respectively. The neutral fraction is

$$\frac{I_{n1}}{I_{n2}} = \frac{j_1(0)}{j_2(0)} \frac{\int_0^{\pi/2} f_1(\theta) \sin \theta d\theta}{\int_0^{\pi/2} f_2(\theta) \sin \theta d\theta}. \quad (5)$$

Now if the neutral detector measurements are made at $\theta = \theta_o$, substituting Eq. (3) into Eq. (5) and multiplying by 10^2 to obtain percent,

$$\%N = \frac{I_{n_1}}{I_{n_2}} 10^2 = \frac{j_1(\theta_o)}{j_2(\theta_o)} \cdot \frac{f_2(\theta_o)}{f_1(\theta_o)} \frac{\int_0^{\pi/2} f_1(\theta) \sin \theta d\theta}{\int_0^{\pi/2} f_2(\theta) \sin \theta d\theta} \cdot 10^2 \quad (6)$$

This is the general expression for the percent neutral efflux when the distribution changes with acceleration potentials applied and removed. If the distributions are identical, it reduces to Eq. (1):

$$\%N = \frac{j_1(\theta_o)}{j_2(\theta_o)} \times 10^2 = \frac{I_{ND1}}{I_{ND2}} \times 10^2 .$$

Turning to the question of what distributions are measured, as mentioned previously, $f_2(\theta) = \cos \theta$. Figure 15 shows the typical form (not normalized) of $f_1(\theta)$, the angular distribution of an operating ionizer. The peak at 0° in this case is about 3.5 times higher than the extrapolated value of the distribution elsewhere. We conclude that this forward peak is mainly due to a focused beam of neutrals caused by charge exchange between the ions and the neutral cesium density resulting from the departure of the neutral fraction from the ionizer itself. The two main observations supporting this conclusion are that the excess of cesium neutrals in the forward peak varies directly as the neutral fraction and also the ion current density. Since we normally do not measure neutrals in the forward direction, and since little integrated neutral emission is represented by this peak, we ignore its presence in determining $f_1(\theta)$.

By extrapolating the data between 4° and 40° to 0° and normalizing, the curve in Figure 16 is obtained. (For comparison, a cosine θ distribution and a Clausing² distribution from a cylinder one-diameter deep are also shown.)

In the case of temperatures above critical and electric fields higher than necessary to overcome space charge, there is a single distribution for neutrals that is independent of temperature, field and ion current density. (Neutrals that are emitted because of insufficient accelerating potential or ionizer temperature below critical have a cosine distribution.)

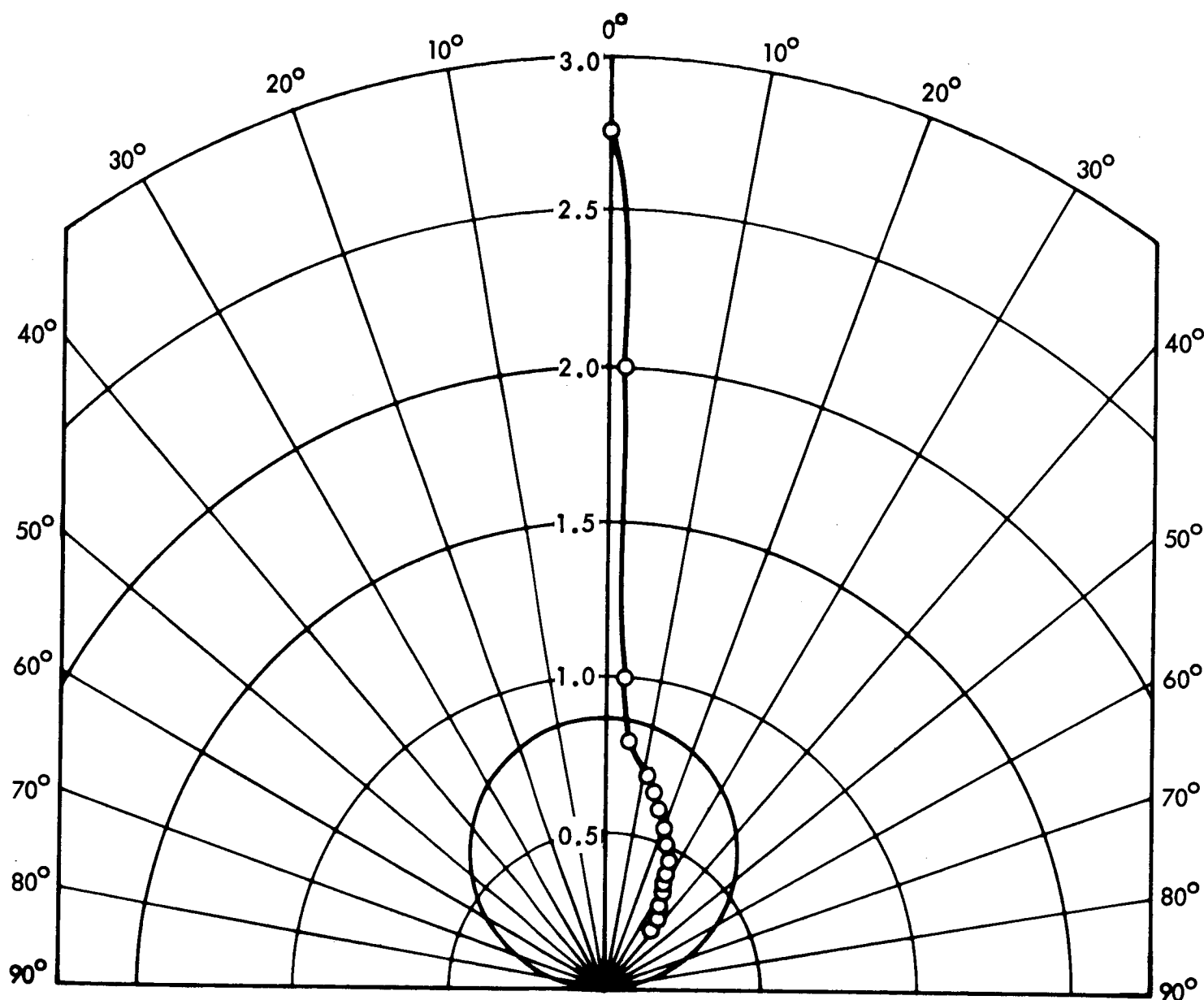


Figure 15. Neutral detector readings vs angle from Hughes 324-S Sample B at 10 ma/cm^2 , non-oxygenated. Circle represents cosine distribution with zero-degree value of extrapolated Sample B data.

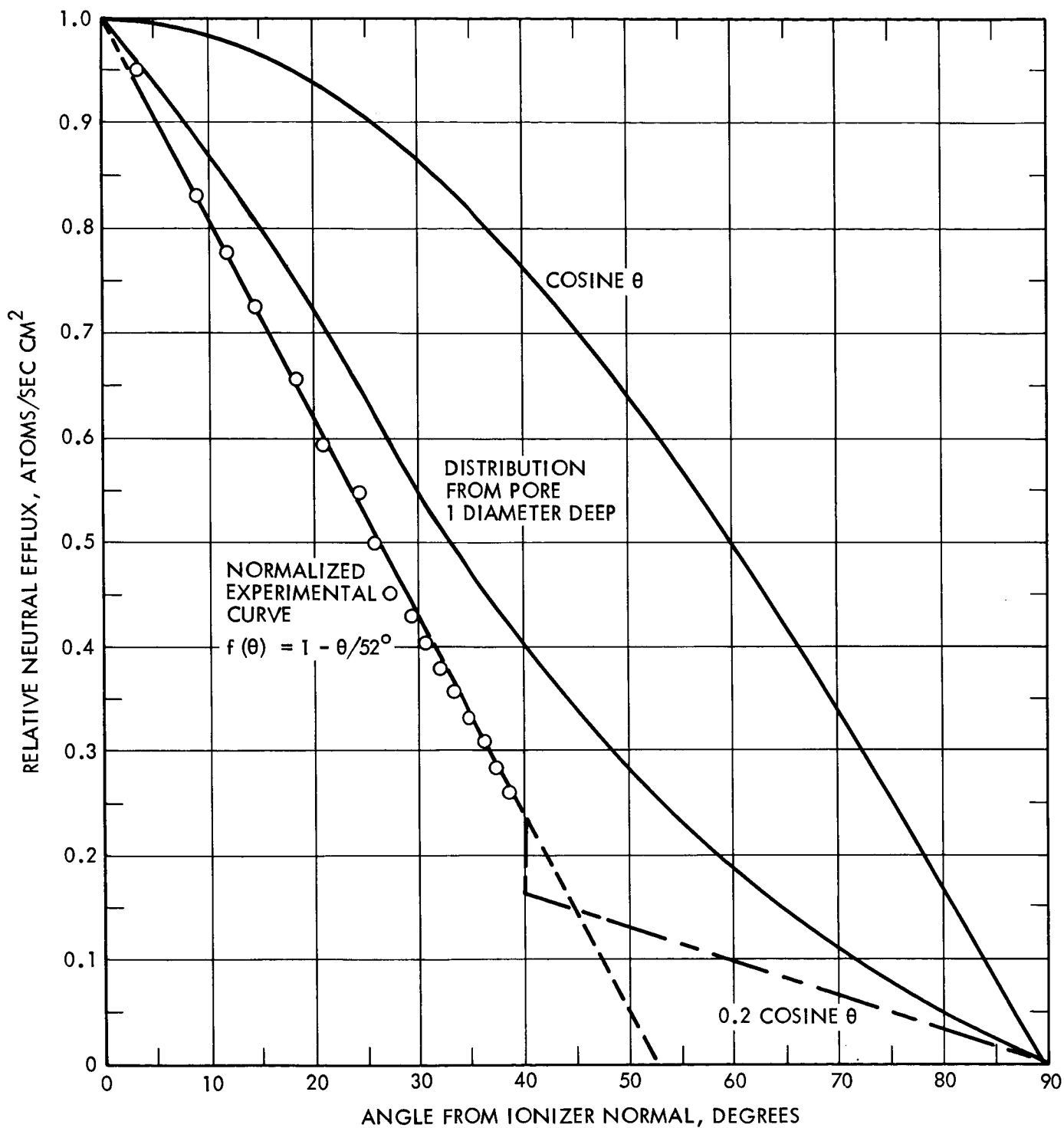


Figure 16. Normalized neutral detector readings vs angle from Hughes 324-S Sample B at 10 ma/cm². Also shown are Case I and II estimates of readings above 40°, Clausing distribution from pores one-diameter deep, and cosine distribution.

Slight changes in slope have been observed as the ion current density is varied or the surface condition changed in testing a sample. Typically, the slope will increase approximately 10 percent as the current density is increased from 5 to 10 ma/cm² or when a clean surface is oxygenated.

The equation of the best line through the data presented in Figure 16 is $f_1(\theta) = 1 - \theta/52^\circ$. To date, the angular distributions of all the samples tested have been substantially linear, with slopes usually between 1/49° to 1/66° at 5 ma/cm² and between 1/49° to 1/60° at 10 ma/cm². We now substitute the $f_1(\theta) = 1 - \theta/52^\circ$ case into Eq. (5) to obtain the corrected value of the total neutral efflux.

The major difficulty in performing this substitution should be apparent from Figure 16. The distribution between 40° and 90° is unknown. Two physically reasonable and mathematically convenient approximations for this portion of the curve have been considered; the actual value of the neutral fraction is expected to fall between the values obtained from these two approximations.

In the first, a simple linear extrapolation to zero at 52° is used:

$f_1(\theta) = 1 - \theta/52^\circ$, $0^\circ < \theta < 52^\circ$. In the second case, a tail is added to the distribution: $f_1(\theta) = 1 - \theta/52^\circ$ for $0^\circ < \theta < 40^\circ$ and $f_1(\theta) = 0.2 \cos \theta$ for $40^\circ < \theta < 90^\circ$. For these two cases Eq. (6) becomes

$$\%N = 0.40 \frac{j_1(\theta_o)}{j_2(\theta_o)} \times 10^2 \quad (\text{Case 1})$$

and

$$\%N = 0.52 \frac{j_1(\theta_o)}{j_2(\theta_o)} \quad (\text{Case 2})$$

Here our standard reference angle θ_o of 20° has been used. To indicate how this correction factor depends on the slope of $f_1(\theta)$, we note that in the Case 1 extrapolation 1/45° leads to 0.34 and 1/62° gives 0.51.

The important aspect of this analysis is that the neutral fraction measured at 20° to the normal on the assumption that $f_1(\theta) = \cos \theta$ should be multiplied by $\sim 1/2$ to obtain the actual neutral fraction. (Measurements of neutral fraction at angles greater than 20° will require less and less correction out to $\sim 40^\circ$, where the correction is unity.)

Not only does this Clausing-like distribution have considerable impact on the value of the neutral fraction itself; it has further ramifications in the calculation of the life expectancy of high ion current density contact thrusters. In such thrusters life expectancy depends heavily on grid bar erosion by charge-exchange ion sputtering. The density of charge-exchange ions depends, in turn, on the density of neutral cesium between the ionizer and the grid. The ramifications of the Clausing-like distribution observed may be summarized as follows:

- 1) The value of the total neutral efflux is $\sim 1/2$ the value implied by uncorrected measurements.
- 2) A larger fraction of this total value escape between grid bars than for a cosine distribution and should not be multiplied by the back-scattering factor.
- 3) For the same total neutral efflux in a Clausing-like and a cosine distribution, the resulting number density of atoms in the accelerating region from the former is reduced in comparison with the latter by its increased average outward velocity component.

Significance of noncosine distribution. - We hoped initially that the observation of the angular distribution and its change with temperature, applied voltage, and ion current density would give some clue as to the site of ion emission. We were quite surprised to find the distribution very insensitive to these parameters. Since the distribution is noncosine, the emission of neutrals does not follow Lambert's law. From this we may conclude that (1) the emission is from within the pores and (2) the cesium coverage on pore walls is a function of distance from the mean surface. Apparently this distribution of cesium coverage is independent of temperature, applied voltage, and cesium feed rate, because the observed angular distribution is insensitive to their values.

Conclusion (1) follows from the fact that any linear combination of point sources with cosine distributions is also a cosine distribution; there would be no way to vary the cesium coverage over a planar surface and not obtain a cosine distribution of neutral efflux.

Conclusion (2) may be illustrated by proving that Lambert's law holds for a porous surface if the coverage of cesium on pore surfaces is uniform. For simplicity, suppose that the surface is composed of a number of sawtooth-shaped pores, all within the collimation area of the neutral detector (as illustrated in Figure 17). The number of neutrals detected from a particular pore is proportional to $L \sin (\theta + \phi)$. This product is equal to the construct B, the projected "area" normal to the neutral detector axis. However, B, to which the number of neutrals detected is proportional, is independent of ϕ and depends only on the cosine of θ : $B = \chi_0 \cos \theta$.

Thus under the condition of uniform cesium coverage, a cosine distribution would obtain whether the pores were deep, shallow, or absent. This proof can be generalized to three dimensions and any arbitrary pore shape. If, however, the areas that are exposed to the detector at low angles have a lower cesium coverage than those seen at angles nearer the normal, the distribution will be noncosine, a result which accords with our observations.

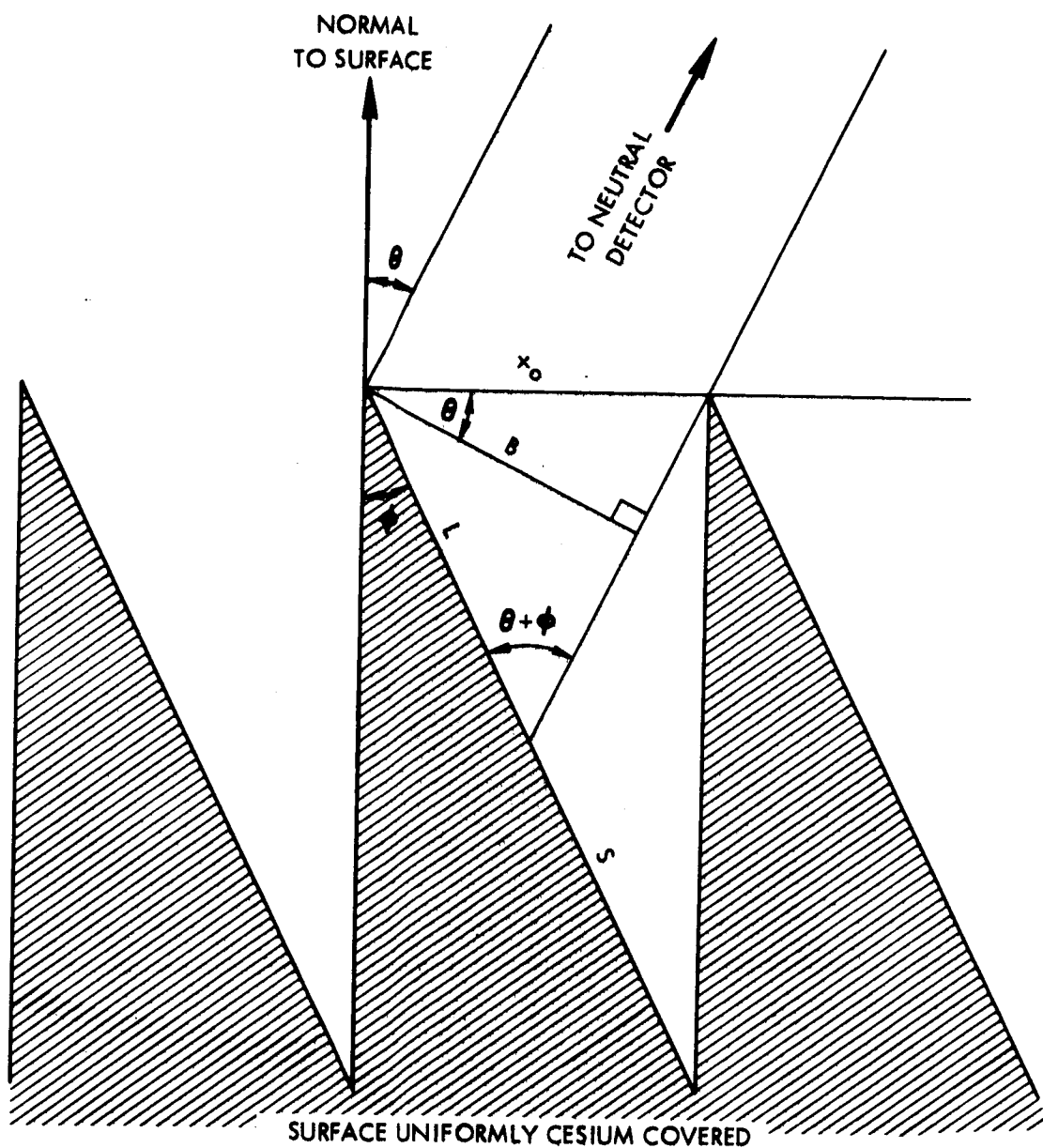


Figure 17. Cross section of hypothetical surface used to demonstrate that uniform cesium coverage leads to a cosine distribution of neutral efflux.

EFFECT OF OTHER ELEMENTS ON TUNGSTEN SURFACES

The surface of tungsten has been studied more than that of any other element, primarily because an atomically clean surface can be achieved by the simple expedient of heating reasonably pure tungsten to extremely high temperatures. However, the porous tungsten used in ion emitters cannot be cleaned by this method because of limitations imposed by the method of heating such large areas, by the necessity of preventing undue sintering, or by the braze material. The lower operating temperature allows a large number of materials to reside on the surface — often completely degrading the ion emission characteristics of the porous ionizer. This fact, i.e., that porous tungsten is often not "tungsten," is probably one of the main reasons cesium contact ionization engines have fallen into disfavor.

Earlier research traced "poisoning" problems to calcium in the interior of the porous tungsten, presumably as CaWO_4 which was decomposed by cesium after the oxygen concentration was finally reduced by lengthy high vacuum operation. Barium was shown to act similarly. Any fluorine or chlorine present desorbed rapidly and so did not "poison" the emitter.

Oxygen. - This research program has continued to study this aspect of porous tungsten development. In past programs the commonly encountered contaminating impurities were studied. Oxygen has always been recognized as being extremely important, first because of its ubiquity, being present in a vacuum system as H_2O and CO_2 and on the surfaces of the porous tungsten previously exposed to air as surface oxides, and second because of its creating a large increase of work function.³ It has long been recognized that oxygen lowers the neutral fraction — usually at the expense of an increase in the necessary operating temperature. This appears to be uniformly true at low current density levels, when a continuous oxygen pressure either is present or has recently been present. More careful continuing study of this phenomenon suggests that at high levels of cesium feed rate, and presumably high coverage, the situation is more complicated.

Evidently there is a reaction between the two materials on the surface. At these higher current densities the effects of a continuous oxygen supply are quite different from those caused by remnant oxygen. Remnant oxygen is recognized by a monotonic increase in neutrals with decreasing temperature and a rounded critical temperature. The clean surface has decreasing neutrals with decreasing temperature and a sharp critical temperature. A tentative conjecture is that a partial oxygen coverage leaves sites for very tightly adhering cesium, resulting in a lower work function and a high neutral fraction for the cesium that desorbs from this composite W-O-Cs surface.

Carbon.— The diffusion of carbon to the surface and its variation with temperature explained many of the observations with oxygen. Carbon present in sufficient quantity to remove quite high oxygen arrival rates for a reasonable time had no effect on the work function of tungsten or the binding energy of cesium. Tungsten carbide WC, and presumably also W_2C , had the startling effect that the neutrals and the critical temperatures were both lower.³

Present studies continue to confirm these observations, and carbon is routinely used to remove remnant oxygen or provide a barrier to remove oxygen that would otherwise migrate from the interior to the surface under study. In this present program we were given the opportunity of repeatedly measuring ion-emitting characteristics of what we believe to be pure carbon. It is practically impossible to make this observation on tungsten except at very low temperatures because of the carbide formation. However, when carbon was cracked from acetylene on iridium a quite stable surface of carbon could be studied for some time over a reasonable temperature range when the carbon layer was only a few atoms deep. Figure 18 shows the ion emission of such a carbon surface. The work function was found to be 4.45 volts, and obviously the critical temperature was very low.

Numerous materials that might be sputtered onto the porous tungsten from adjacent electrodes were studied, both with respect to their adsorption

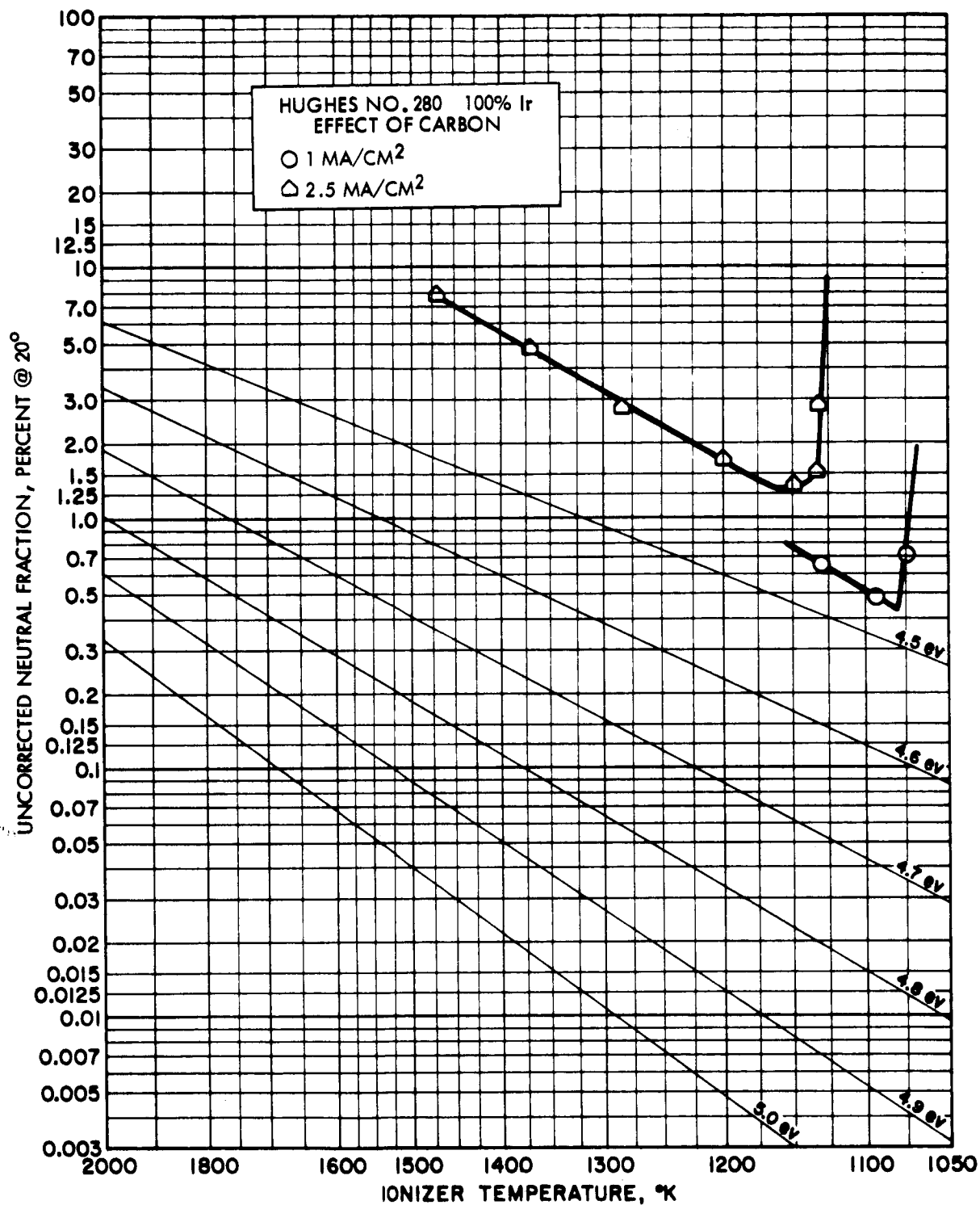


Figure 18. Uncorrected neutral fraction from bulk carbon on Hughes No. 280 100% Ir at 20° from the normal vs ionizer temperature for two ion current densities.

lifetime⁴ and their work function effects on porous tungsten emitting cesium ions. The lifetimes of the materials that would be expected to reevaporate from the porous tungsten at its operating temperature were studied last year. For low coverages at 1500°K from clean tungsten the lifetimes are (in seconds) Cu, 0.01; Cr, 3.; Be, 0.05, Ni, 1.; and Fe, 0.7. All of these may be tolerated at arrival rates up to one monolayer per second except chromium. Trace amounts of it are difficult to remove and increase neutral efflux. Titanium and zirconium have very long lifetimes and are very bad with respect to their effect on the work function.

In the current research program the materials to be studied were mostly those that would not reevaporate but would alloy with the tungsten. These materials were iridium, rhenium, tantalum, molybdenum, rhodium, niobium, platinum, silicon, and carbon. The surface migration, or bulk diffusion, was to be inferred mainly from the transient effects, the arrival rate needed to maintain some surface effect, and the depth necessary to sputter to remove the material. All such information is qualitative at best. More quantitative is the effect of these materials on the tungsten. One material, aluminum, yielded quantitative adsorption lifetimes.

Aluminum. - The adsorption lifetimes of aluminum on polycrystalline solid tungsten have been measured and are shown in Figure 19. As in the past, the lifetimes at low coverage are most accurately measured. The low coverage lifetime τ satisfies the equation $\tau = 10^{-16} \times 10^{+5040 \times 5.3/T}$, where T is the tungsten temperature in degrees Kelvin. The adsorption energy is 5.3 volts.

Since the lifetime of aluminum from clean tungsten is about four orders of magnitude longer than its lifetime from aluminum, as calculated from the vapor pressure of Honig, lifetime would logically vary strongly with coverage. However, the variation lies within about a decade for coverages less than a value called one monolayer ($\theta = 1$) beyond which the lifetime rapidly decreases the additional three decades. The sketched

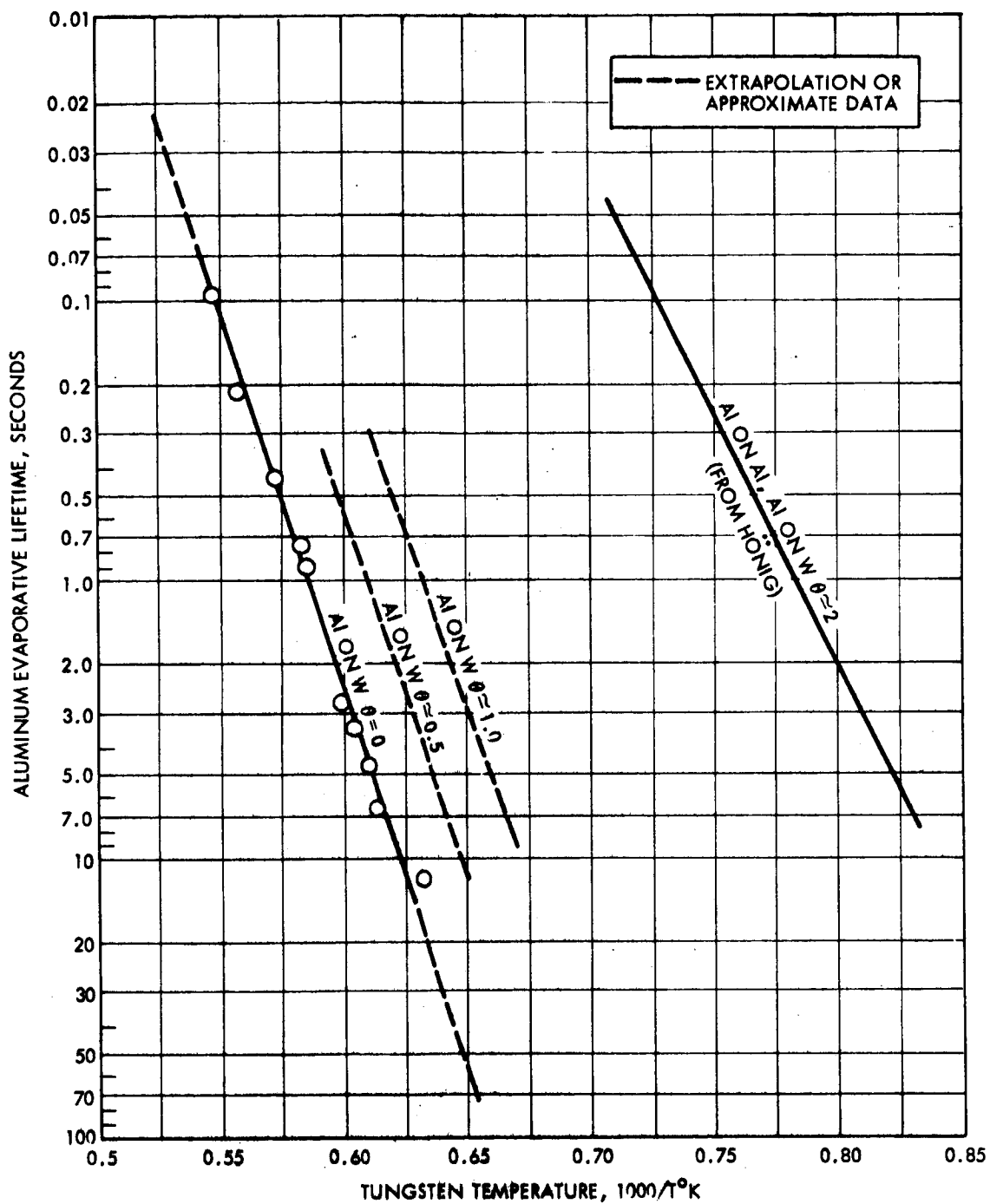


Figure 19. Evaporative lifetime of aluminum on polycrystalline tungsten vs tungsten temperature for several aluminum coverages (in number of monolayers).

position of the $\theta \approx 0.5$ line indicates a nearly linear decrease in the adsorption energy with coverage: within experimental error, this appears to be true. The coverage before bulk accumulation commenced was approximately 2 monolayers. The lifetimes for this coverage agreed reasonably with the upper line, which represents aluminum evaporation from bulk aluminum.

The low-coverage lifetime of aluminum is about 1/2 decade longer from oxygenated tungsten than it is from clean tungsten. From tungsten carbide it is about 2-1/2 decades shorter than from clean tungsten. No diffusion of aluminum into the tungsten was observed. Also, no deviation of the sticking coefficient from 1.0 was observed.

Aluminum was also evaporated onto hot porous tungsten emitting cesium ions. Because we feared that evaporating Al onto a porous W ion emitter might permanently ruin it, the Union Carbide material whose performance characteristics had already been seriously degraded was chosen to test the effect of Al on the ion-emitting properties of porous W. The results are shown in Figure 20. Curve a represents the condition of the surface essentially as it was before the test was begun and to which it returned after sputtering or prolonged periods of operation reduced the Al coverage to a small value. Curve b resulted from a high arrival rate of Al (a few monolayers/sec) continuously incident on the surface. The condition represented by curve c was obtained within a few seconds after turning off the Al. This surface condition has quite a long life at temperatures of about 1500°K — probably in excess of two hours. The initial overshoot and undershoot of the neutral fraction upon raising and lowering the temperature, followed by a return to the stable value within a few minutes, suggest that surface diffusion is the dominant moderating mechanism. This is consistent with the observation that the decay from curve b to c is much faster than the adsorptive lifetime (about 50 sec) and also with the fact that a high continuous arrival rate of Al must be maintained to produce even a fractional monolayer coverage when little material is evaporating off.

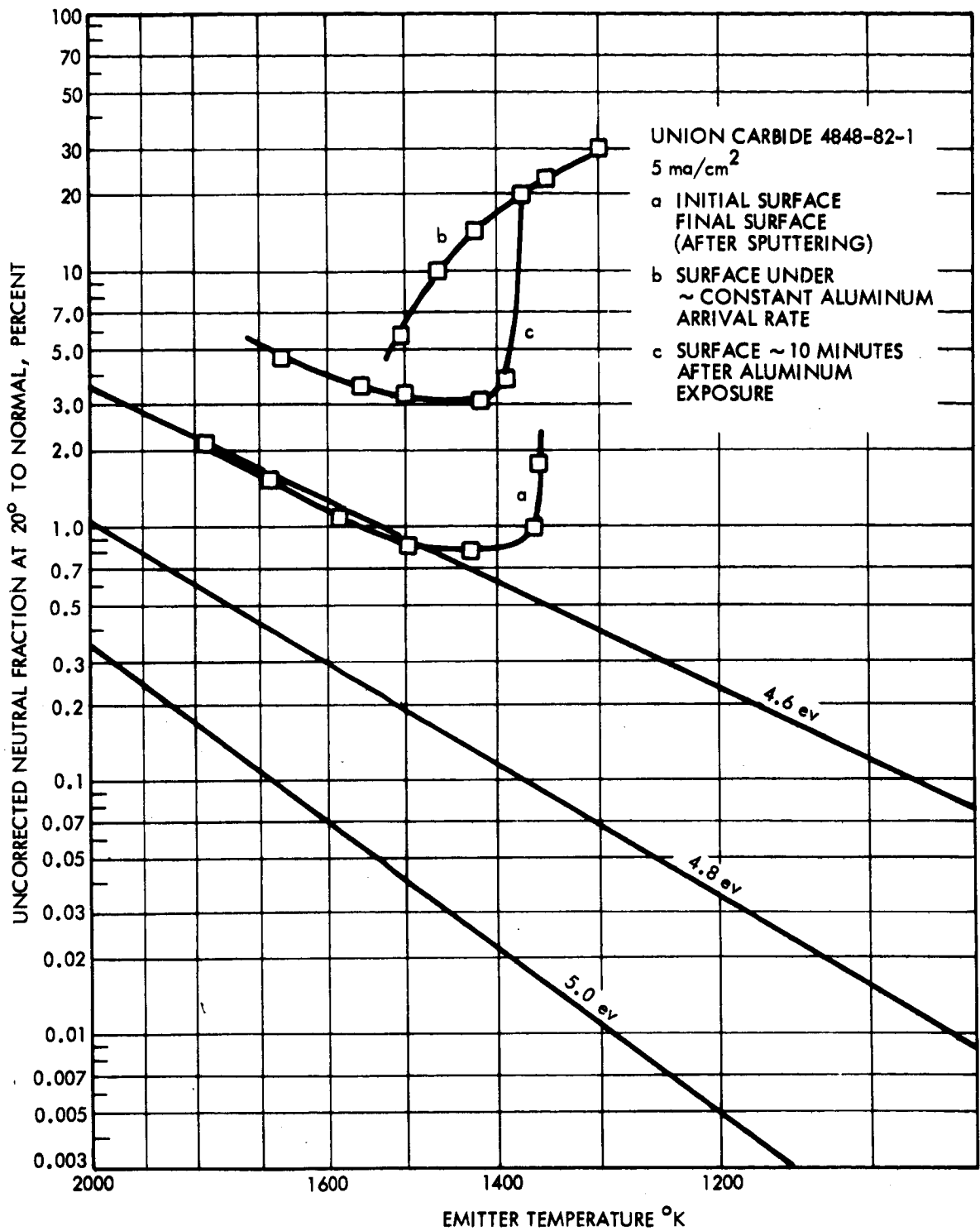


Figure 20. Uncorrected neutral fraction from Union Carbide 4848-82-1 vs temperature for various surface conditions.

Trace amounts of Al do not seem to be very serious. Significant amounts of Al probably remain even when curve a is obtained. Even with quite a bit of Al present (curve c) the critical temperature is not high. Also, in the presence of continuous or remnant oxygen, the characteristics of an Al-contaminated surface are similar to those of a clean surface. Of course, for continuous exposure to Al, the arrival rate must be low enough so that the equilibrium coverage is much less than a monolayer. The equilibrium coverage is given by $\sigma = \Gamma\tau$, where Γ is the arrival rate and τ is the evaporative lifetime. (This assumes that the concentration of Al in the source is so high that evaporation dominates diffusion.) In this connection, a carbided surface can be exposed to about 300 times as high an arrival rate as can clean W because of the very much shorter lifetimes of Al on tungsten carbide.

Iridium. - The effects of iridium were observed in individual tests on emitters in which this material was coated on the surface of tungsten, alloyed with the tungsten, or used in its pure form. In each case, oxygen was found to adhere tightly, seeming to reside within the interior and continually diffuse to the surface, and was very difficult to remove when iridium was contained in the porous ionizer. The intrinsic work function appears to be about 5.15 volts with a slightly higher critical temperature than of tungsten ($\sim 50^\circ\text{K}$). Thin coatings of Ir seemed to alloy rapidly and soon closely resembled pure tungsten. Porous Ir and Ir alloys sinter more rapidly than tungsten. (See Tests 2a, 2b, 3, 7, 8, and 9.)

Rhenium. - Rhenium has a higher work function than tungsten, but it alloys and therefore rapidly depletes itself if a small quantity is placed on the surface. The resulting alloy behaves very much like tungsten but has a work function up to 0.1 volts higher. (See Tests 6 and 11.)

Tantalum. - The cesium neutral fraction from a porous tungsten surface on which tantalum has been deposited by sputtering is shown in Figure 21. Neutrals are higher and the critical temperature knee is less sharp. Also, remnant oxygen produces a sloppy knee with a higher critical

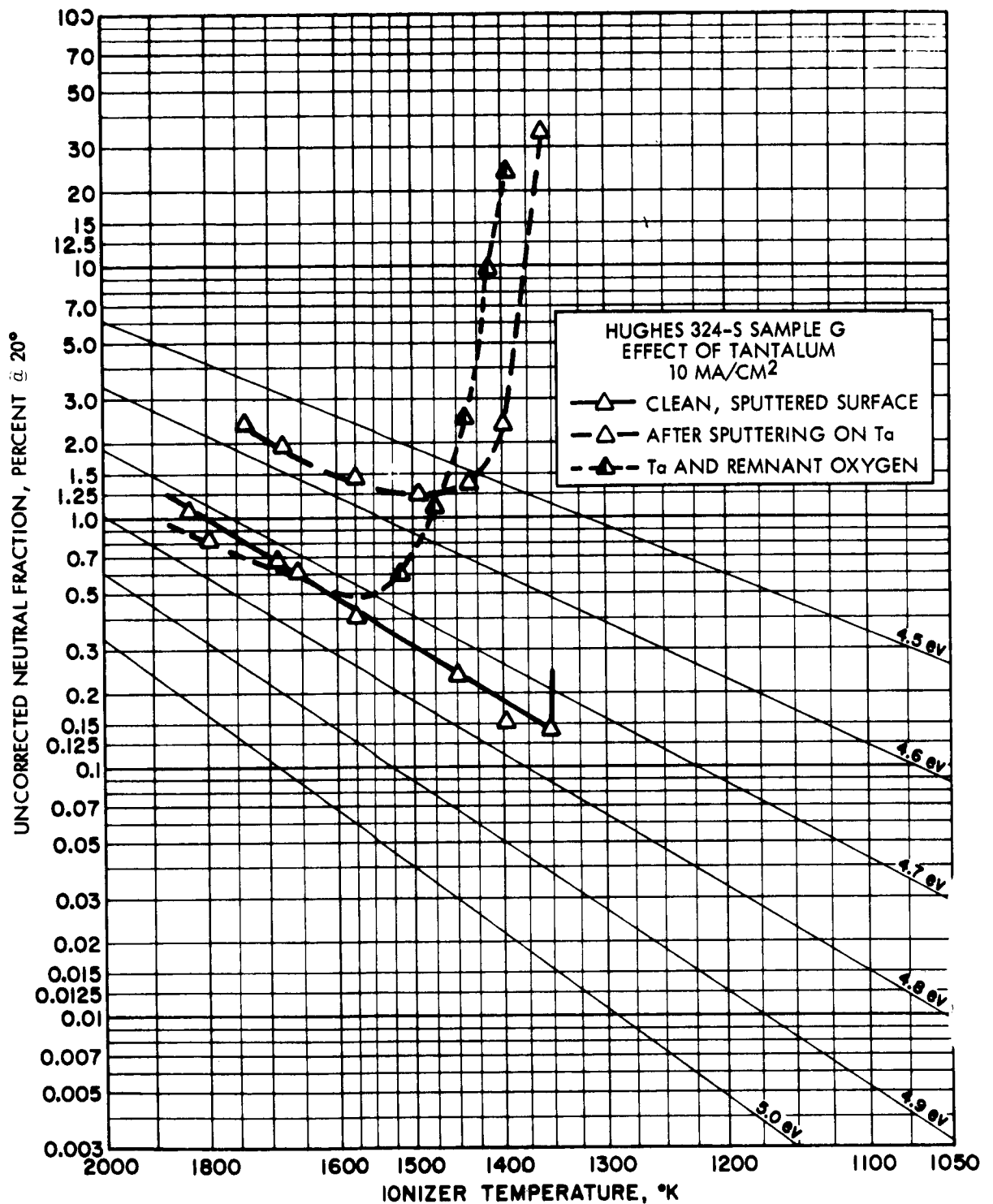


Figure 21. Uncorrected neutral fraction from Hughes 324-S Sample G at 20° from normal vs ionizer temperature showing the effect of sputtered tantalum at 10 ma/cm².

temperature and results in low neutral fractions occurring only at quite a high temperature. Remnant oxygen cannot be removed by cracking carbon on the surface. Tantalum diffused little: small doses gave a large effect, and the bulk of the tantalum could be removed readily by sputtering. However, some evidence exists that small traces of tantalum (probably associated with carbon or oxygen) can produce very much worse effects than a fair fraction of tantalum. The characteristics of remnant Ta are a low neutral fraction but very high critical temperatures.

Niobium. - The main effect of a niobium surface can be seen in Figure 22. The addition of Nb decreases the work function and hence increases the neutrals. Also, the critical temperature is lower and the knee is not so sharp. A small amount of exposure suffices to produce large effect. A small dilution of the effect occurs after initial exposure, implying diffusion of Nb into the interior, and more doses have to be applied to produce the maximum effect. However, the material diffused very much less than some materials tested (e.g., molybdenum), and hence most could be removed by short periods of sputtering, although small amounts remained even after quite extensive sputtering. This behavior can be seen from the dotted curve. Tantalum and niobium are very similar in behavior as would be expected from their chemical similarity.

Molybdenum. - When molybdenum was sputtered onto clean porous tungsten that had been prepared and studied as a control, the neutrals increased by a factor of 2, indicating a slightly lower work function of the resulting alloy (less than 0.2 volt). The following observations all imply rapid diffusion over grain surfaces and alloying: the surface appeared stable and was not altered by the addition of more Mo; the work function of Mo itself was never observed; and lengthy sputtering was required to remove this alloy.

Rhodium. - The initial effect of sputtering Rh on the clean, sputtered surface was to raise its work function by approximately 0.08 volt. However,

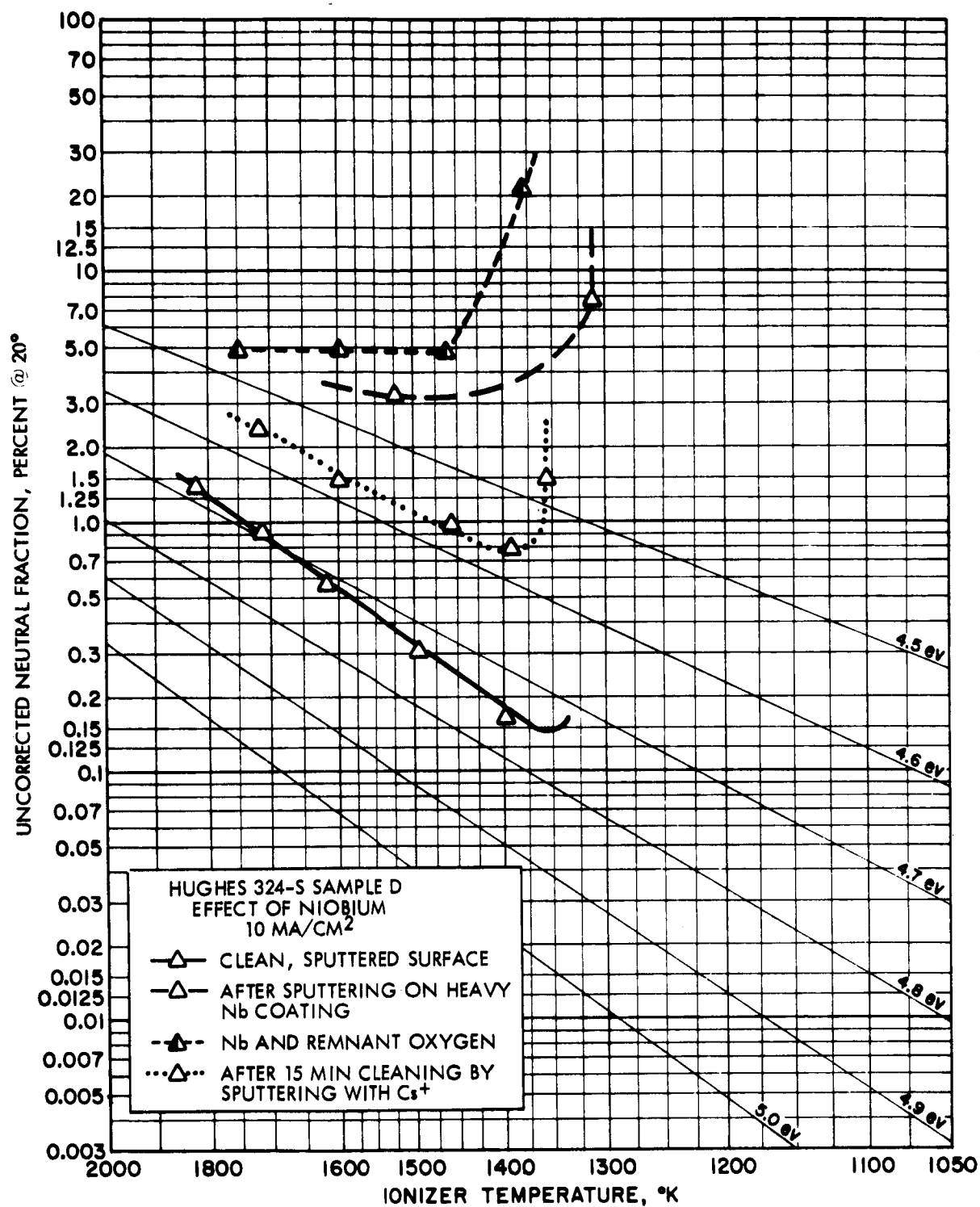


Figure 22. Uncorrected neutral fraction from Hughes 324-S Sample D at 20° from the normal vs ionizer temperature showing the effect of sputtered niobium at 10 ma/cm².

after more exposure and short periods of high-temperature operation, the neutral efflux increased by more than a factor 10. The criticals were elevated and the curve shape was very rounded. Under these conditions the neutral efflux increased 10 times when the current density was increased from 2 to 10 ma/cm², indicating pore blockage. It was possible to recover the original surface by heavy cleansing sputtering with Cs ions. We conclude that although a Rh surface coverage raises the work function slightly, Rh easily diffuses into the ionizer and dramatically enhances further sintering.

Platinum. - Evidence of a sintering effect of platinum on porous tungsten is shown in Figure 23. A brief lowering of neutrals and an increase in critical temperature due to high work function was seen, but soon the operation deteriorated. (The increase of neutral fraction with lowering temperature and increasing current density is typical of surface closure.) These results were expected in view of experiences of others as described verbally to present experimenters. Also, the similarity of platinum to rhodium, except for a lower melting point, heightened this expectation.

Metallographic examination of the porous sample on which platinum had been sputtered showed a thin layer of solid platinum-bearing metal on the surface — not a deep diffuse region of further sintering. However, these metallographic conclusions have not been substantiated by repeated test and are considered somewhat suspect.

Silicon. - The attractiveness of silicon as an accelerator grid material and the encouraging results obtained in earlier tests prompted repeated careful tests of the effects of silicon. Since three tests gave almost the exact results, there is no doubt that the tungsten silicide surface is an ideal ion emitter — quite similar in nature to tungsten carbide. Both neutral efflux and critical temperature are low. Figure 24 shows the very superior low-current-density results obtained with tungsten silicide. The sequence of testing indicated in Figure 24 was adopted in the

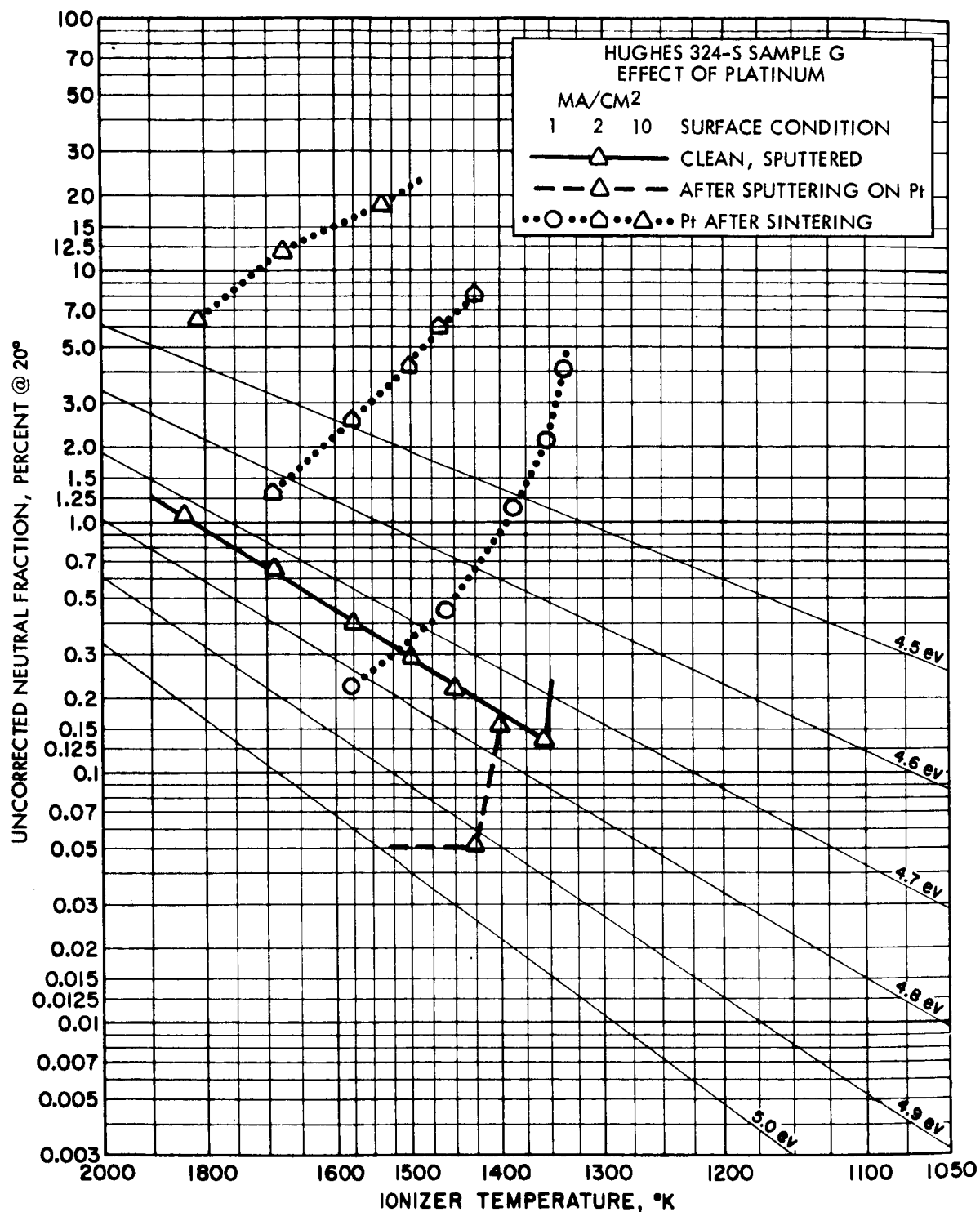


Figure 23. Uncorrected neutral fraction from Hughes 324-S Sample G at 20° from the ionizer vs ionizer temperature showing the effect of sputtered platinum at various current densities.

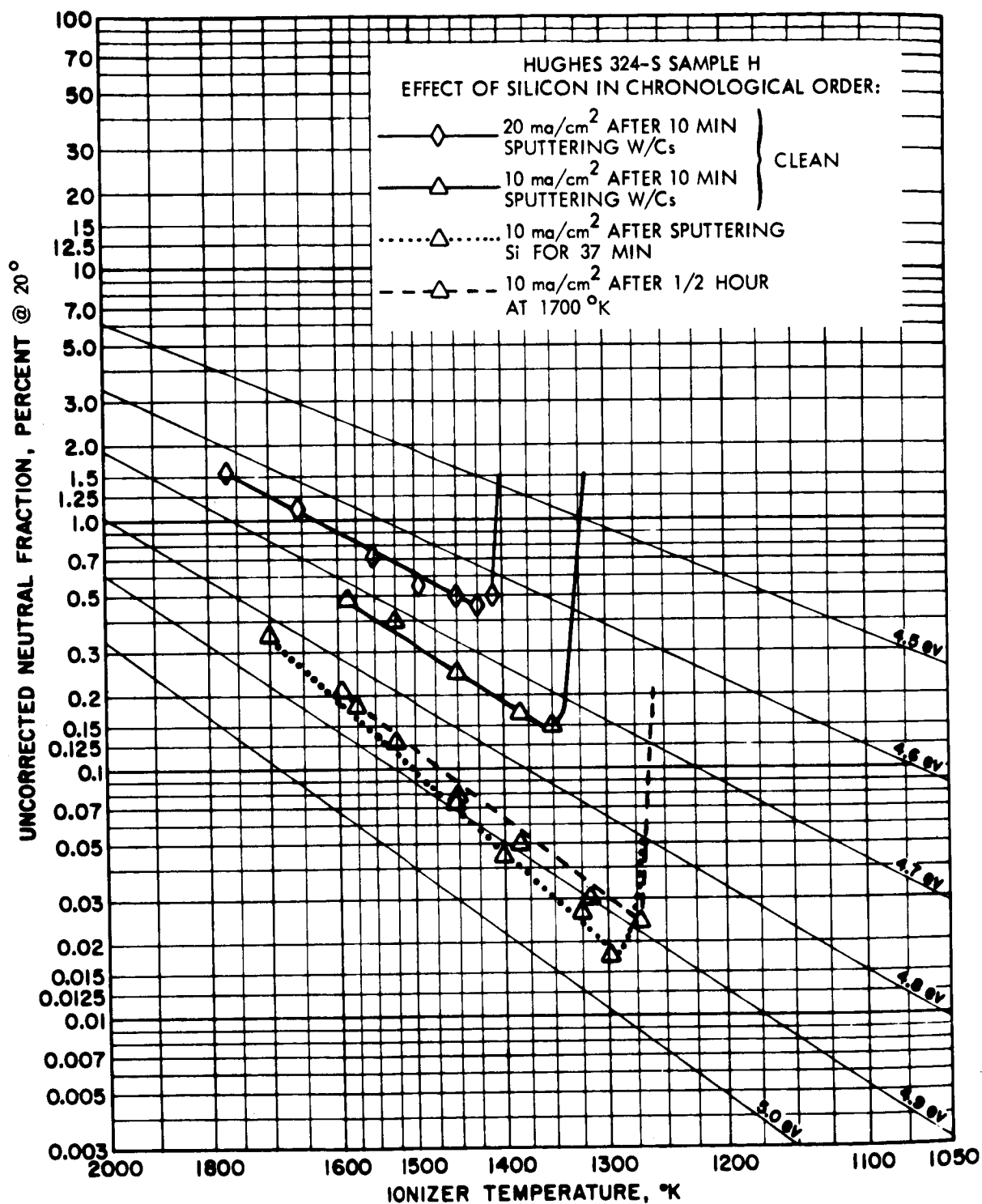


Figure 24. Uncorrected neutral fraction from Hughes 324-S Sample H at 20° from the normal vs ionizer temperature showing the effect of sputtered silicon at 10 ma/cm^2 .

hope of showing that if the silicon is deposited on a very hot surface, less will accumulated and no molten phase will form. The tests showed that high-temperature operation does not prevent silicon from being deposited nor does it remove the silicon. After more silicon was deposited at lower temperature and the emitter then operated at high temperature, the sample become solid and had zero transmittivity, an effect that started to occur in the previous test. Because of a strong correlation between the rapidity of this solidification and the melting point of silicon and tungsten silicide, it is suspected that a liquid might have been present throughout the porous tungsten, although the metallographic examination does not necessarily support this. The startling fact revealed by the microphotographs that were taken is that solid single crystals many times larger than the original grains of porous tungsten had grown, as can be seen in Figure 25.

These results and an unsuccessful attempt to measure the adsorption lifetime of silicon on tungsten makes us suspect that silicon rapidly forms a compound with tungsten and has a very low partial pressure of silicon in equilibrium with this surface. The experimental evidence for these assumptions is that we have never been able to detect silicon leaving a tungsten surface.

A summary of the data obtained from the current and past contaminate and desorption studies is presented in Table I.



Figure 25. Photomicrograph at 1000X of center of cross section of Hughes 324-S Sample H, which received a total of 70 minutes of sputtering with silicon. The material is virtually solid.

TABLE I. Properties of Studied Contaminants on Porous Tungsten

Contaminant	Lifetime τ , sec	Diffusion	Effect on Neutral Efflux	Effect on Critical Temp.	Remarks
Aluminum	$\theta \approx 0, 170$ $\theta \approx 1, 8$	Solid: none Porous: Surface dif. observed	$\sim 3X$ increase	Slightly higher	Little effect from trace amounts. Oxygen has little effect. Carbiding raises Al tolerance $\sim 300X$.
Beryllium	$\theta \approx 0, 0.3$ $\theta \approx 1, 0.04$	None observed	Increased \dagger	No effect Lower \dagger in presence of O_2	Sticking probability varies w/ θ , strongly w/ O_2 present. Oxygen increases $\tau \sim 10^4X$.
Boron			No effect $\dagger\dagger$	No effect $\dagger\dagger$	
Calcium		Yes (surface)	Very high to moderate depending on coverage	High temp. required to reduce θ	Very bad poison
Carbon	∞	Rapid	Lower when carbide is formed; higher when graphite is formed	Lower	Combines readily w/ adsorbed oxygen to form volatile CO.
Chlorine	Very short		No effect $\dagger\dagger$	No effect $\dagger\dagger$	Metals may be evaporated onto the sample as a chloride.
Chromium	$\theta \approx 0, 3$ $\theta \approx 0, 0.09$	Yes	Increased	No effect	Oxygen decreases τ slightly. Trace O_2 raises crit, lowers neut. Trace amounts, difficult to remove, effect ionization.
Copper	$\theta \approx 0, 0.02$ $\theta \approx 1, 0.02$	None observed	No effect $\dagger\dagger$	No effect $\dagger\dagger$	Oxygen increases $\tau \approx 2X$.
Fluorine			Decrease	Increase	Similar to effects of oxygen, but less tightly bound.

\dagger Desorption time from polycrystalline tungsten at $1500^\circ K$ and coverage θ . ($\theta = 1$ is one monolayer.) From Reference 2.

\dagger May have resulted from additional unknown contaminant.

$\dagger\dagger$ After exposure.

TABLE I. Contd. Properties of Studied Contaminants on Porous Tungsten

Contaminant	Lifetime [†] τ , sec	Diffusion	Effect on Neutral Efflux	Effect on Critical Temp.	Remarks
Iridium (sputtered)			Lowers $\sim(1/2)X$ from 10-40 ma/cm ²	Slightly higher	Improvement completely gone after ~ 1 hr at 1750°K.
Iridium ($\sim 1\mu$ chem. coating)		Uncertain	Lower than polished surface below 15 ma/cm ² ; \sim same above. (1/3)X lower than sputtered surface at all J_+ .	Slightly lower than sputtered surface; slightly higher than polished surface.	Oxygen adheres tenaciously producing poor results. 16 hrs operation and/or O ₂ eliminated improvement on sputtered surface.
Iridium (50% bulk alloy)			Very high at 5 ma/cm ² and above	High	Results probably reflected poor ionizer fabrication. Oxygen produces very poor curve shape and higher "criticals".
Iridium (100%)			Neut. \sim same as high quality porous W ₂ above ~ 1 ma/cm ²	Very high	Ionizer sintered closed after $\sim 1/2$ hr. at 1800°K. Results probably reflected poor ionizer fabrication.
Iron	$\theta \approx 0, 0.7$ $\theta \approx 0, 0.2$	None observed	No effect ^{††}	No effect ^{††}	Oxygen decreases τ slightly.
Molybdenum			$\sim 2X$ increase	No effect	Evidence of rapid alloying w/ W.
Nickel	$\theta \approx 0, 0.9$ $\theta \approx 1, 0.2$	None observed	No effect ^{††}	No effect ^{††}	Oxygen decrease $\tau \sim 10X$.
Oxygen	$\theta \approx 0, \infty$	Mobile at high temp.	Drastic decrease due to high ϕ	Usually increase	Trace amounts can increase neutrals

[†] Desorption time from polycrystalline tungsten at 1500°K and coverage θ . ($\theta = 1$ is one monolayer.) From Reference 2.

[‡] May have resulted from additional unknown contaminant.

^{††} After exposure.

TABLE I. Contd. Properties of Studied Contaminants on Porous Tungsten

Contaminant	Lifetime [†] τ , sec	Diffusion	Effect on Neutral Efflux	Effect on Critical Temp.	Remarks
Rhenium (sputtered on W-5% Re)			Slightly lower	No effect	$\sim 1.3\mu$ layer partially closed surface. Stable for at least surface several hours.
Rhenium (5% bulk alloy)			No effect	No effect	
Rhodium			Slight de- crease	No effect	Heavy application plus 1800°K produced severe surface sintering.
Silicon			$\sim (1/2) \times$ decrease	No effect	Suspect rapid alloying.
Tantalum (bulk; 2, 5, 10%)			Lower	High by >100°K	Has high affinity for oxygen.
Titanium	$\theta \approx 0, \sim 10^6$ $\theta \approx 1, \sim 20$	Yes	$\sim 10 \times$ increase	Little effect w/ low cover- age	Very bad poison.
Zirconium	$\sim \infty$	Yes	Very high	Little effect w/ low cover- age	Very bad poison.

[†] Desorption time from polycrystalline tungsten at 1500°K and coverage θ . ($\theta = 1$ is one monolayer.) From Reference 2.

[‡] May have resulted from additional unknown contaminant.

^{††} After exposure.

Ionizer Test Results

During the contract period 12 porous metal ionizer samples were tested to determine their ion and neutral cesium emission characteristics. Presentation and discussion of the data attained follows in chronological sequence.

Test 0: Astromet 10-1. — To verify that the new experimental configuration gave results consistent with those obtained in the past, the sample of Astromet 10-1 tested under previous contract (NAS 3-5254) was again tested. The results were in agreement with those previously obtained.

Test 1: Hughes 324-S Sample C. — In addition to being a test of this porous tungsten material, this test was to have served as a control for later tests of the material with thin coatings of Ir and Re on its surface. However, clean surface was never obtained because of the unfortunate choice of Ta to patch a break in the lip of the Mo plenum. Therefore Test No. 5 was made the control.

Test 2a: Hughes 324-S Light Ir Coating. — This sample, B, received a 0.5 to 1 micron thick chemical coating of Ir by Hughes Research Laboratories (H.R.L.) after it was brazed into the plenum at TRW Systems. According to a private communication with Frank Kavanagh and Tom Riley of NASA LeRc, the coating procedure consisted of dissolving 0.037 grams IrCl_3 in 1 ml H_2O and spraying this solution onto the sample while its temperature was 120°C . It was subjected six times to a wet hydrogen firing at 1000°C after each spray. Following the final spray it was held for 2 hours at 1500°C in dry hydrogen. Because of the thinness of this coating, no sputtering was done on its surface during the early part of the test.

At first the surface appeared quite contaminated, but after the ionizer was held at 1765°K for 1 hour, its performance improved dramatically. In the course of two days of operation the stable, reproducible curves presented in Figures 26 and 27 were obtained. The results were not influenced by short periods of operation at temperatures as high as 1875°K .

These curves were superior to any we had previously from either clean or carbided porous W. The critical temperatures were comparable to or lower than

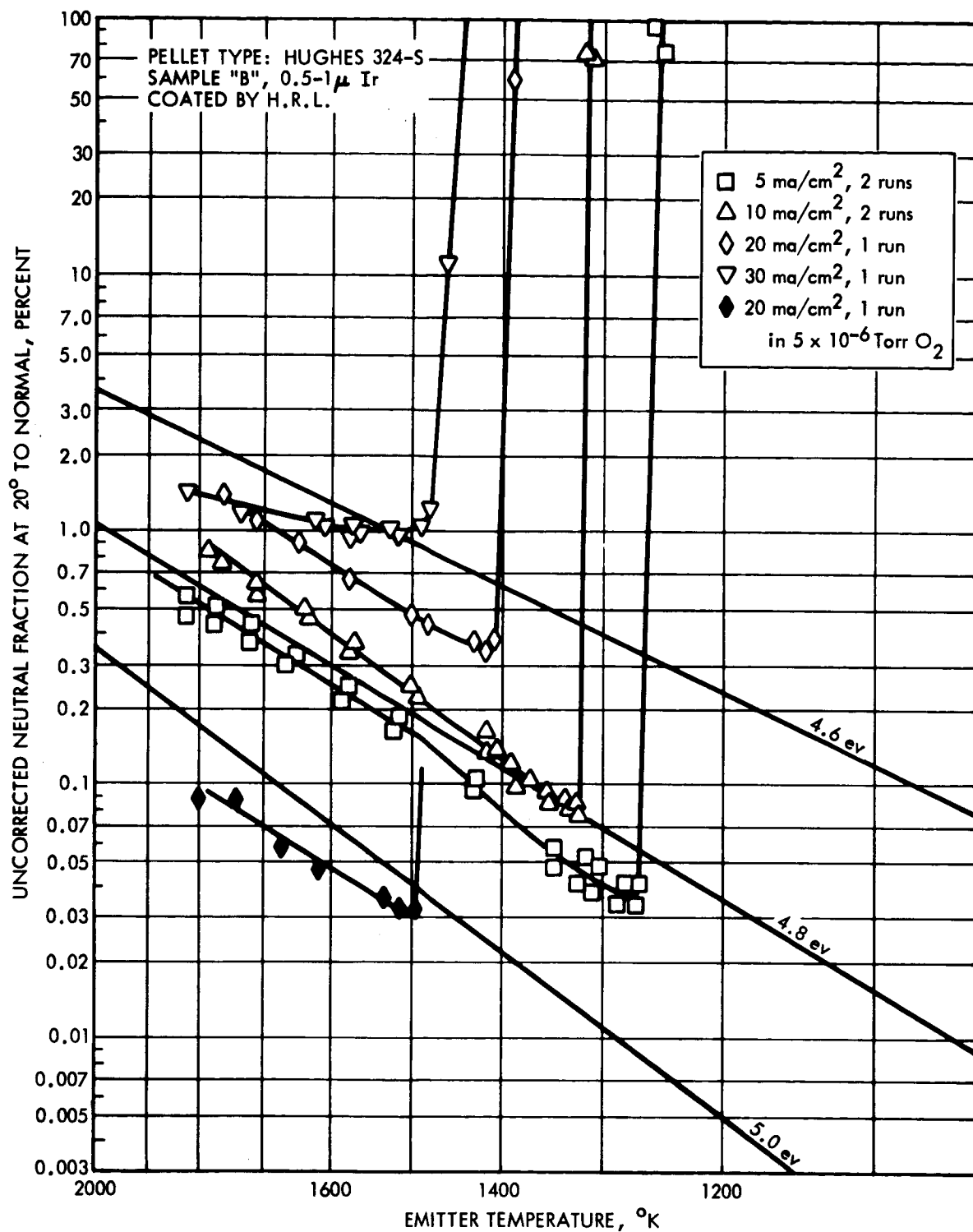


Figure 26. Uncorrected neutral fraction from Hughes 324-S Sample B (lightly coated with iridium) at 20° from normal vs ionizer temperature at various ion current densities before initial oxygen exposure.

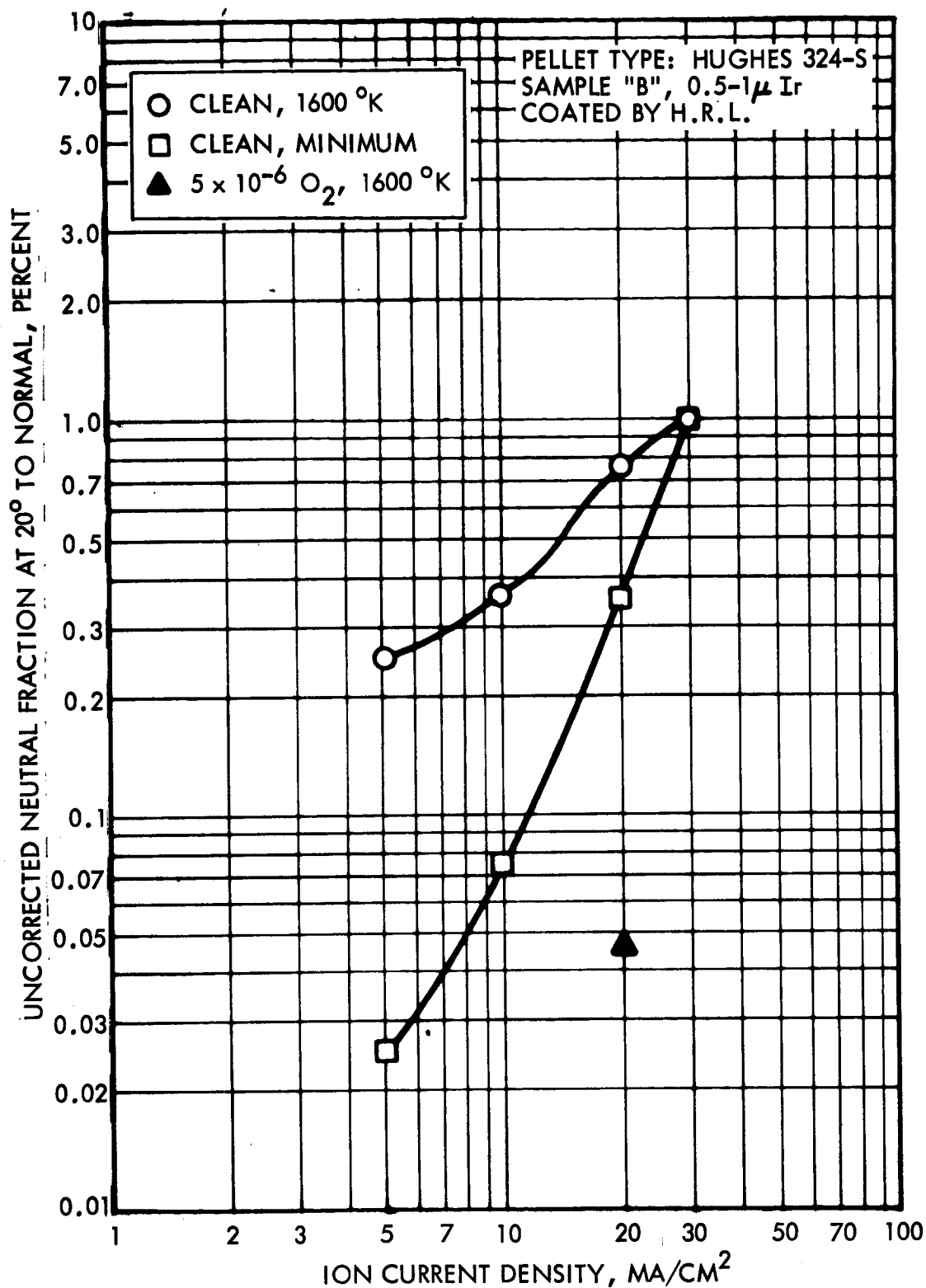


Figure 27. Uncorrected neutral fraction from Hughes 324-S Sample B at 20° from normal vs ion current density with clean and oxygenated surface at 1600°K. Also uncorrected minimum neutral fraction at 20° vs ion current density with clean surface.

the best previously tested ionizers. The critical knees are very sharp; we were unable to obtain data points between those shown near critical and those near 100-percent neutral efflux. The minimum neutral efflux at 20 ma/cm^2 was $1/3$ the minimum value of the best clean porous W ionizer previously tested, and was also better than those carbided surfaces that had been tested. (For comparison, refer to test number 9, 14, 19, 20, and 21 in the Summary Report of NAS3-5254.) Constant work function performance was obtained for all but the 30 ma/cm^2 curve. The curve taken immediately following the unoxygenated curve at this current density, is notable for its constant work function (a characteristic not usually observed with oxygenated ionizers), its sharp critical knee, and the low neutral fraction. We note that it is quite similar in appearance to the curve reported by Zimmerman and King (*) from a presumable uncontaminated Ir-coated ionizer operating at 7.5 ma/cm^2 . We also note that the critical temperatures obtained in our test are approximately 200°K lower than those reported by these investigators for some rear-fed Ir-coated samples(**).

Test 2b: Hughes 324-S Following Oxygenation.— After Sample B was exposed to oxygen for 10 minutes at 5×10^{-6} torr its original performance was never duplicated. For clarity the tests prior to the initial oxygen exposure are designated 2a while those following it are designated 2b.

After obtaining data at 20 ma/cm^2 in the presence of oxygen, an effort was made to desorb the oxygen by operation at 1750°K . After 2 hours at this temperature the neutral fraction vs ionizer temperature curve still clearly indicated the presence of remnant oxygen. A 1-minute sputtering of the surface with Cs ions at 5 kv produced no change.

(*) R. L. Zimmerman and J. J. King, "A Status REport on an Ion Engine Development Program," AIAA preprint 65-374, Figure 9

(**) Ibid., Figure 12.

However, a subsequent 10 minutes of 1850°K operation at the end of the day did increase the high temperature neutral efflux approximately 50 percent. Following our usual procedures, we shut down by first cooling the boiler and then turning off the ionizer heater and accelerating potentials. The LN₂ trap warmed up overnight.

The ionizer was started at 5 ma/cm² the following date; the surface provided the 5 ma/cm² curve shown in Figure 28. This curve was duplicated on several later dates but was never significantly improved. The critical temperature is approximately 15° higher and the minimum neutrals are 1.5 times higher than in Figure 26.

The 10 ma/cm² curve in Figure 28 was also obtained on this date; again the critical temperature is only slightly higher than in Test 2a but the minimum neutral fraction is 1.8 times higher. Equipment failure prevented obtaining the curve at 20 ma/cm², but a quick check of the critical temperature indicated a similar situation at this current density.

Following exposure to atmosphere, the ionizer behaved as though it were oxygenated again, an effect duplicated on several later occasions. Again slow and uncertain improvement was effected by operation above 1800°K.

It was later demonstrated that a much more rapid and certain technique for obtaining a clean surface was available. The surface of the sample was heavily oxygenated when work was begun. After improving the surface somewhat by high-temperature operation, C₂H₂ was admitted into the system. Ten minutes of operation at 3×10^{-6} torr produced a dramatic improvement in ionizer performance, which was stable the rest of the day with respect to both temperature and ion current density. The improvement resulted from cracking the hydrocarbon on the hot surface and removing the oxygen by the formation of CO. To demonstrate that the surface was not carbided, 5×10^{-6} torr of O₂ was admitted. In less than 2 minutes the neutrals suddenly dropped to 1/20 their previous value. At this time the O₂ was turned off. Within 10 minutes at 1610°K the clean surface was restored.

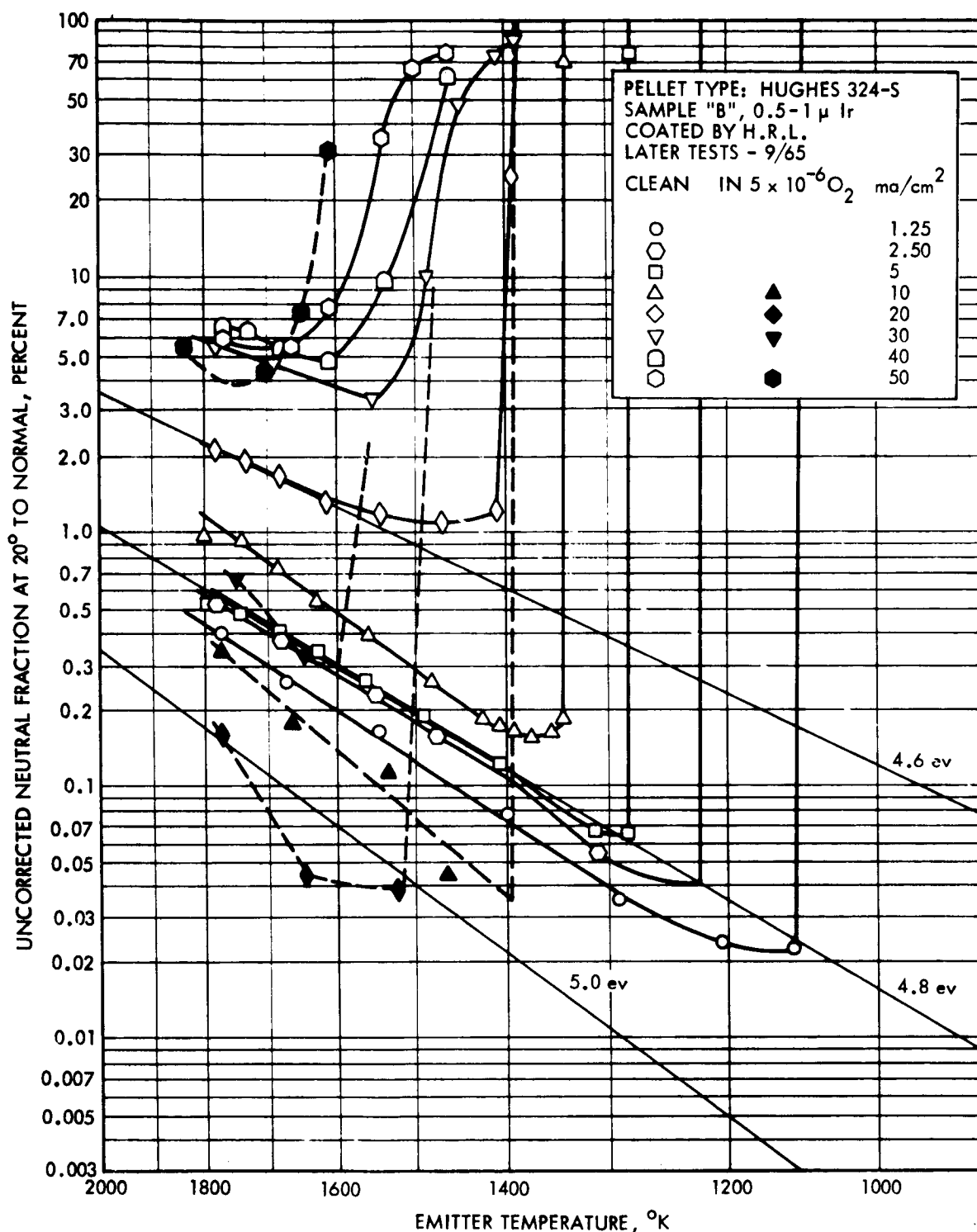


Figure 28. Uncorrected neutral fraction from Hughes 324-S sample B at 20° from normal vs ionizer temperature for various ion current densities and surface conditions. The data were obtained subsequent to the initial exposure of ionizer to O_2 .

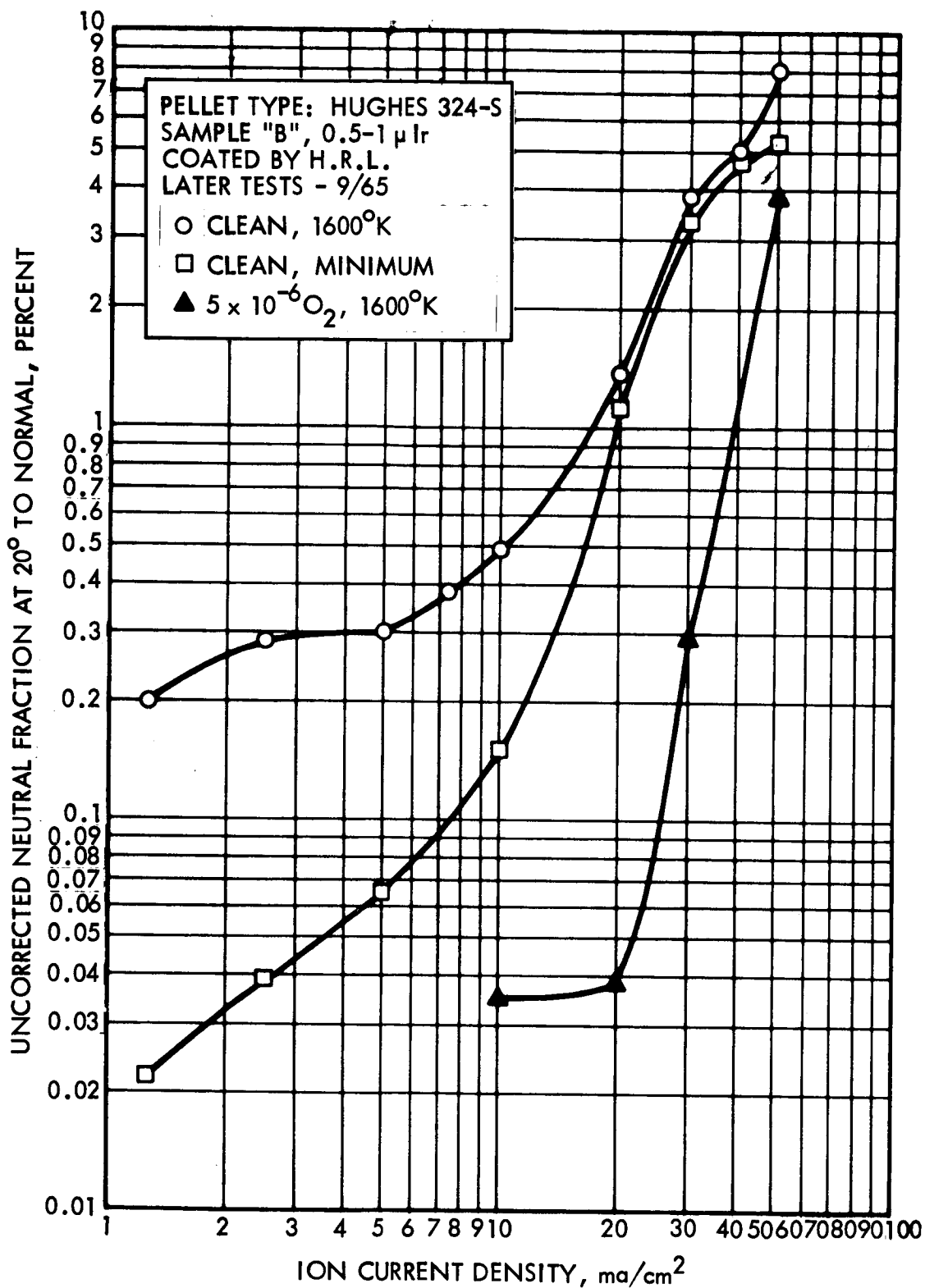


Figure 29. Uncorrected neutral fraction from Hughes 324-S sample B vs ion current density with clean surface at 1600°K, oxygenated surface at 1600°K. Also minimum neutral fraction vs ion current density with clean surface.

The curves obtained at 5 and 10 ma/cm² by cleaning with C₂H₂ matched those of Figure 28 very well except that the 10 ma/cm² had a uniform work function (instead of the gradually changing work function of Figure 28), a sharper critical, and a minimum neutral fraction of 0.2 percent instead of 0.15 percent. The 20 ma/cm² curve of Figure 28 was obtained on this day. Its critical temperature is identical to that of Figure 26 but the curve shape is poorer, with a minimum neutral fraction three times the previous one. A similar comparison exists between the 30 ma/cm² in Tests 2a and 2b: a similar critical temperature and a minimum neutral fraction three times larger.

In summary, the performance of Hughes 324-S Sample B subsequent to its first exposure to oxygen while hot was similar to that of very good porous tungsten -- and, as will be seen in Test No. 5, to a heavily sputtered sample of this material. The critical temperatures of the sample were very close to those obtained prior to oxygen exposure, but the curve shapes were poorer and the minimum neutral fraction were two to three times higher than before the exposure.

Test 3: Hughes 324-S Heavy Ir Coating. -- This Sample A was coated with Ir in a manner similar to that used for Sample B with the exception that 0.073 gm of IrCl₃ were dissolved in 1 ml of H₂O and applied in four sprays by H.R.L. The resulting coating had an estimated thickness of 1 to 2 microns.

The initial performance of Hughes 324-S Sample A was much the same as that of Sample B. That is, the critical temperature at 6.6 ma/cm² was approximately 200°K higher than those achieved later, and the minimum neutral fraction was about 10 times higher. As with Sample B, slow and rather unsure improvement resulted from operating in excess of 1850°K for a few minutes. The competition between the rate of oxygen diffusing from the interior of the ionizer and its evaporation is seen as the explanation for this phenomenon. However, when C₂H₂ was admitted to the system at a pressure of approximately 5 x 10⁻⁶ torr for approximately 10 minutes, the performance of the ionizer improved dramatically and was good for the rest of the day. The data

obtained with this surface are shown in Figure 30 and 31. In general, the minimum neutral fraction is slightly higher than that of Test 2b below 10 ma/cm^2 and slightly higher than data of Test 2a above 10 ma/cm^2 . The critical temperatures are lower than for sample B. This was therefore a very high performance sample. The required boiler temperatures were substantially higher than normal, reflecting the poor transmittivity of this heavy Ir coating and, as was discovered later, the 40-percent coverage of the rear surface by braze run.

An interesting time sequence of the response of the surface to oxygen is presented in Figure 32. Here the clean-surface, 17 ma/cm^2 curve is labeled (1), the curve obtained in 5×10^{-6} torr of O_2 are labeled (2), the curve obtained approximately 1 minute after O_2 turn-off is labeled (4). Curve 2 is similar to those obtained in O_2 in the past, although the elevation of critical temperature is a little high. Curves 3 and 4 demonstrate that as the degree of surface oxygenation decreases, the ionizer performance first becomes extremely poor and then begins to improve. We have often observed a degradation in performance following O_2 turn-off, but changes of this magnitude have been observed only with this sample.

Test 4: Union Carbide ORGDP 4848-82-1. - When the Union Carbide sample was first placed in operation, its neutral fraction was extremely high. The neutral fraction decreased significantly after about 1 hour of operation at temperatures up to 1825°K . The stable clean conditions represented by the curves in Figures 33 and 34 were obtained by an additional 4 hours of operation and by increasing the current density to 20 ma/cm^2 . These curves exhibit minimum neutral fraction about twice as high as shown by Astromet 10-1 (Test 21 last year) and critical temperatures roughly 100°K higher than those of Astromet 10-1. (Astromet 10-1 is representative of high-performance clean porous tungsten.)

The large increase in cesium neutral fraction as the current density was increased beyond even 2 ma/cm^2 indicates poor pore count or distribution. The decreased neutrals and increased critical temperature obtained while operating in a pressure of oxygen and the degraded performance when traces of oxygen were present are characteristic.

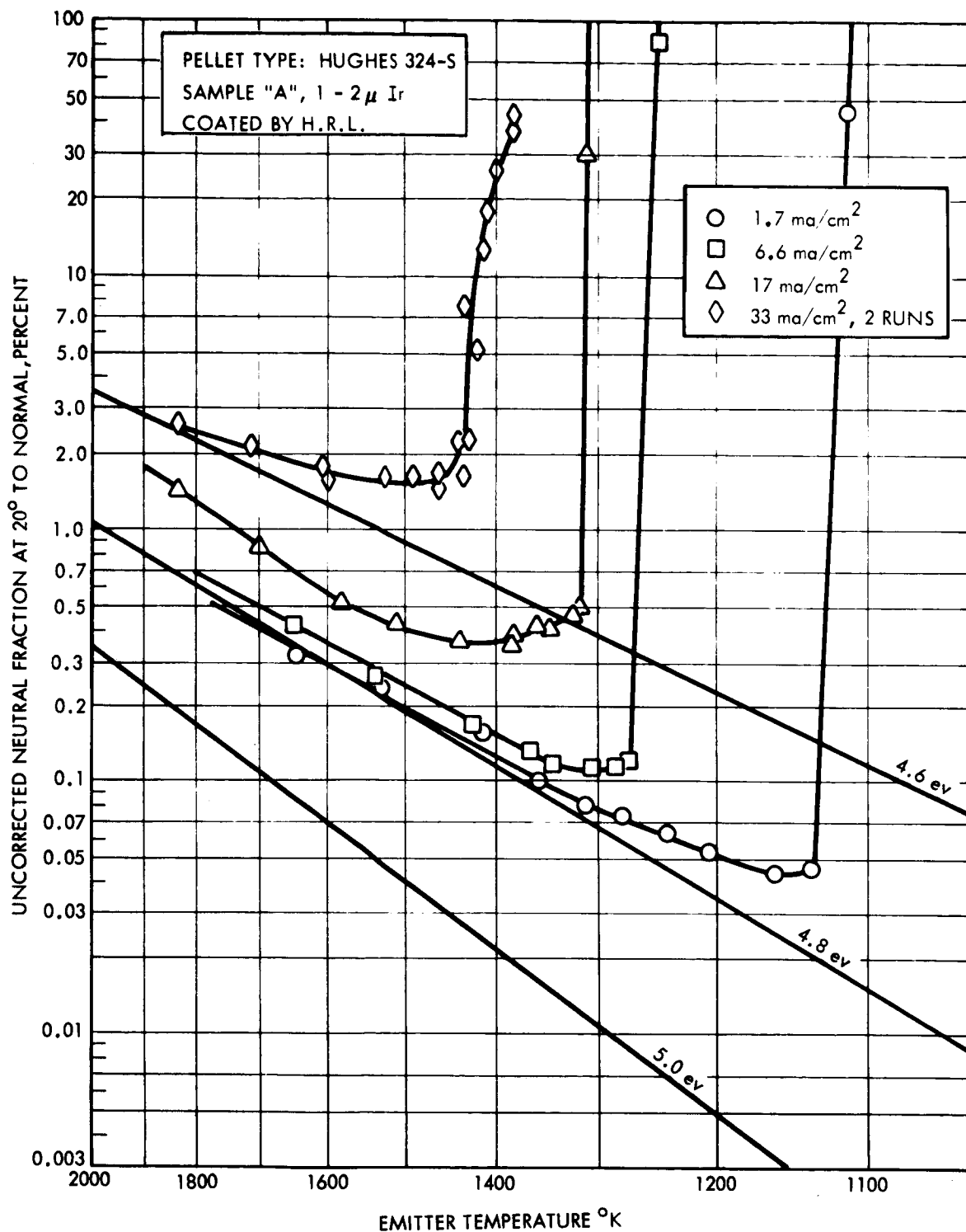


Figure 30. Uncorrected neutral fraction from Hughes 324-S Sample A at 20° from normal vs ionizer temperature for various ion current densities and surface conditions.

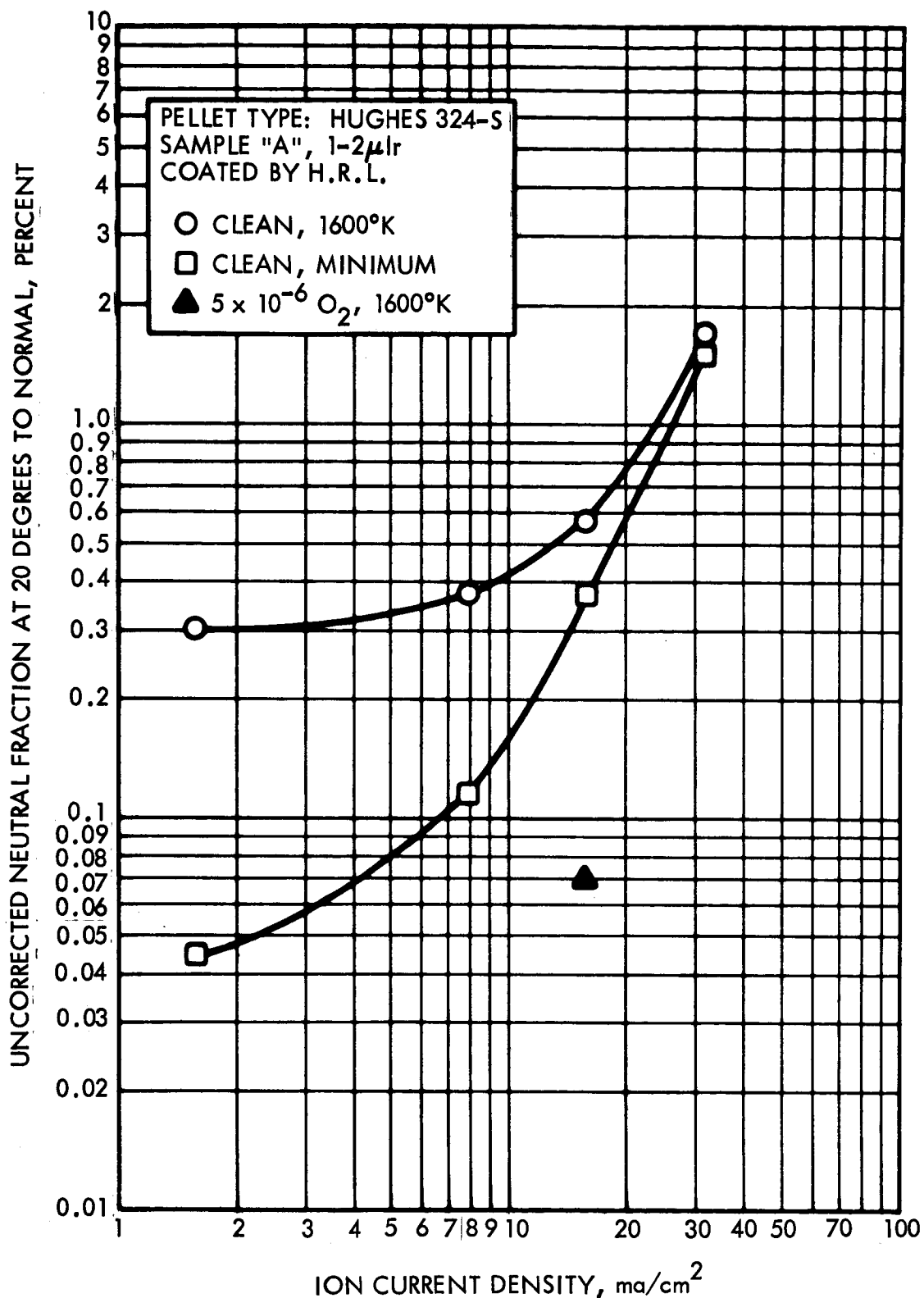


Figure 31. Uncorrected neutral fraction at 1600°K and minimum neutral fraction, both at 20° from normal vs ion current density from Hughes 324-S Sample A. Also neutral fraction from oxygenated surface at 1600°K.

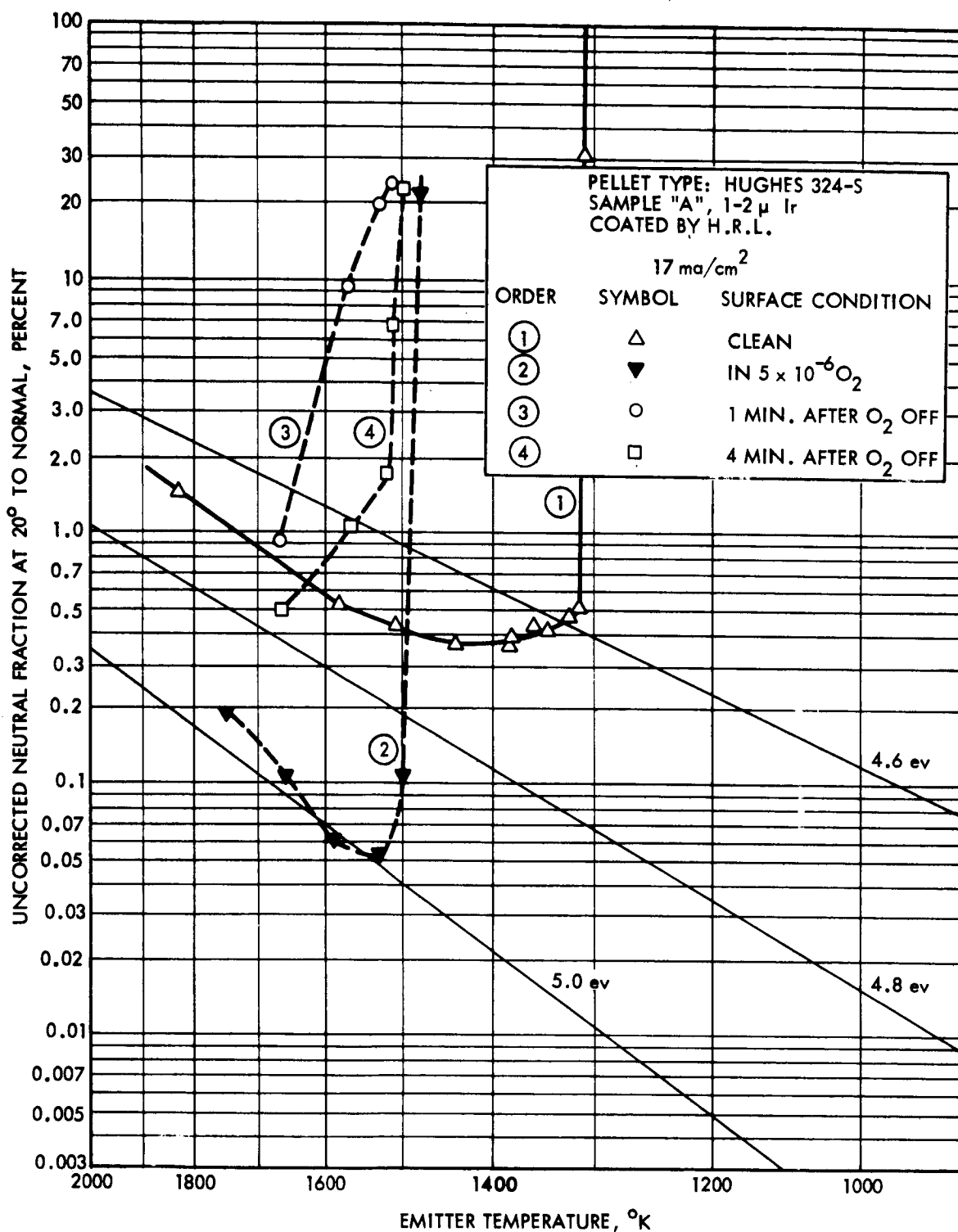


Figure 32. Uncorrected neutral fraction from Hughes 324-S Sample A at 20° from normal vs ionizer temperature at 17 ma/cm² for various surface conditions in time sequence.

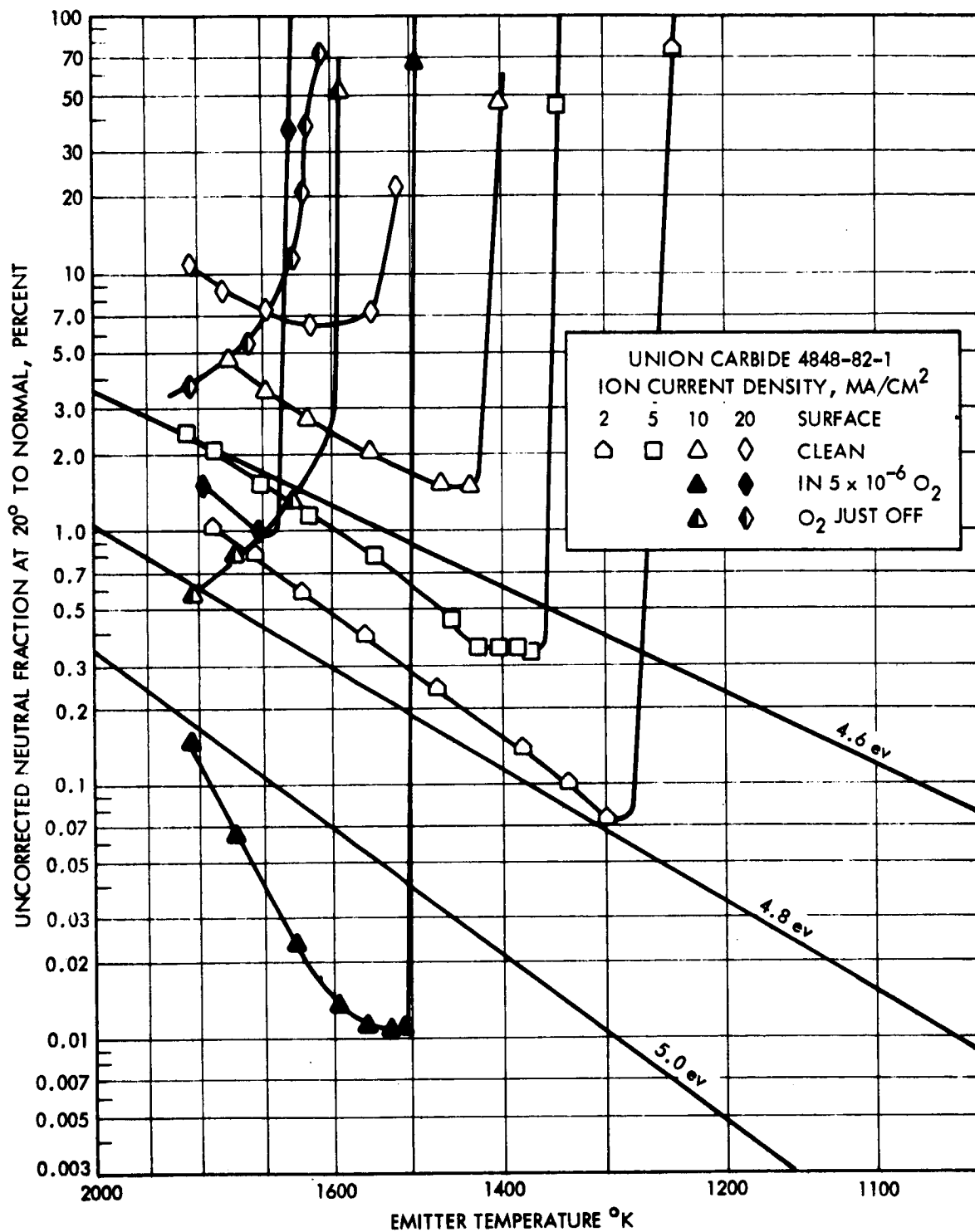


Figure 33. Uncorrected neutral fraction from Union Carbide 4848-82-1 at 20° from normal vs ionizer temperature for various ion current densities and surface conditions.

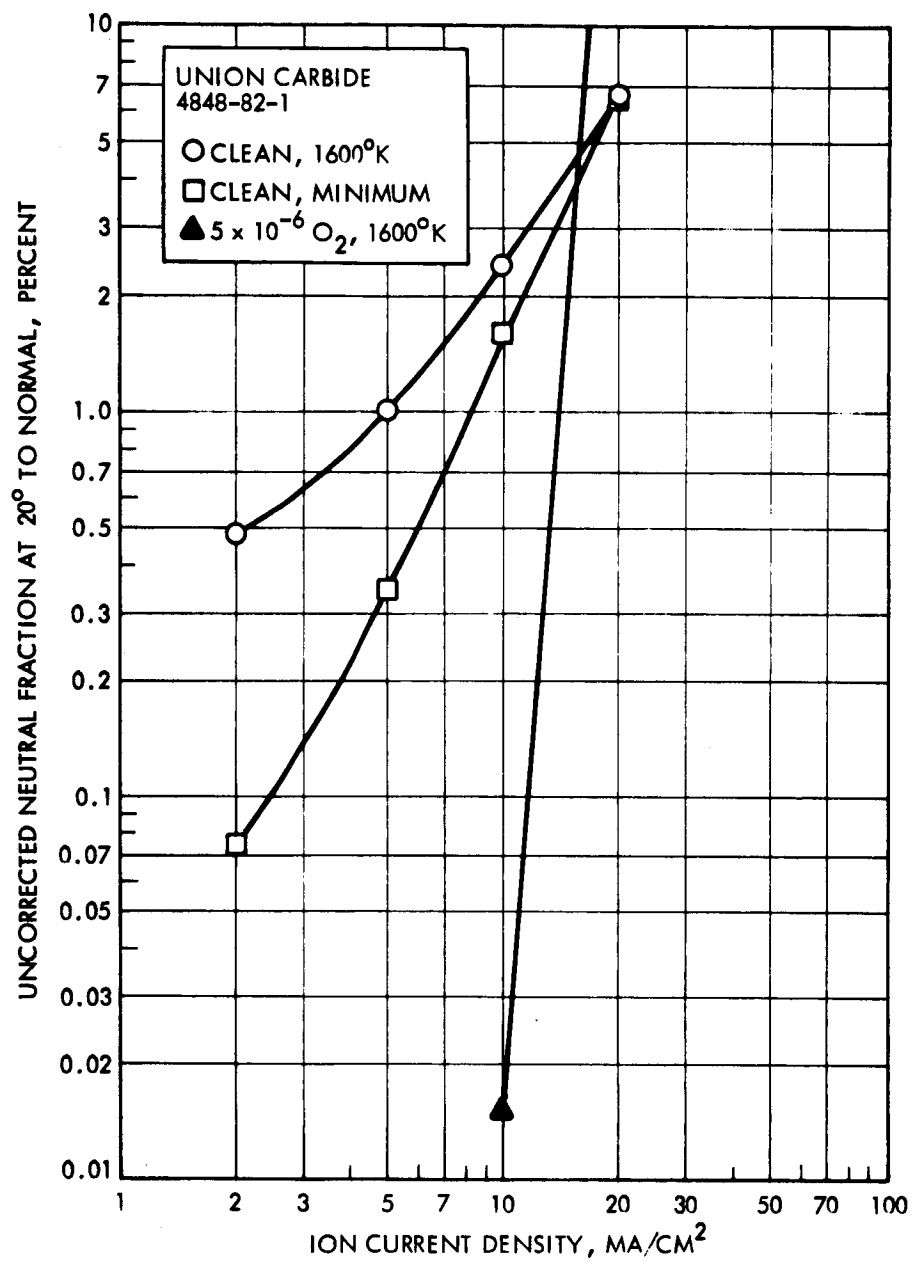


Figure 34. Uncorrected neutral fraction from Union Carbide 4848-82-1 ion current density with clean surface at 1600°K and oxygenated surface at 1600°K. Also minimum neutral fraction vs ion current density with clean surface.

The performance of this sample degraded further after a few days of operation. Metallographic examination revealed that both the front and back surfaces had many large voids, whereas the central portion was more uniformly dense -- possible a near-solid. There was also a fair amount of braze run on the rear surface. This further sintering could conceivably have been enhanced by the proximity of rhodium.

Test 5: Hughes 324-S Sample F. - This sample was intended as a control sample for the tests on Ir and Re-coated ionizers of the same material. (The original control sample, C, was not given a fair test, as discussed under Test 1.) The front surface of the Cu-infiltrated sample was metallurgically polished. Neither the front nor the back surface was etched. The curves shown in Figure 35 indicate very superior performance: both neutral fraction and critical temperature are low, and the degradation of performance with increasing current density is quite slow.

After these curves were obtained the surface was heavily sputtered with Cs ions. The performance was essentially the same at low current densities but poorer at high current density. This evidence tended to suggest that the polished surface was superior to the sputtered surface, but many later tests on this same material failed to support this contention. It is now felt that the polished surface had enough dissolved carbon in it from being brazed in an atmosphere containing a slight amount of hydrocarbon with the result that it was not bothered by oxygen. We have observed more recently effects of oxygen at high current densities related to the poorer vacuum caused by outgassing of parts under bombardment of the high power ion beam.

Tests of this sample in oxygen are shown in Figure 36. The lower current density curves show the usual beneficial effects of continuous oxygen pressure with the less beneficial effects of residual oxygen. The inverse relationship between the 50 ma/cm^2 and the 30 ma/cm^2 is strange. We tend to explain this effect by presuming that we did not have enough oxygen present for the 30 ma/cm^2 curve to represent the continuous oxygen situation and so measured a remnant oxygen curve. The observations that remnant oxygen effects are worse at the high current densities and that more oxygen is need-

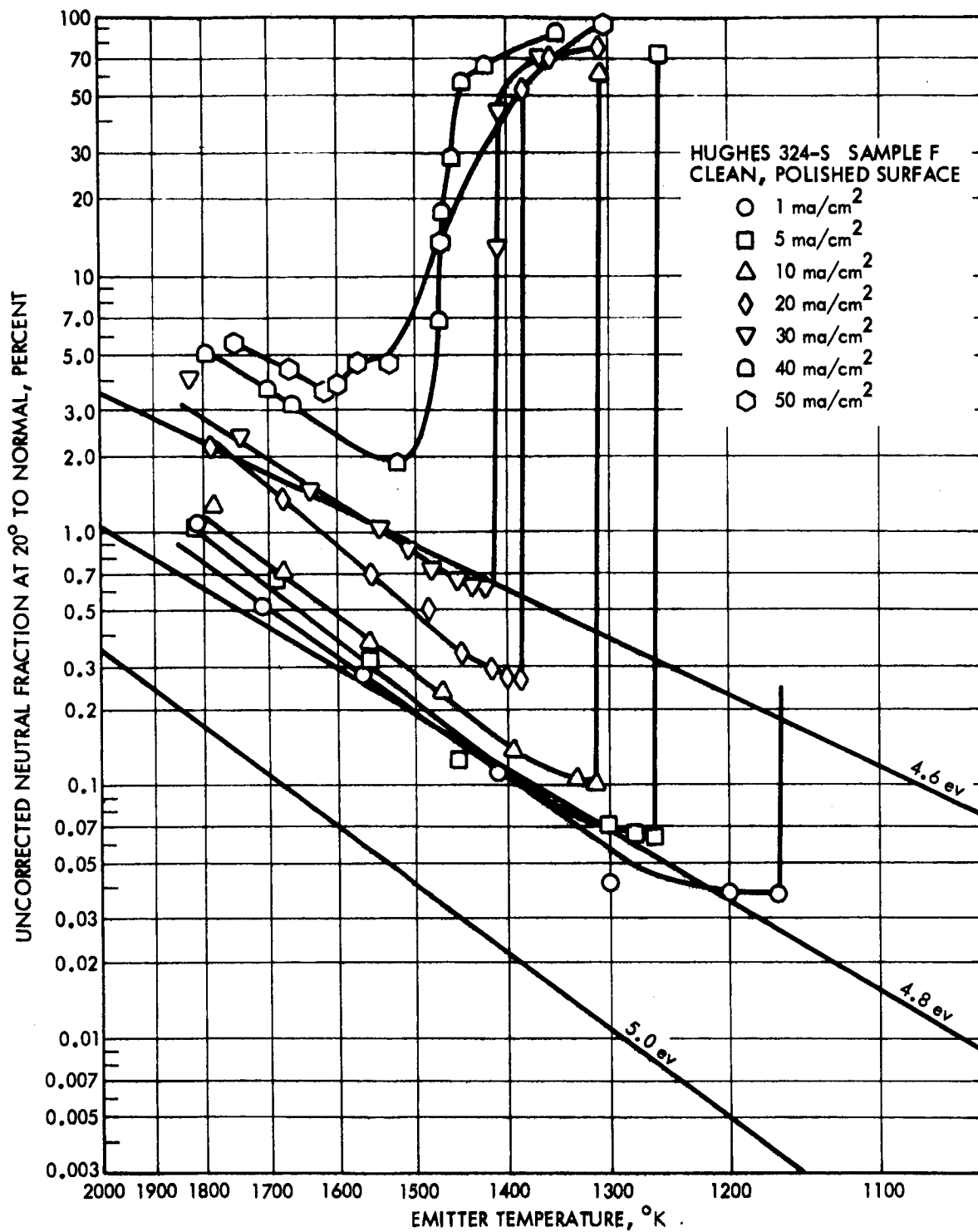


Figure 35. Uncorrected neutral fraction from clean, polished Hughes 324-S sample F vs temperature for various ion current densities.

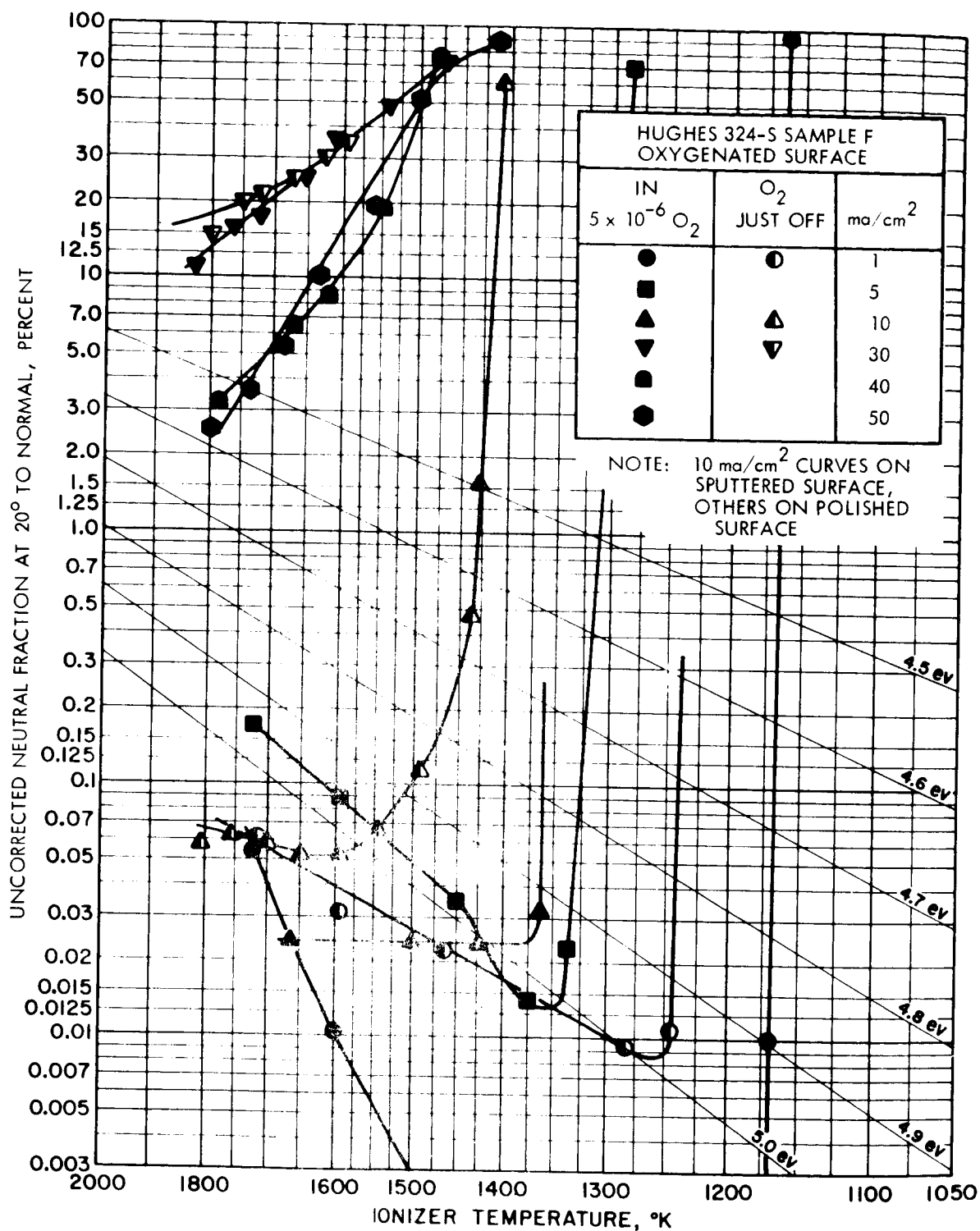


Figure 36. Uncorrected neutral fraction from heavily sputtered Hughes 324-S Sample F at 20° from normal vs temperature in the presence of 5×10^{-6} torr O₂ at various ion current densities.

ed at the higher current densities to produce low neutrals suggests that oxygen can be removed from the surface by large surface coverages of cesium. These observations also support the hypothesis that the cesium binding energy is higher on tungsten with a fractional monolayer coverage of oxygen than on tungsten with a complete monolayer coverage of oxygen.

The neutral fraction versus ion current density for both clean and oxygenated for this test is shown in Figure 37.

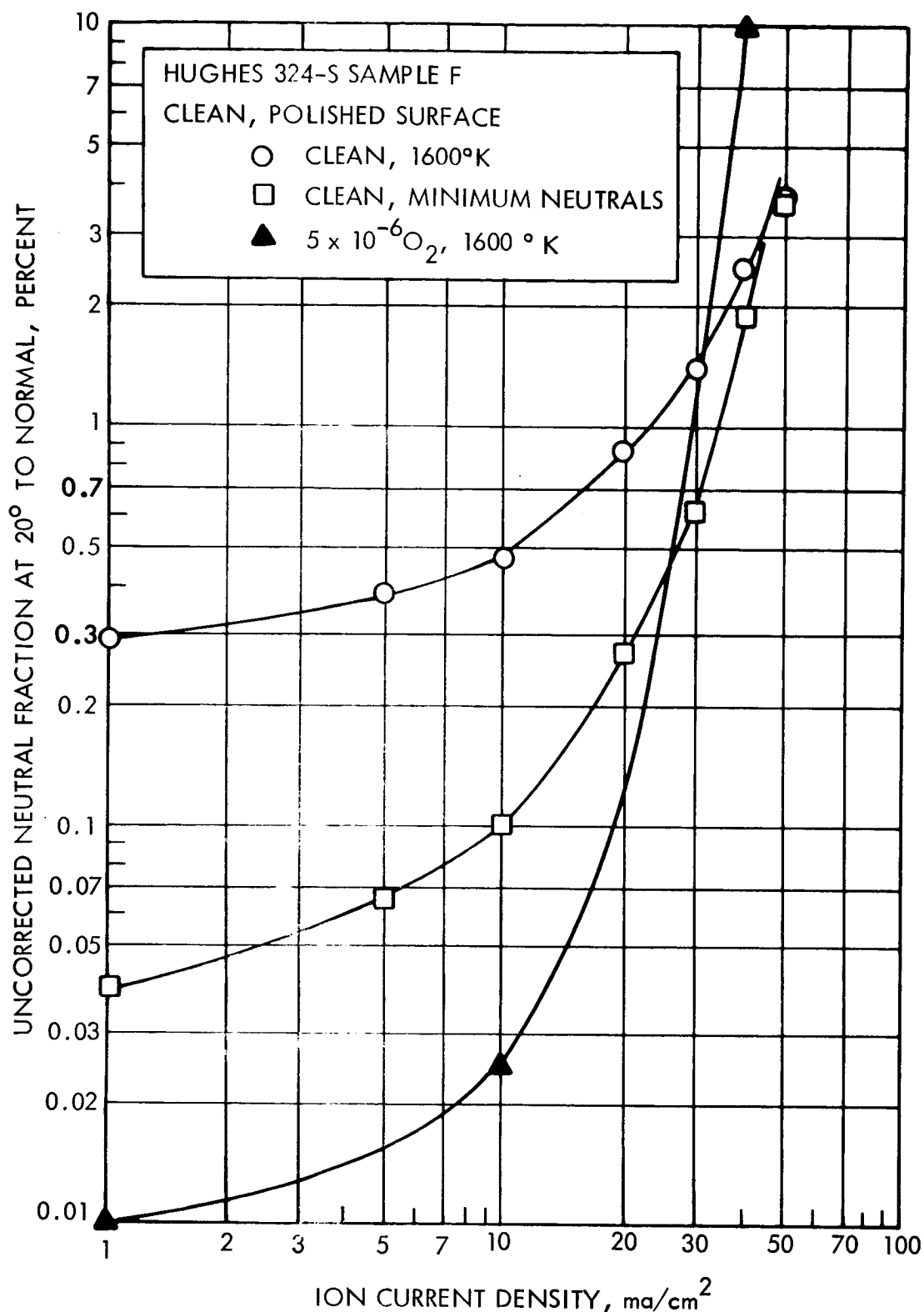


Figure 37 Uncorrected neutral fraction from Hughes 324-S Sample F at 20° from normal vs ion current density with clean, polished surface at 1600°K and oxygenated, sputtered surface at 1600°K. Also uncorrected minimum neutral fraction at 20° vs ion current density with clean, polished surface.

Test 6: TRW W-5% Re No. 2 Prealloyed - The performance of the ionizer when it was first placed in operation was characterized by a high critical temperature and very high neutral efflux. Some improvement was effected over a 2-hour period by operating at modest temperatures with occasional short periods at $\sim 1850^\circ\text{K}$ and a brief exposure to C_2H_2 . A significant improvement was effected at about 2 hours by a 1-minute sputtering with Cs ions. An additional 2-minutes of sputtering produced a surface which was reproduced several times on later dates. It is regarded as the clean surface and is presented in Figure 38. The performance indicated by these curves, though inferior to those obtained from clean Hughes 324-S, would have been regarded as quite good by last year's standards. One qualification is that the critical temperatures increase more rapidly with current density than is observed from high quality clean porous W.

One characteristic of almost all of the curves obtained on both the clean and the Re-sputtered surfaces is a decrease of apparent work function with increase in temperature above critical.

In Figure 39 are shown the curves taken in $5 \times 10^{-6} \text{ O}_2$ along with clean curves taken just before the O_2 was admitted at each current density. One curious effect is noted: above 20 ma/cm^2 the critical temperature is elevated by the presence of O_2 , whereas at and below 10 ma/cm^2 it is lowered. In the past we have observed O_2 to raise critical temperatures at all current densities on some samples, to lower critical temperatures at all current densities on some samples, and occasionally to have practically no effect. But only once during last year (Test 14 of EOS Bar, G-3) did we see critical elevation at high current densities and critical depression at low current densities as in Figure 39. Figure 40 shows α vs current density.

The neutral efflux vs angle measurement was made at 5 ma/cm^2 . A very good fit to the normalized line $f = 1 - \frac{\theta}{66^\circ}$ was obtained. A smaller correction to the neutral efflux data taken at 20° to the normal is implied for this sample than for previously measured samples.

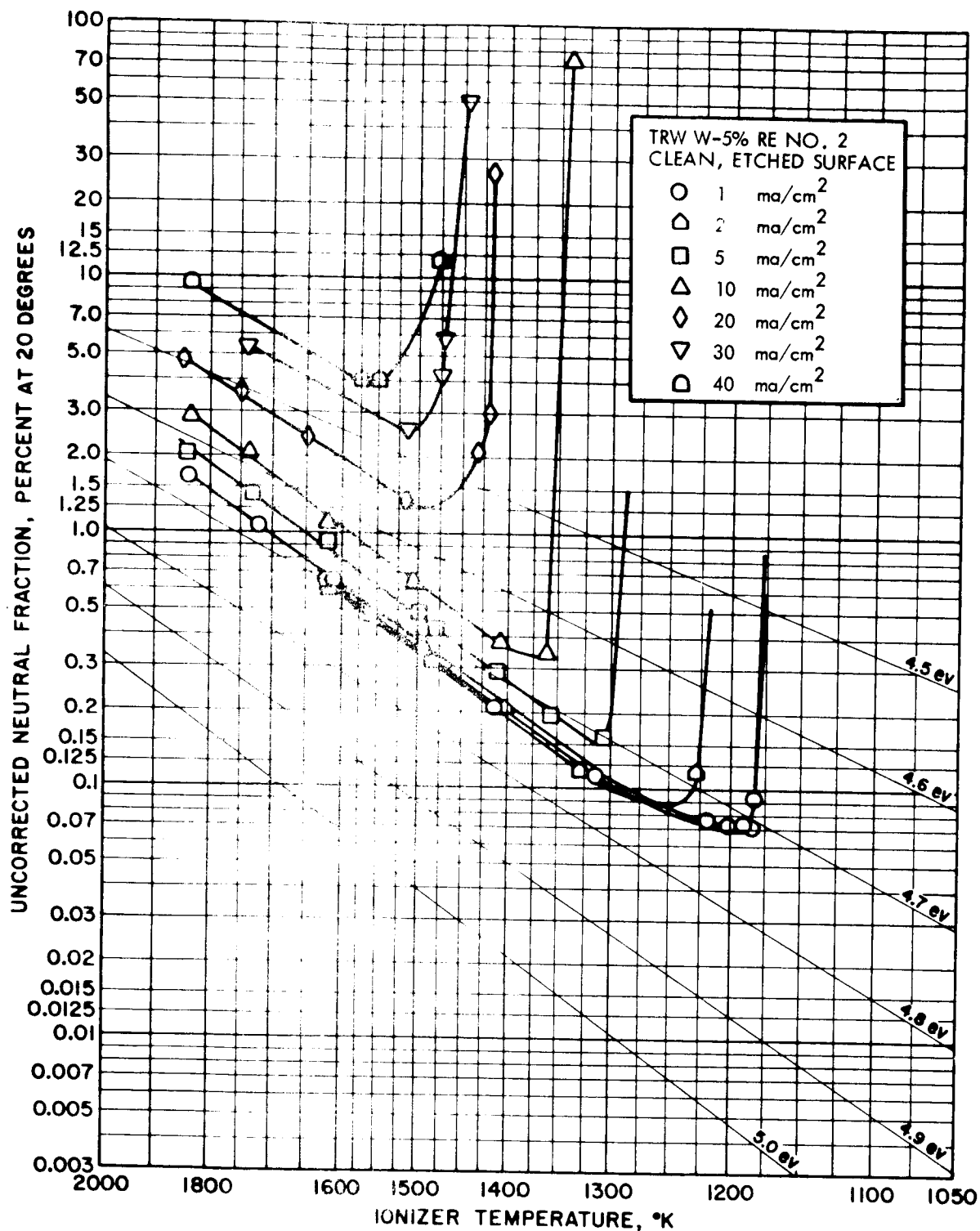


Figure 38. Uncorrected neutral fraction from clean TRW W-5% Re No. 2 pre-alloy at 20° from normal vs ionizer temperature for various ion current densities.

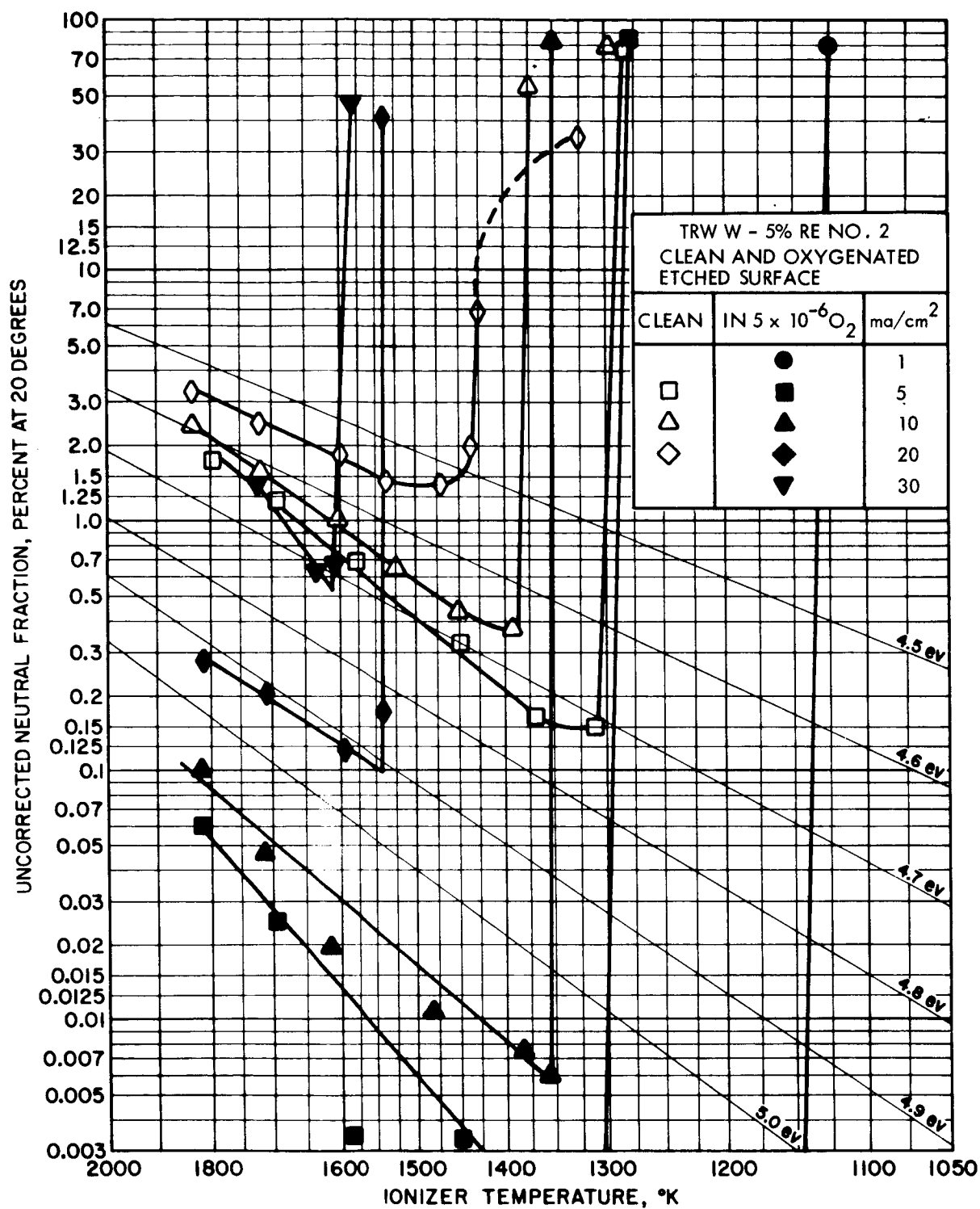


Figure 39. Uncorrected neutral fraction from TRW W-5% Re No. 2 pre-alloy at 20° from normal vs ionizer temperature for various ion current densities and surface conditions.

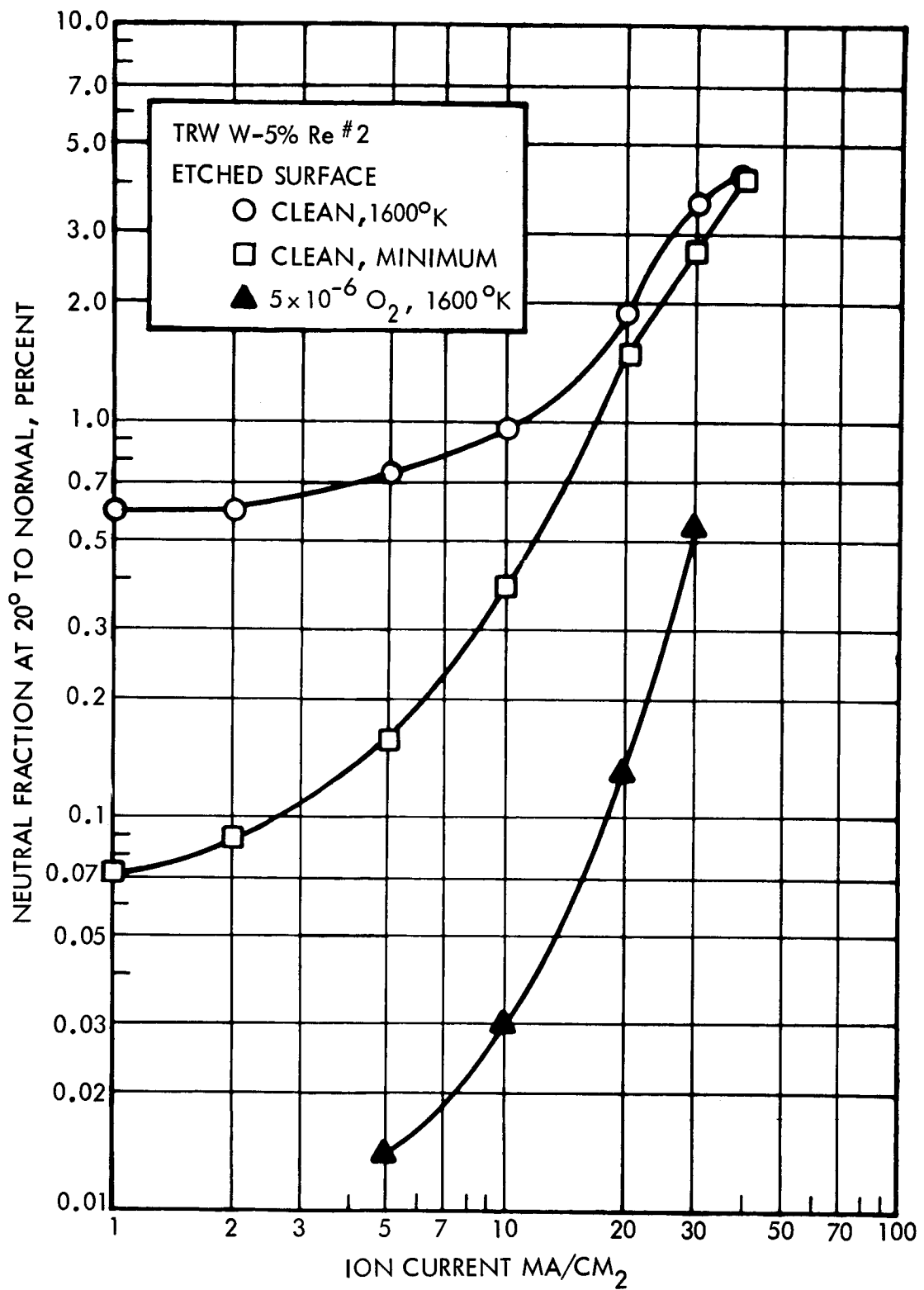


Figure 40. Uncorrected neutral fraction from TRW W-5% Re No. 2 pre-alloy at 20° from normal vs ion current density with clean surface at 1600°K and oxygenated surface at 1600°K. Also uncorrected minimum neutral fraction at 20° vs ion current density with clean surface.

To determine the effect of additional rhenium sputtered on to the surface, a sheet of Re was positioned over the ionizer operating at 10 ma/cm^2 . An estimated thickness of 1.3μ of Re was applied in this manner with three sputterings of equal length. As shown in Figure 41, at 10 ma/cm^2 the Re produced relatively little effect (and that effect was observed after the first sputtering). A more noticeable effect was observed at 1, 2, and 5 ma/cm^2 : the neutral fraction was reduced to that associated with an effective work function of 4.8 volts. In the clean surface data of Figure 38 this value was ~ 4.7 volts. On the other hand, the performance at 20 ma/cm^2 was degraded. We suspect that the additional Re did raise the work function of the surface ~ 0.1 volts but that the coating thickness, which is of the order of a pore diameter, closed the surface enough to compensate for the higher work function at 10 ma/cm^2 and that this closure overcompensated at the higher current densities.

Test 7: Hughes No. 276 W-50% Ir Prealloy. - The first sample prepared of this material had a crack (believed to have been present in the billet before machining) and also showed numerous pits after it was polished. Therefore, a second sample was prepared. This sample, like the first, was metallurgically polished while still infiltrated with silver and was then deinfiltreated. Many pits were visible in the polished and deinfiltreated material, as can be seen in Figure 42 (taken at 50X). Furthermore the deinfiltreated material was quite susceptible to being cracked, and the transmittivity of the sample was measured as 6.9×10^{-4} , which is five to ten times the value normally associated with high-quality porous W. The over-all impression, then, was that the sample had little structural integrity.

The 1000X photomicrograph of the polished surface in Figure 43 indicates a coarse pore distribution. Notice that the large solid areas between pores exhibit a hint of grain boundaries. Attempts to etch this surface with the usual solution of nitric and hydrofluoric acids did not

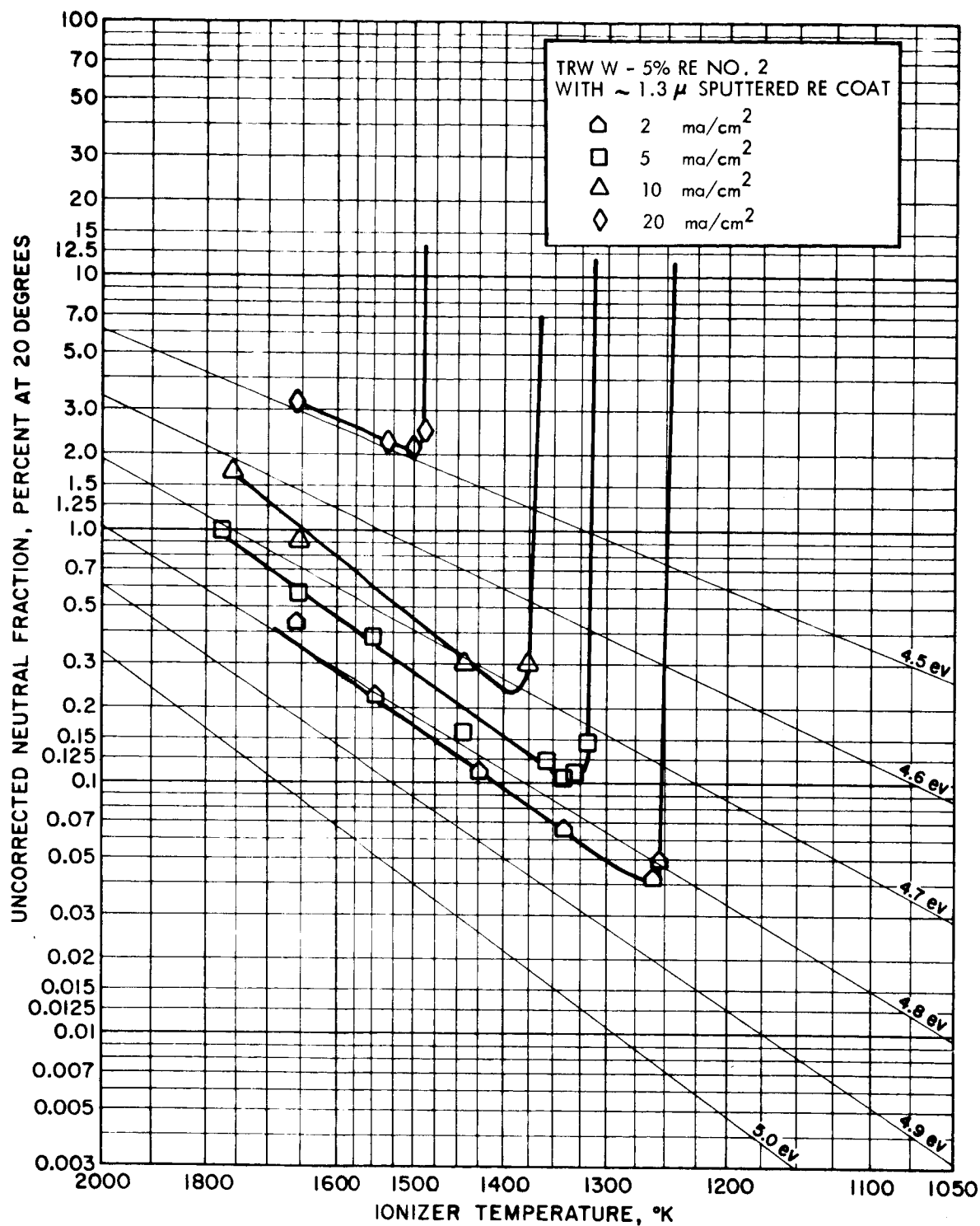


Figure 41. Uncorrected neutral fraction from TRW W-5% Re No. 2 pre-alloyed with $\sim 1.3 \mu$ Re coating at 20° from normal vs ionizer temperature at various ion current densities.

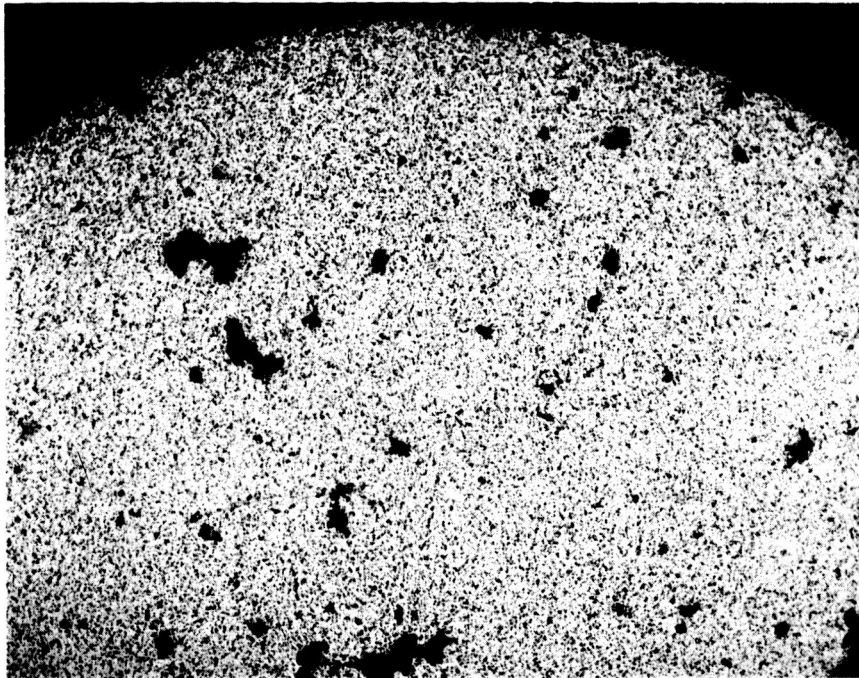


Figure 42. Photomicrograph of Hughes No. 276 W-50% Ir Prealloy, polished surface at 50X, showing large pits and coarse pore structure.

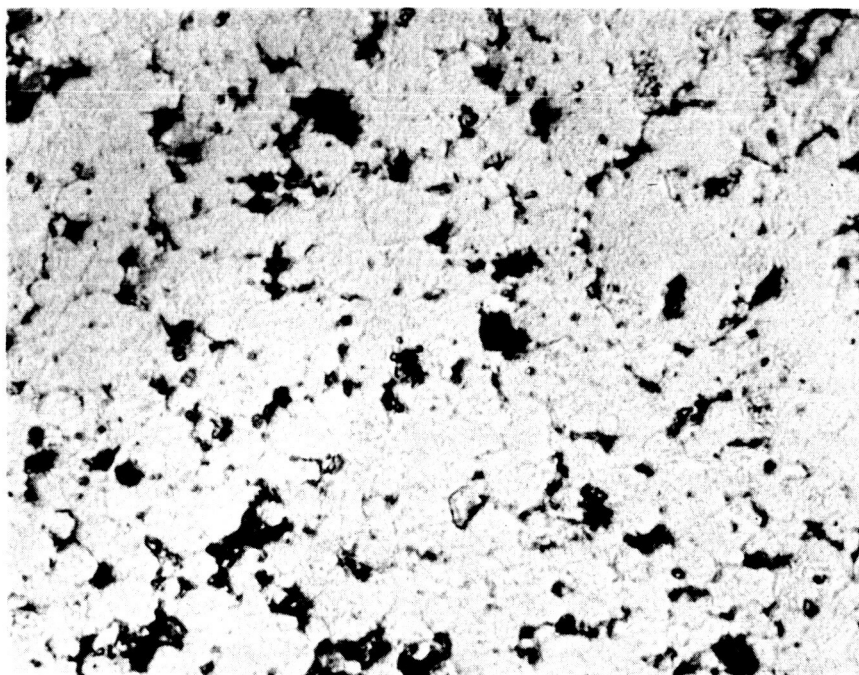


Figure 43. Photomicrograph of Hughes No. 276 W-50% Ir Prealloy, polished surface at 1000X, showing coarse pore distribution and grain clusters. Pores are probably not completely exposed.

alter its appearance, presumably because Ir is so chemically inert. After the ionizer was operated, a portion of the surface that was at most lightly sputtered had a much improved appearance (see Figure 44). This change was probably due to annealing of the surface by the heat of brazing or testing.

Finally, Figures 45 and 46 at 150X and 1000X indicated yet another pore distribution. They were taken from the cross-section of the sample after testing. A pore count of the material will not be given because we are not convinced that the pores are exposed in the photomicrographs taken before testing or that those photomicrographs taken after testing do not represent "pull-out" of material during polishing or annealing and sintering during testing.

When the sample was first operated, the neutral efflux was 250 per cent at $2\frac{1}{2}$ ma/cm². It improved to 10 per cent at 5 ma/cm² after 1 hour of low-temperature operation. Because we felt that the surface represented in Figure 43 might have resulted from burnishing during polishing, it was decided to sputter it. The initial sputtering reduced the neutrals to 1.4 per cent at 5 ma/cm², which proved to be a repeatable value on successive days. The curves of Figure 47 represent this equilibrium surface. As can be seen from Figure 47 or Figure 48, the neutral fraction increases almost linearly at 1550°K from 1 ma/cm² to 20 ma/cm². Furthermore, the critical temperatures are high in comparison with those of high quality, clean porous W, especially at high current densities.

The fact that at 1 ma/cm² and 1500°K the neutral fraction is associated with an effective work function of 4.8 ev convinces us that the neutral efflux observed is not dominated by an exceptionally large pit or crack. The low values of acceleration potential at the onset of space charge limitation also confirm this assumption.

In the data presented, the maximum temperatures shown are 250°K less than those usually used. This was to assure that the ionizer was not further sintered before a set of curves were obtained. The reported sintering

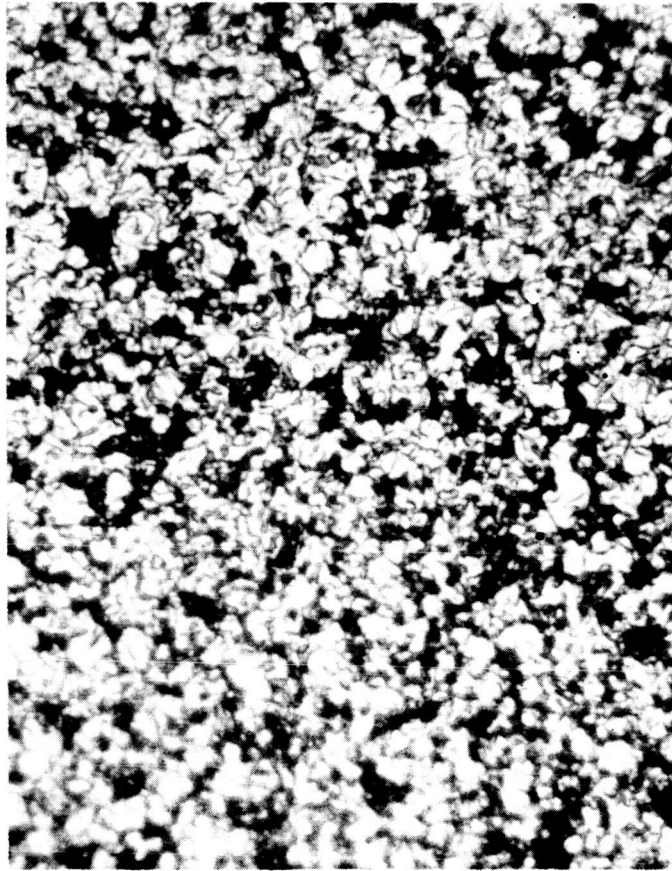


Figure 44. Photomicrograph of Hughes No. 276 W-50% Ir Prealloy at 700X showing a lightly sputtered area of the surface after test.

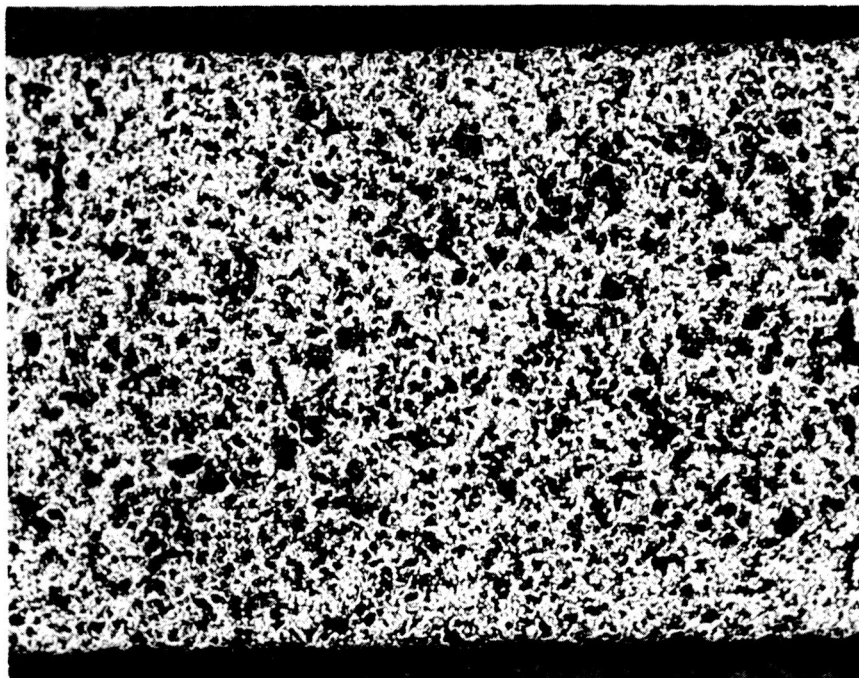


Figure 45. Cross-section of Hughes No. 276 W-50% Ir Prealloy at 150X after test showing extremely coarse structure.

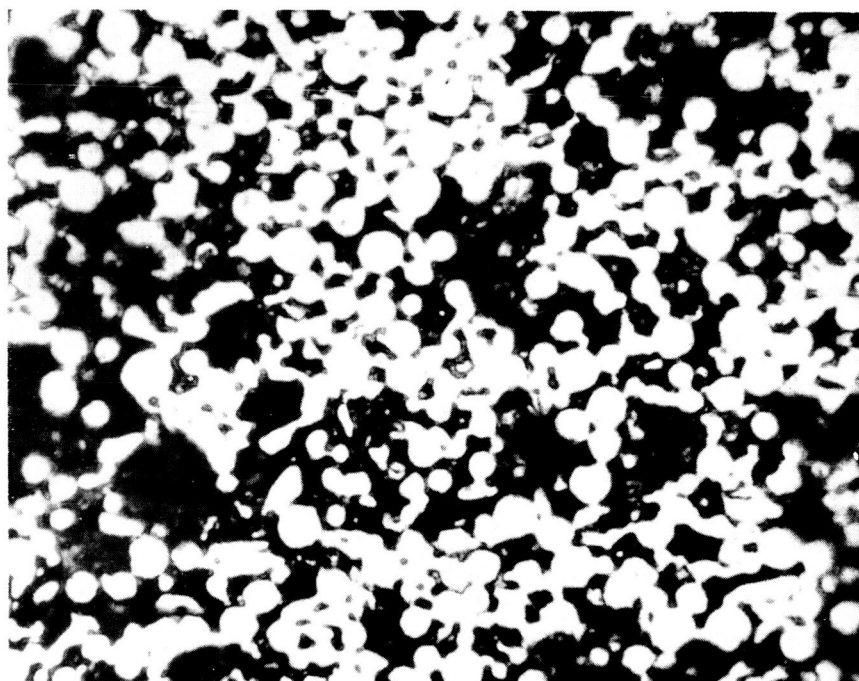


Figure 46. Cross-section of Hughes No. 276 W-50% Ir Prealloy at 150X after test showing extremely coarse structure.

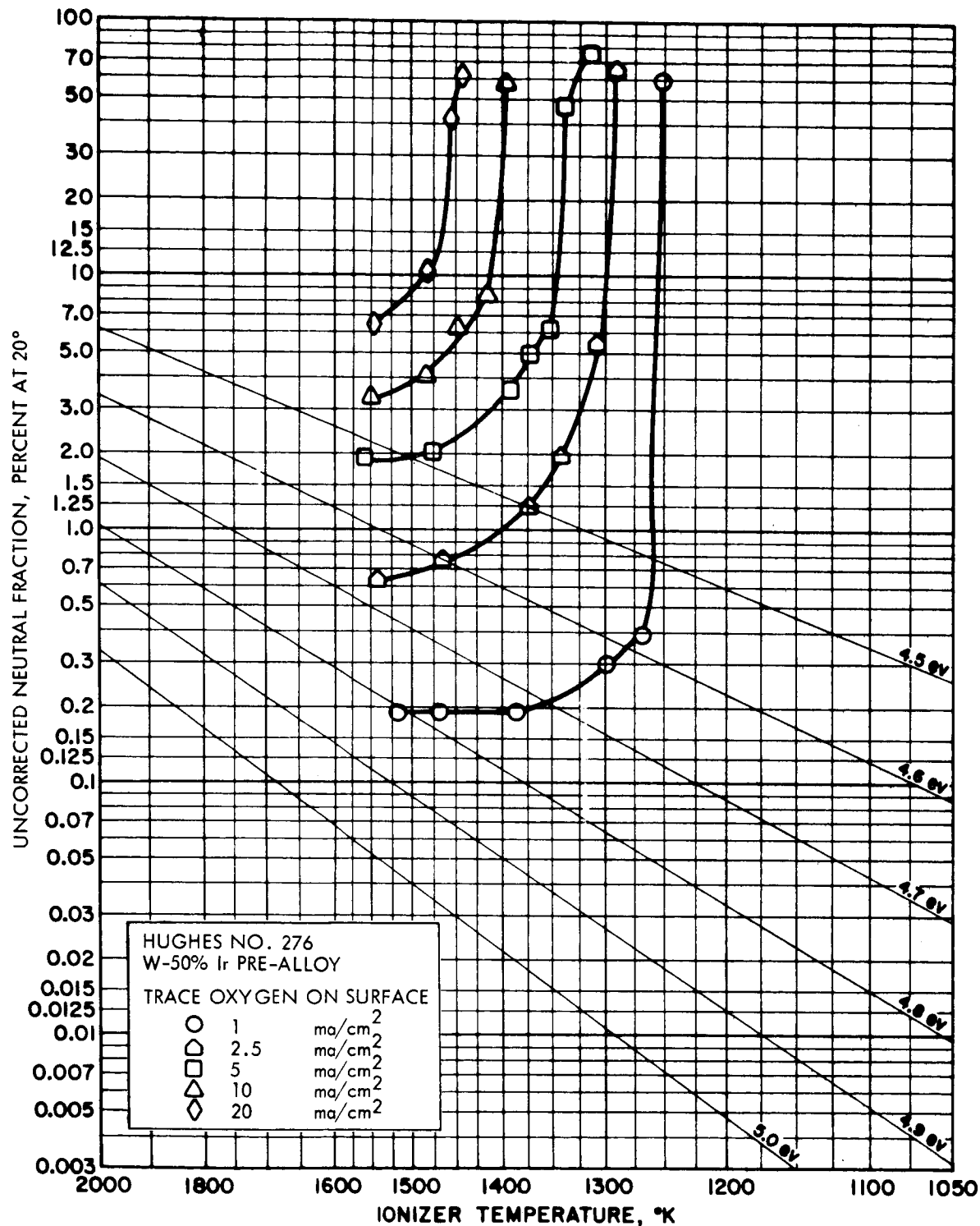


Figure 47. Uncorrected neutral fraction from Hughes No. 276 W-50% Ir Prealloy at 20° from normal vs ionizer temperature for various ion current densities. Sputtered surface; probably contaminated with trace oxygen from bulk contaminant.

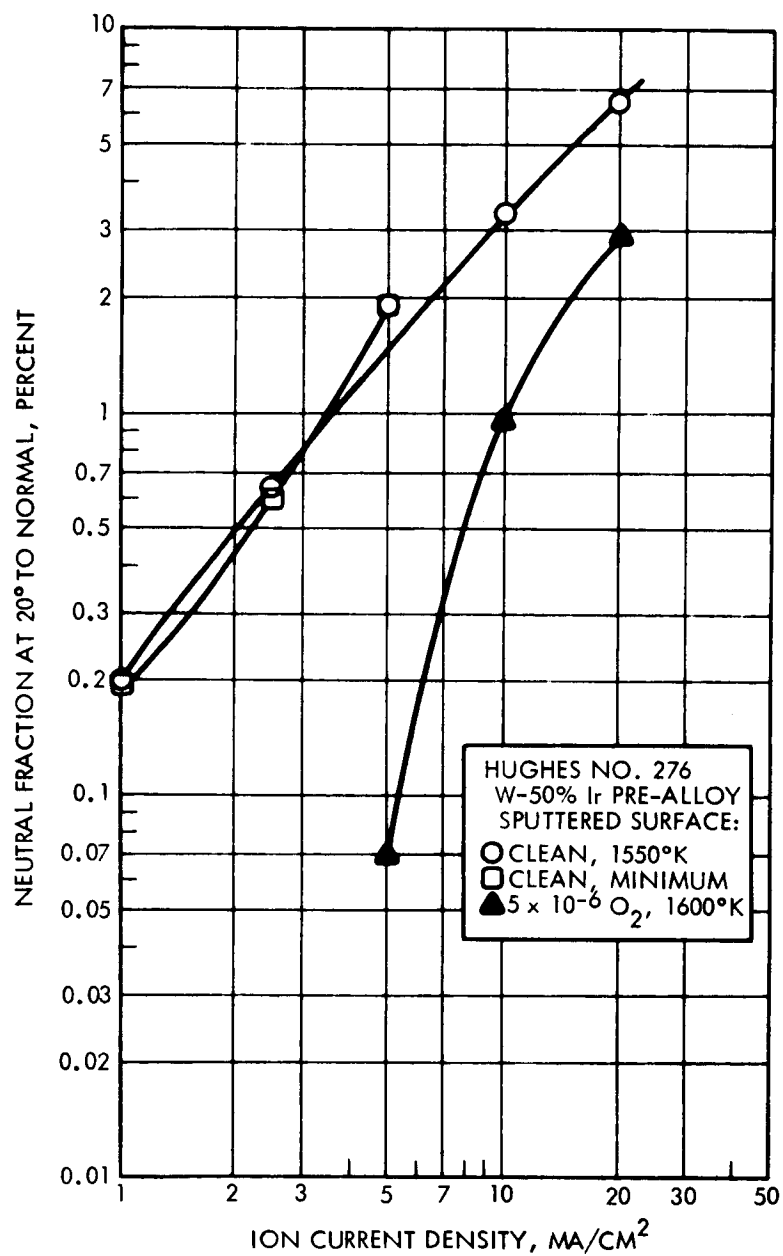


Figure 48. Uncorrected neutral fraction from Hughes #276 W-50% Ir Prealloy at 20° from normal vs ion current density with "clean" surface at 1550°K and oxygenated surface at 1600°K. Also uncorrected minimum neutral fraction at 20° vs ion current density with "clean" surface.

schedule for the sample was 1875° for 2 hours. This temperature is 400° lower than a typical value for sintering porous W, and the sintering time period is also shorter.

As can be seen in Figure 49, the performance of this material in 5×10^{-6} torr of O_2 is not attractive either. At the 20 ma/cm^2 current density the oxygen pressure was raised to 5×10^{-4} torr briefly to assure that the lower pressure produced a fully oxygenated surface. No change was noted with the increase in pressure.

The distribution of neutral efflux with angle again yields a straight line at 5 ma/cm^2 ($f = 1 - \theta/49^{\circ}$). This sample did not exhibit the enhanced neutral detector readings at 0° seen on previous samples; the peak value fell on the above line within experimental error.

We developed the following general ideas about the material from its behavior. As in the case of Ir-coated W, oxygen is more tightly bound to WIr than to W. Furthermore, the evidence suggests that oxygen is present in the ionizer as a bulk contaminant. Consequently the data presented in Figures 47 and 48 represent a slightly oxygenated surface and a neutral fraction at 1550°K that is slightly low. Not only do the curve shapes and the response of the surface to C_2H_2 support this theory, but so does the following experiment. The surface was first heavily exposed to C_2H_2 , with the result that a heavy surface layer of carbon formed, and then heated to diffuse the C into the ionizer. During the process of removing C, the surface approached an equilibrium performance similar to that of the 5 ma/cm^2 curve in Figure 46 but with slightly higher neutrals. We believe that the diffused C layer was acting as a barrier to the diffusion of bulk oxygen to the surface.

Test 8: Hughes No. 225 W-50% Ir Mixture. - The sample, reportedly made by sintering a mixture of equal proportions of W and Ir powder, also had very poor physical characteristics. It tended to crumble under even delicate handling. Figure 50 shows the result of lightly scratching a deinfiltreated but unpolished sample. The grain size seen from the polished

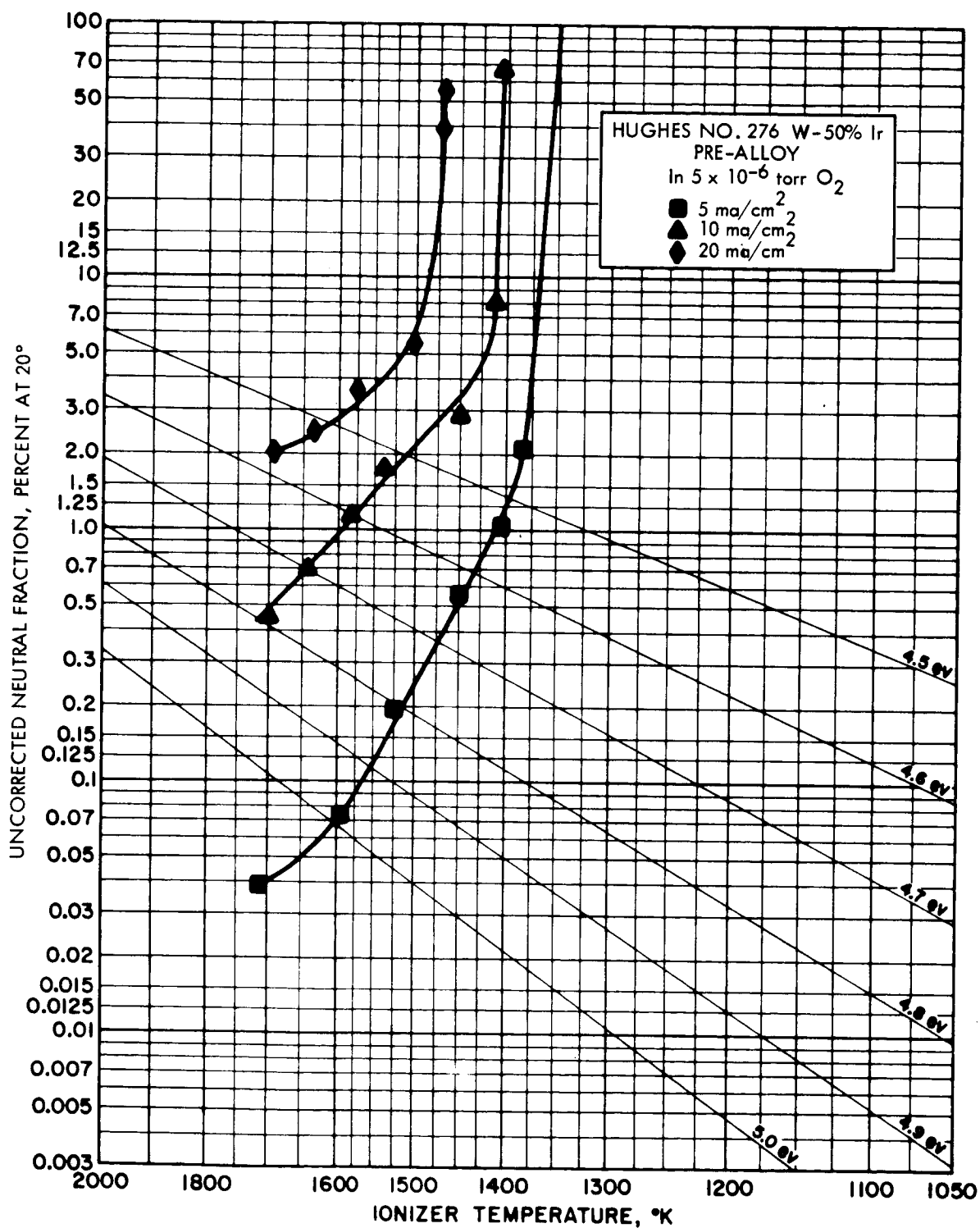


Figure 49. Uncorrected neutral fraction from Hughes No. 276 W-50% Ir Prealloy at 20° from normal vs ionizer temperature for various ion current densities in the presence of 5×10^{-6} torr O_2 .

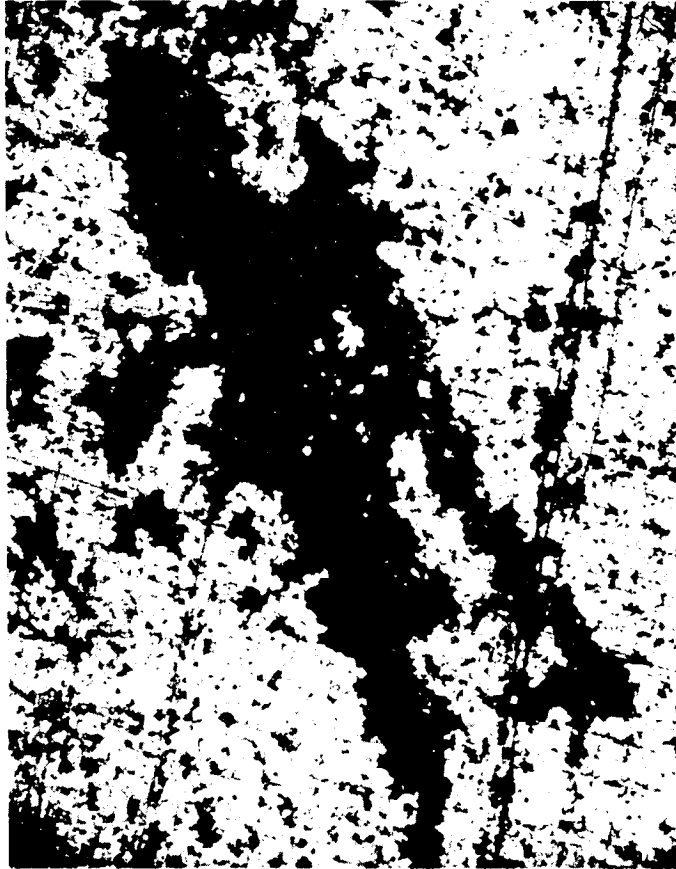


Figure 50. Photomicrograph at 100X of Hughes No. 225 W-50% Ir Mixture showing effect of light scratch on machined surface.

surface at 500X in Figure 51 is very large. It is difficult to know if the large dark areas in this figure represent single pores or an aggregate of smaller pores. From the latter point of view, the average pore diameter is $\sim 3.5\mu$ and the pore count 3.5×10^6 pores/cm². These figures would be drastically changed if the view was taken that the aforementioned dark areas were single pores. The transmittivity of this sample was very high.

The sample was quite similar in performance to Hughes No. 276 W-50% Ir Prealloy. Carbon immediately increased its neutral efflux, suggesting oxygen contamination. The best surfaces attained were those following sputtering, and they are shown in Figure 52. As shown in Figure 53 and 54, the presence of 5×10^{-6} torr or oxygen failed to improve performance, even at low current densities.

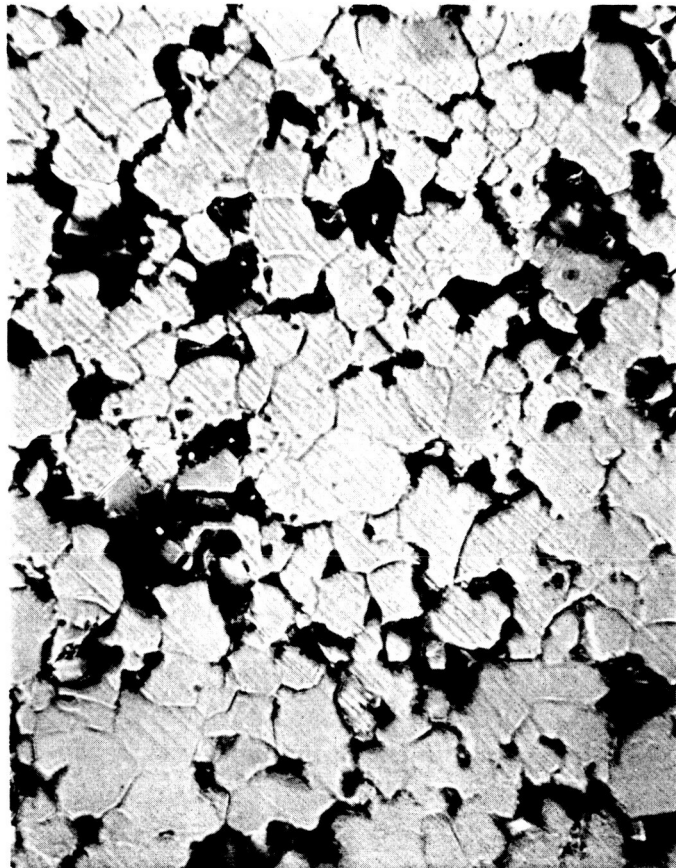


Figure 51. Photomicrograph at 500X of Hughes No. 225 W-50% Ir Mixture showing extremely large surface pores and grains prior to testing.

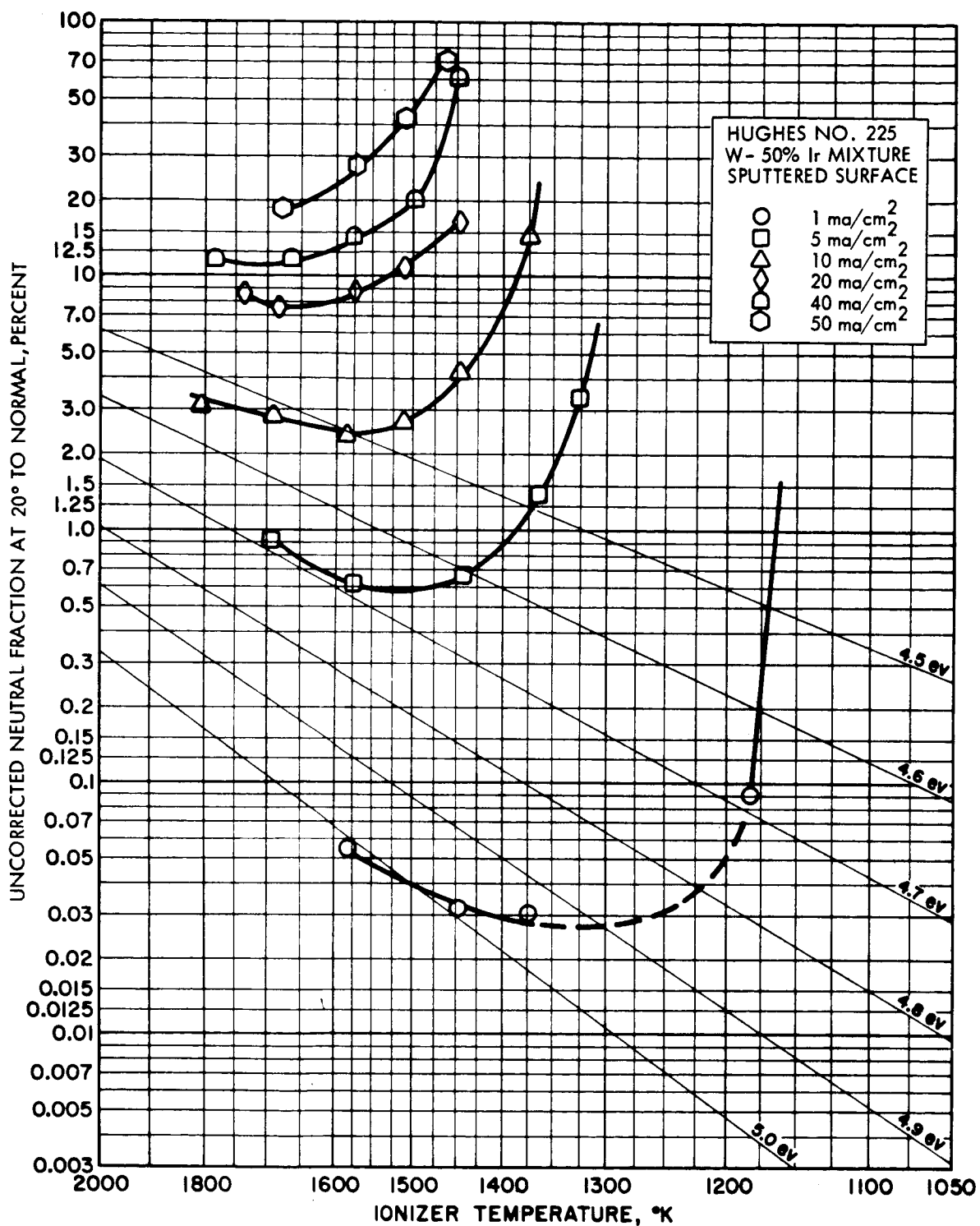


Figure 52. Uncorrected neutral fraction from Hughes No. 225 W-50% Ir Mixture at 20° from normal vs ionizer temperature for various ion current densities. Sputtered surface; probably contaminated with trace oxygen from bulk contaminated.

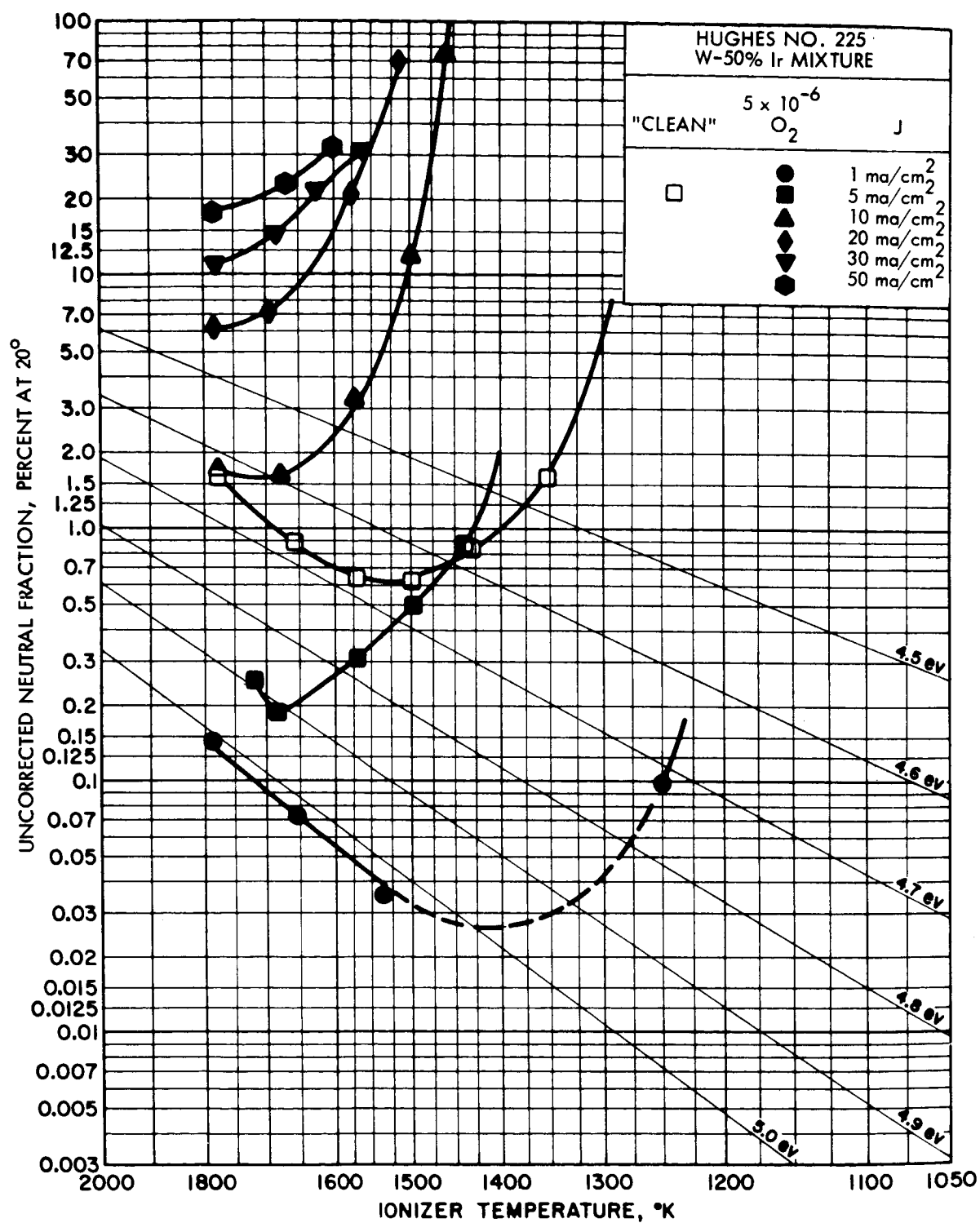


Figure 53. Uncorrected neutral fraction from Hughes No 225 W-50% Ir Mixture at 20° from normal vs ionizer temperature for various ion current densities and surface conditions.

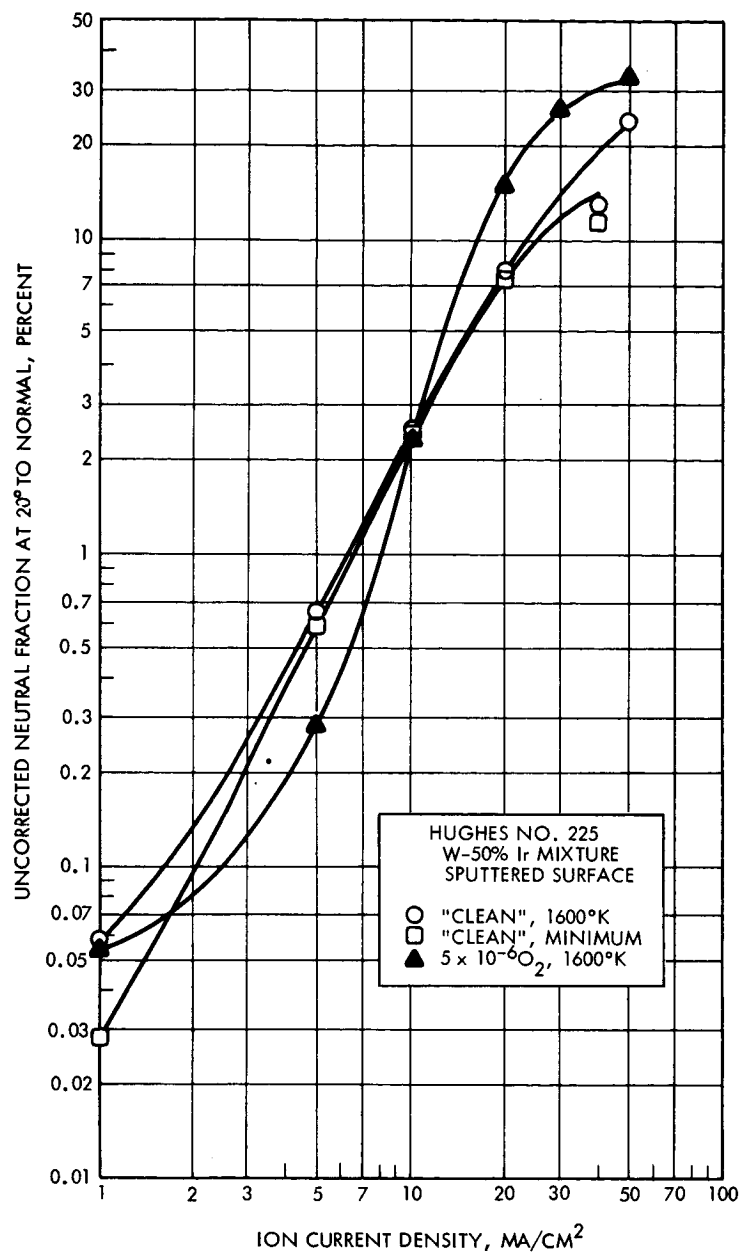


Figure 54. Uncorrected neutral fraction from Hughes No. 225 W-50% Ir Mixture at 20° from normal vs ion current density with 'clean' surface at 1600°K and oxygenated surface at 1600°K. Also uncorrected minimum neutral fraction at 20° vs ion current density with 'clean' surface.

Test 9: Hughes No. 280-100% Ir. - A sample of porous iridium was routinely machined from a silver-impregnated billet supplied to us by the manufacturers (H. R. L.), and designated 280-100% Ir. It was then polished, deinfiltred, and rhodium-brazed into our molybdenum holder. The transmittivity of the 1/2-mm thick sample was 1.6×10^{-4} at this time. No electrolytic etching of the surface was, or could be used to remove any surface cold work present because of the chemical passivity of iridium, but the 1000X photomicrograph of Figure 55 suggests that the surface was substantially open. (Notice the tendency for contiguous pores.)

The test results shown in Figures 56 and 57 were obtained after the surface was materially improved by sputtering. The results obtained previous to sputtering are shown at a single current density of 10 ma/cm^2 for comparison (dotted line). The sketchy results at the high current densities are due to arcing problems associated with the higher Cs feed pressure that was required as sintering reduced the transmission of the porous iridium and the subsequent leakage in our differentially pumped feed line.

Interpretation of the results is straightforward. The effective work function of the material at higher temperatures and low current densities seems to be a definite 5.15 volts. The results at lower temperatures and higher current densities can easily be ascribed to poor pore distribution on the surface. Possibly lengthy sputtering resulting in more uniform pore distribution over the entire face of the sample would have improved performance.

In the tests with oxygen the almost complete reduction of the sample transmittivity to zero terminated the experiment before extensive data could be obtained; however, many qualitative observations were made. Ample oxygen seemed to be ever-present (possibly from bulk solubility) and could be removed only by treatment with carbon. Continuous oxygen exposure reduced neutrals and lowered and sharpened the critical temperature, whereas remnant oxygen lowered the neutrals and raised and sharpened the critical temperature.

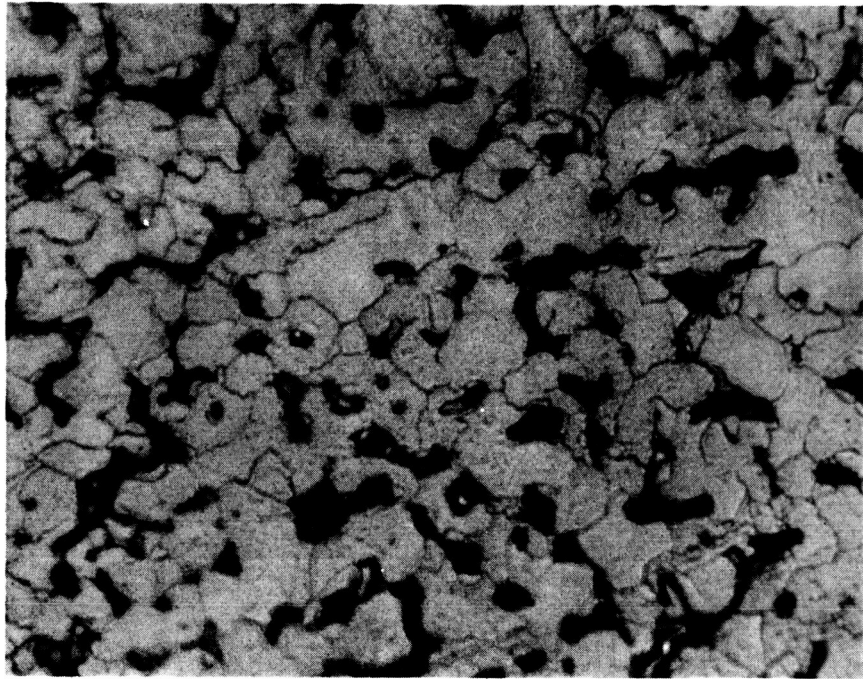


Figure 55. Photomicrograph of Hughes No. 280 100% Ir at 1000X after polishing and deinfiltration.

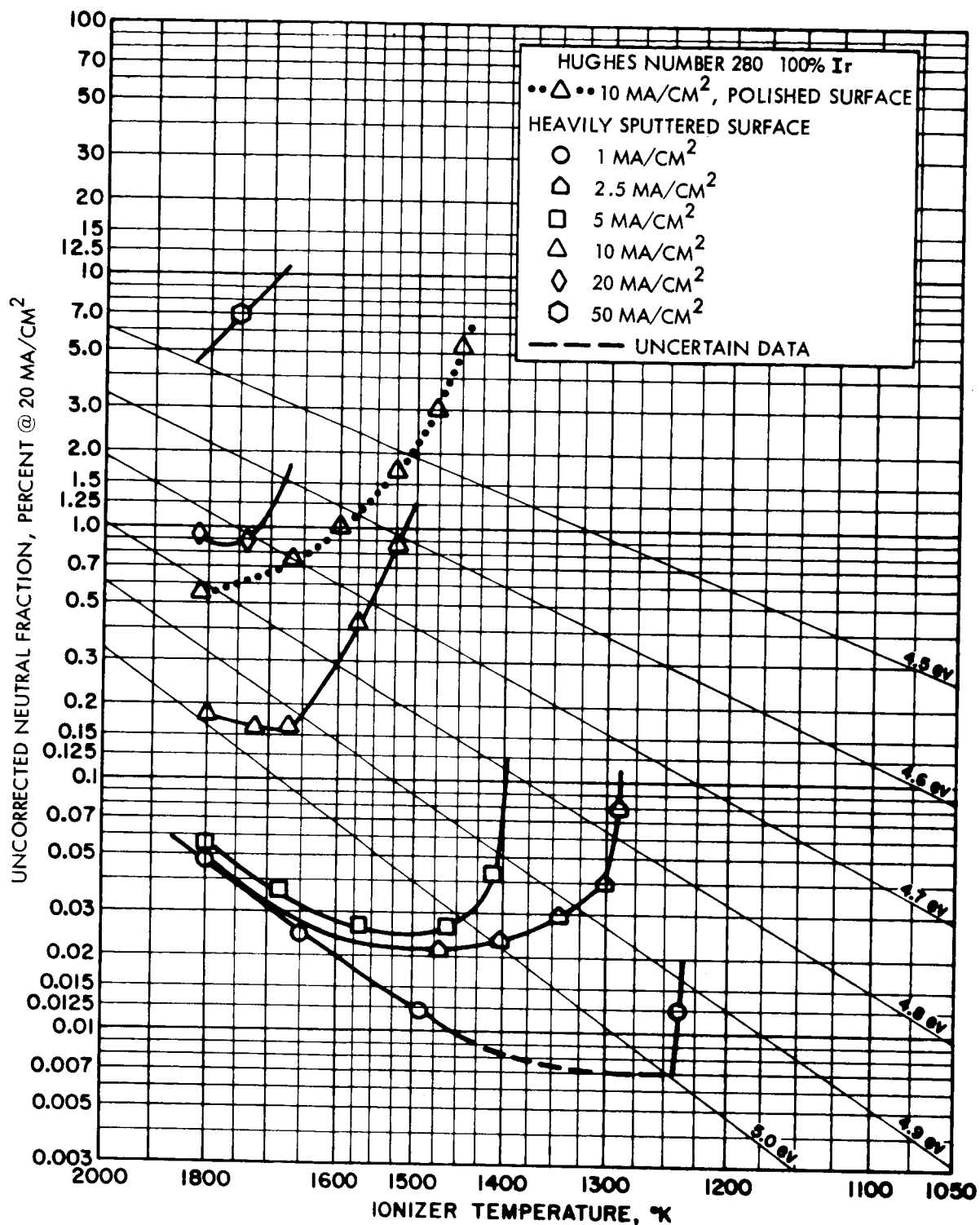


Figure 56. Uncorrected neutral fraction from Hughes No. 280 100% Ir at 20 degrees from the normal vs ionizer temperature for various current densities and surface conditions.

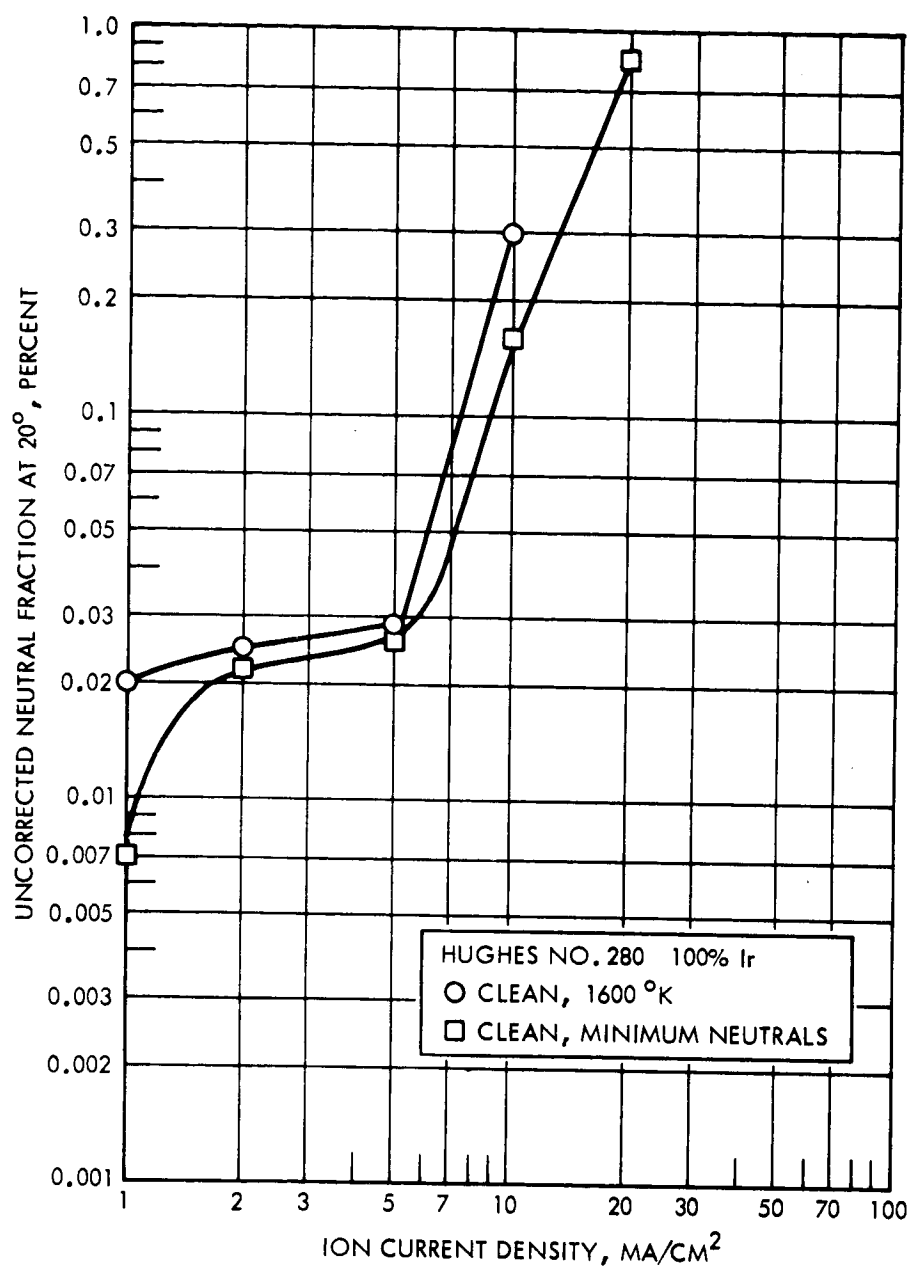


Figure 57. Uncorrected neutral fraction from Hughes No. 280 100% Ir at 20 degrees from the normal vs ion current density with clean surface at 1600°K. Also uncorrected minimum neutrals at 20° vs ion current density with clean surface.

In about 12 hours of testing, during which time a maximum temperature of 1750°K was held for about 1/2 hour, the transmittivity of the porous iridium decreased, as evidenced by the need for ever-increasing boiler temperature to obtain a given ion current density. Transmittivity measurement after test showed a transmittivity less than 10 percent of the original. Bubble tests at high pressure showed some small transmittivity. Photomicrographs, such as Figure 58 at 1000X, did not show solid iridium but did suggest large, unconnected pores surrounded by solid iridium sintered from smaller grains and a disappearance of the small interconnecting pores. We noted that in the region of the rear surface there were fewer pores than the average. Probably the two surfaces sintered preferentially to the interior, but we kept the front open by sputtering. The braze was successful; completely solid Ir was found only in the immediate region of the fillet.

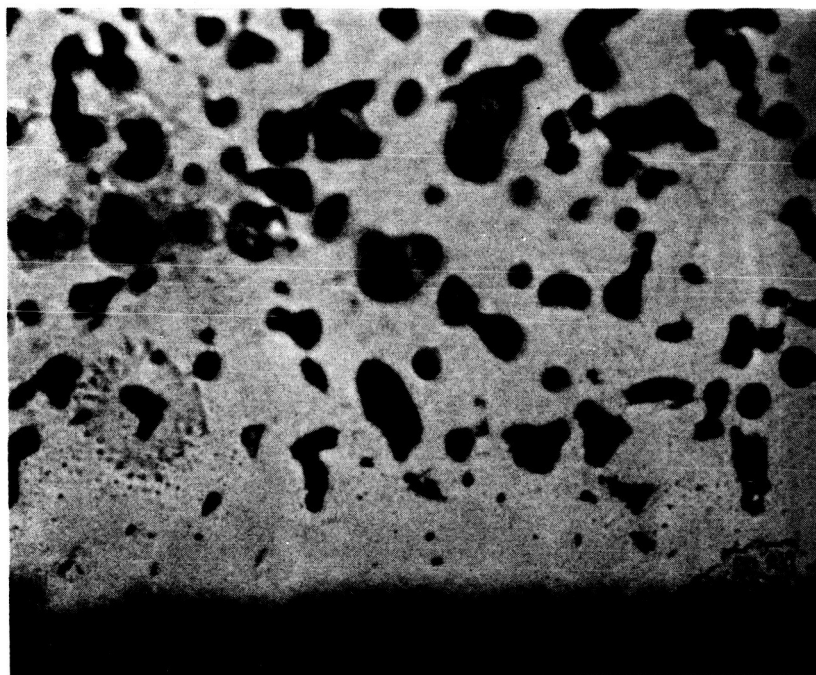


Figure 58. Photomicrograph at 1000X of Hughes No. 280 100% Ir after test. Rear surface at bottom appears almost completely sintered closed; elsewhere large, unconnected pores appear.

Test 10: TRW ST 1-9. - This test was carried out using porous tungsten manufactured by TRW Systems from graded spherical tungsten powder. The results can be seen in the neutral fraction vs temperature curves of Figure 59. The performance of the material was excellent through 10 ma/cm² but degraded rapidly in the vicinity of 20 ma/cm². The behavior when the sample was operated at high current density in oxygen and then with a remnant oxygen coverage is indicated. In an oxygen pressure of 5×10^{-6} torr, the neutrals were low but a large hysteresis existed. Operation shortly after the oxygen was turned off showed the monotonic increase in neutrals as the temperature decreased.

Test 11: TRW 57-3. - The material for this test was manufactured by TRW Systems under the direction of M. Kirkpatrick from a melt of rhenium-tungsten alloy. Upon cooling a dendritic array of tungsten with the limit of rhenium in solid solution dispersed itself, this being separated by an intermetallic compound. The latter compound is more chemically reactive and can be preferentially removed; however, in practice the operation was difficult and the removal was not complete, as can be seen in the photomicrographs of Figures 60 and 61. The results of the cesium ion test were poor as might be expected with a very dense solid material having only a few over-fed passageways connecting the sides. The transmittivity to Knudsen flow was found to be almost nonexistent. Also high cesium boiler temperatures were required to get as little as a nominal 5 ma/cm² of cesium neutral current density. The largest percentage of ions measured was about 20 percent. This current was highest with high temperatures and high electric fields. The electron work function of the source assembly was measured to be about 4.2 volts. This, of course, could result from the molybdenum holder and only indicates that the porous sample is not contaminated by a low work function material. A work function of around 3.5 volts would be necessary to explain the large neutral fraction.

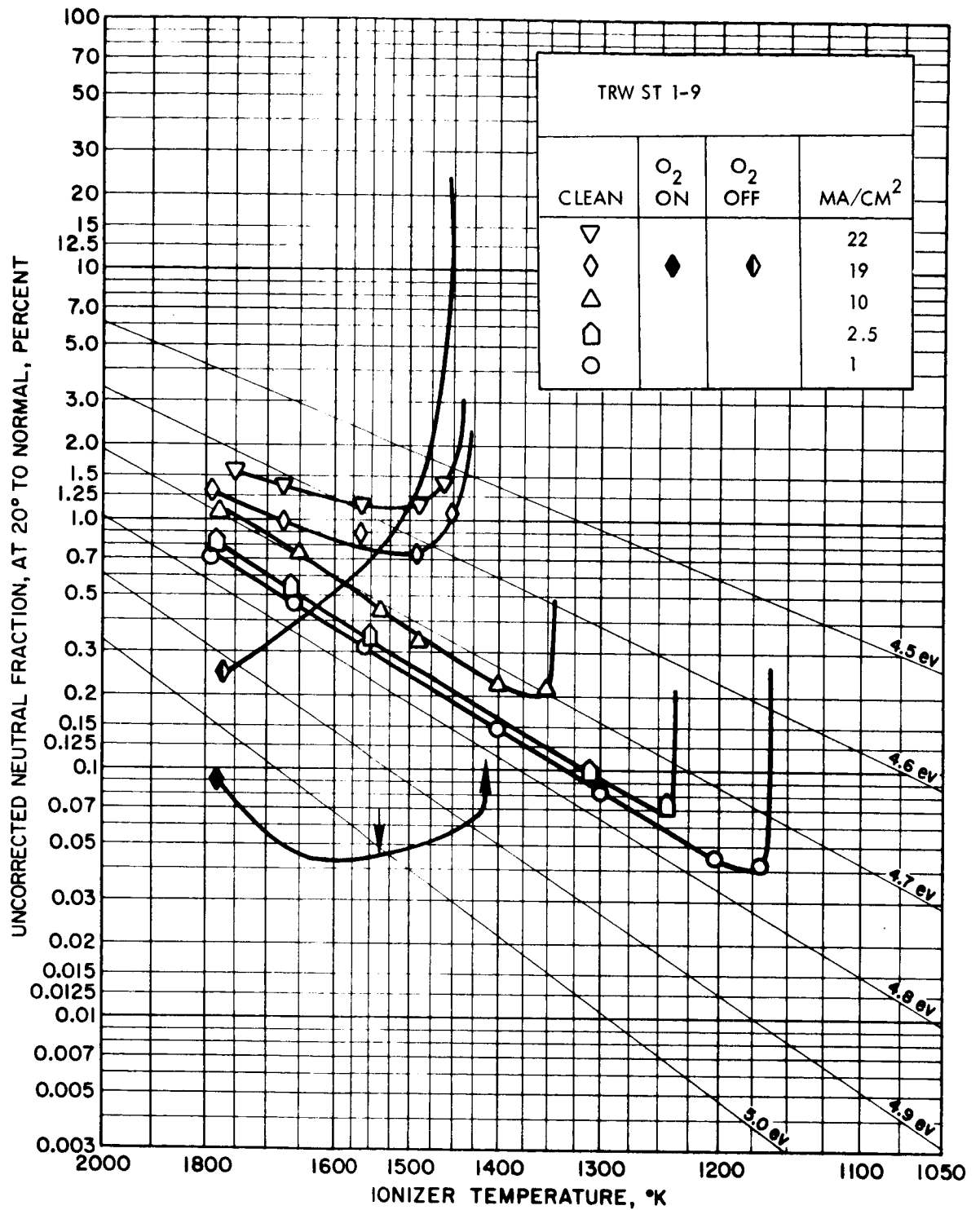


Figure 59. Uncorrected neutral fraction from TRW ST 1-9 at 20° from normal vs ionizer temperature at various ion current densities and surface conditions.



Figure 60. Photomicrograph at 1000X of cross-section of TRW W-Re 57-3 showing pore structure near surface. Sample was rounded in polishing so only center of photo is in focus.



Figure 61. Photomicrograph at 400X of cross-section of TRW W-Re 57-3 showing that the center of the ionizer was not etched open. Sample was rounded in polishing so only center of photo is in focus.

Test 12: E.O.S. 788 Low Density Tungsten. - This low density material was quite difficult to braze, with the result that the test was made on the fifth sample to be brazed. All others showed leaks at the braze because the sample sintered leaving a larger than usual clearance between the sample and the holder. In addition, the high porosity "sopped" the braze away from this region to result in a leak at the braze and more than usual penetration of the braze material into the porous tungsten. A number of metallographic examinations of the porous tungsten revealed a large number of internal "pull away" areas where large cavernous voids were left as further sintering occurred. A typical area exhibiting this effect is shown in Figure 62.

The testing results are shown in Figure 63. The results at low current density were poorer than usually observed, but high current density performance was as good or better than that of any other material tested. The results in oxygen and in remnant oxygen were similar to those observed with other porous tungsten materials.

Careful measurements of the angular distribution of neutrals again showed no variation with current densities up to 40 ma/cm^2 , nor with temperature or electric field. Again, 100-percent neutrals, space charge limited neutrals, or neutrals produced during operation below critical temperature showed a cosine distribution. For this plug, the constant noncosine distribution had a smaller slope than observed with any other porous material; it had the normalized form, $1 - \theta/90^\circ$, from 10° to 40° .

TABULATED TEST PARAMETERS AND EVALUATION SHEETS

In Table II are tabulated the test parameters, sample results, and conclusions, reached during this program. The test evaluation sheets of all of the 12 tests are assembled here and follow the table.

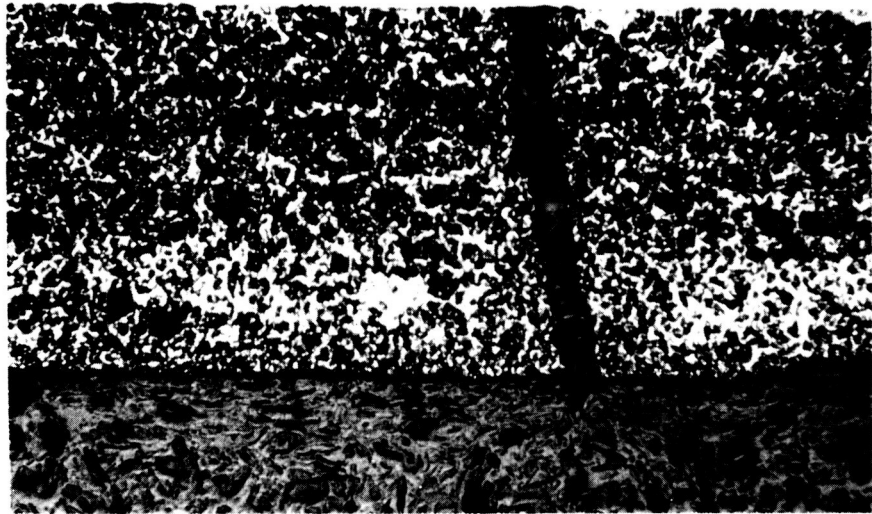


Figure 62. Photomicrograph at 100X of cross section of EOS 788 low density tungsten after brazing. Large, bright areas are solid tungsten. This sample was not tested.

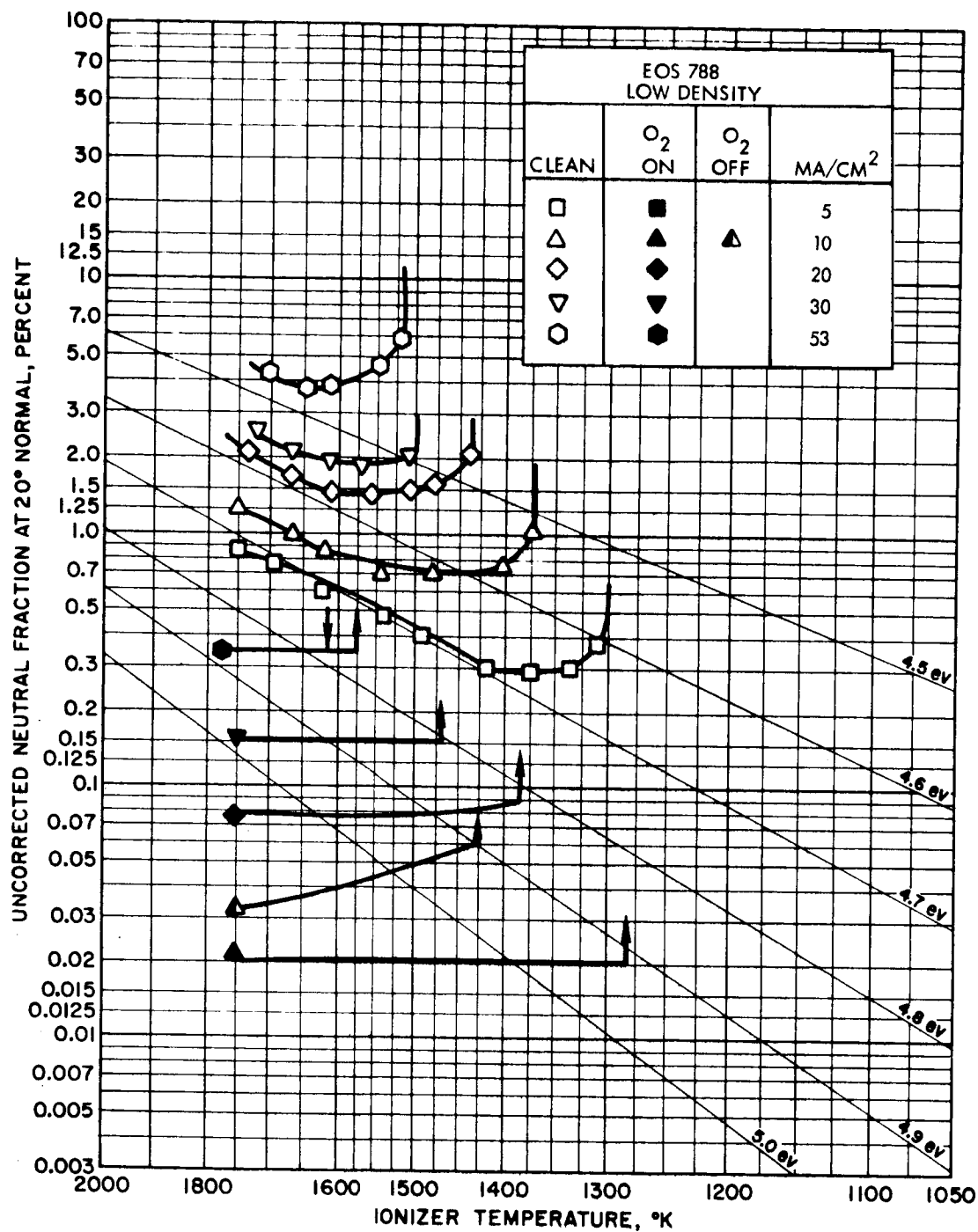


Figure 63. Uncorrected neutral fraction from EOS 788 at 20° from normal vs ionizer temperature at various ion current densities and surface conditions.

Test No.	Ident.	Trans. $\times 10^5$ Before After	Pore Density $\times 10^{-6}$, Diam (μ)	Low j S-L ϕ	At 20 ma/cm ² Min. % Neut. @ Temp °K	Angle Distr.	Comments
1	HRL 324S-C	10 --	--	--	--	--	Poisoned with sputtered tantalum
2	0.5-1.0 μ Ir coat	9.4 8 5	--	4.9	0.35 1420	1- θ /52	Initial results excellent Poorer after lengthy operation
3	1-2 μ Ir Coat	9.5 4.7 3.2	--	4.8	0.5 1400	--	Results basically same as #2- Neutrals & Critical low.
4	Union Carbide	7.3 5.4	4.9 2.3	4.8	6.5 1630	1- θ /52	Poor High j operation
5	HRL 324S-F	15 9.1	7.6 2.0	4.8	0.3 1390	1- θ /60	Very good without Iridium
6	TRW W-5% Re	6.9 6.5	7.2 2.0	4.75	1.25 1500	1- θ /65	Small amount of Re not helping
7	HRL W-50% Ir	69 64	--	>4.8	6 1550	1- θ /49	Poor pore distribution
8	HRL 50%Ir mix	85 83	3.5 3.5	>5	7.5 1680	1- θ /45 1- θ /55	Poor Hi j performance
9	HRL 100% Ir	16 <1	--	5.15	0.9 1750	1- θ /55	Further sintering during operation
10	TRW STI-9	16	5.9 2.0	4.77	1.0 1500	1- θ /52 1- θ /60	Degrade at Hi j
11	TRW W-Re	<1	--	--	--	cosine	Intermetallic compound not completely etched out
12	EOS Low Dens.	65 --	?	~4.75	1.5 1480	1- θ /90	Good at Hi j Shrinks in braze

TABLE II

IONIZER PELLET EVALUATION REPORT

PELLET TYPE Graded, Spherical W
 MADE BY Hughes Research Lab
 AVERAGE PARTICLE SIZE 3.9 μ

TEST NO. 1 DATE August, 1966
 PORES PER CM² 7.6×10^6
 AVERAGE PORE SIZE 2.0 μ

PARTICLE SIZE DISTRIBUTION

MICRON DIAMETER	PERCENT
> 7.5	—
7.5 - 5.0	—
5.0 - 3.3	Std. deviation 0.7 μ
3.3 - 2.25	—
1.5 - 1.0	—
< 1.0	—

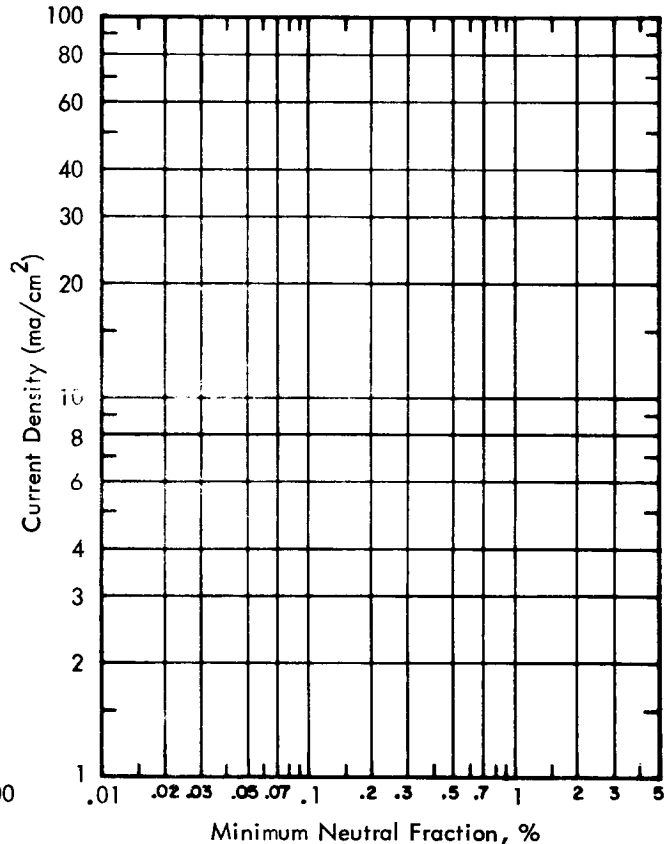
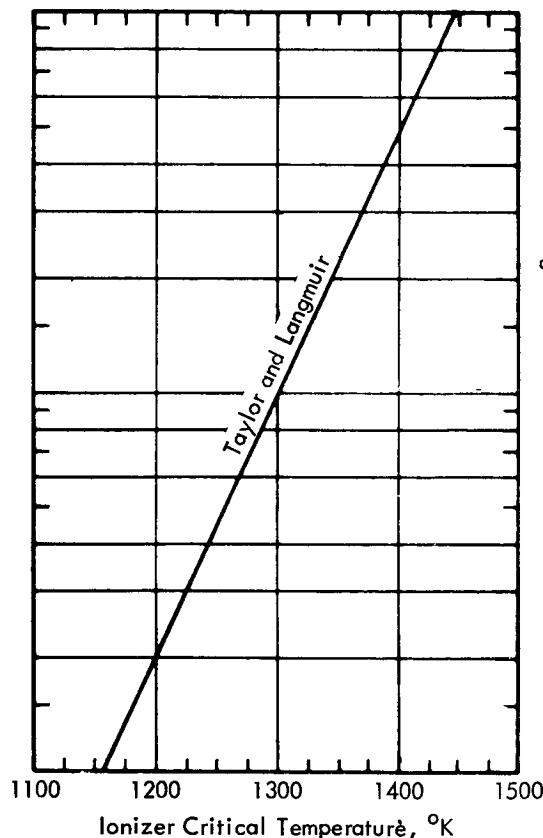
PORE SIZE DISTRIBUTION

MICRON DIAMETER	PERCENT
> 1.6	—
1.2 - 1.6	—
0.8 - 1.2	—
0.4 - 0.8	—
< 0.4	—

PELLET DIAMETER (EFFECTIVE) 0.18
 TRANSMISSION COEFFICIENT 1.0×10^{-4} BY
 PRESSURE 10 (air) TORR
 CALCULATED TRUE DENSITY 79.2 %
 SURFACE TREATMENT Etched & Sputtered
 SAMPLE INFORMATION Hughes No. 324-S
TRW No. C

AVERAGE DISTANCE BETWEEN PORES — μ
 THICKNESS 5×10^{-2} CM, DENSITY — %
 $\Delta p / \Delta t$ — TORR/SEC
 WORK FUNCTION — *, eV

*SAHA-L. EQ. - % NEUTRALS AT 1 Ma/cm



CONCLUSIONS Clean surface was never obtained because of a Ta patch of
break in the lip of the Mo plenum. Therefore data not presented.

TEST MADE BY Shelton/Hall REPORT PREPARED BY D. F. Hall

IONIZER PELLET EVALUATION REPORT

PELLET TYPE Ir Coated (chemically) TEST NO. 2a DATE 8-30-65

MADE BY Hughes Research Lab.

PORES PER CM² _____

AVERAGE PARTICLE SIZE 3.9μ

AVERAGE PORE SIZE _____

PARTICLE SIZE DISTRIBUTION
MICRON DIAMETER PERCENT

> 7.5 _____
7.5 - 5.0 _____
5.0 - 3.3 _____
3.3 - 2.25 Std. deviation 0.7μ
1.5 - 1.0 _____
< 1.0 _____

PORE SIZE DISTRIBUTION
MICRON DIAMETER PERCENT

> 1.6 _____
1.2 - 1.6 _____
0.8 - 1.2 _____
0.4 - 0.8 _____
< 0.4 _____

PELLET DIAMETER (EFFECTIVE) 0.18

AVERAGE DISTANCE BETWEEN PORES _____ μ

TRANSMISSION COEFFICIENT 8x10⁻⁵ BY

THICKNESS 5 x 10⁻² CM, DENSITY _____ %

PRESSURE 10 (air) TORR

Δp/Δt _____ TORR/SEC

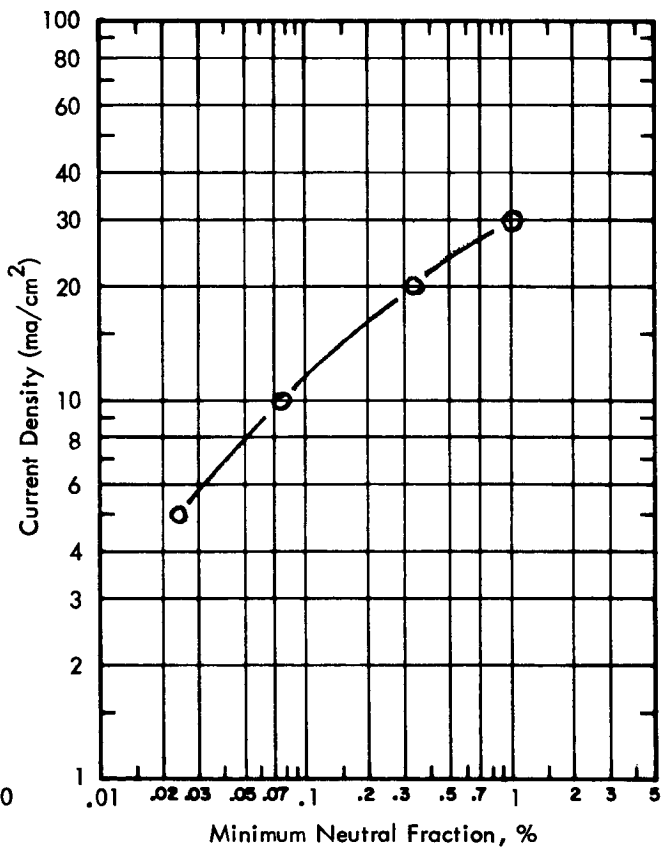
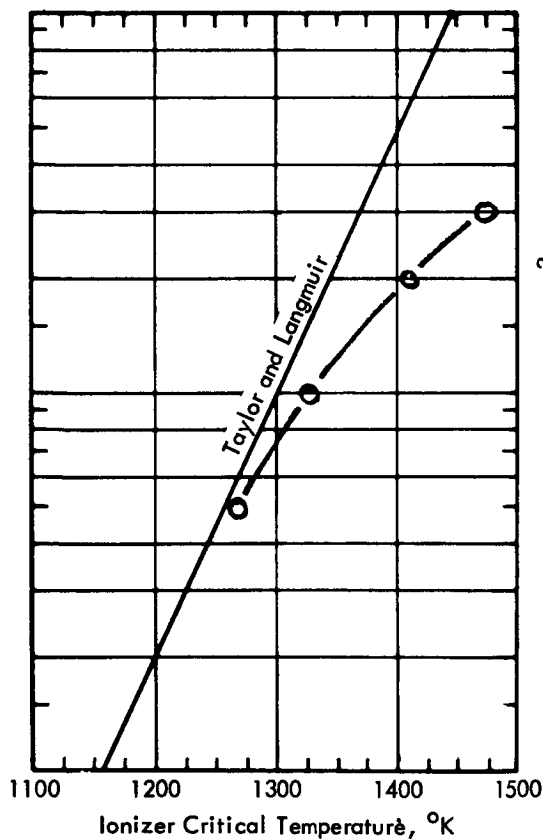
CALCULATED TRUE DENSITY 79.2%

WORK FUNCTION est. 4.9 (4.88 at ^{*}5 ma/cm²)

SURFACE TREATMENT 0.5-1μ Ir coating

SAMPLE INFORMATION Hughes No. 324-S
TRW No. B

*SAHA-L. EQ. - % NEUTRALS AT 1 Ma/cm



CONCLUSIONS Very superior performance. Neutral efflux 0.35% at 1410°K at 20 ma/cm². Minimum neutral efflux at 20 ma/cm² 1/3 of best clean porous W ever tested and better than any carbided ionizer ever tested. Criticals extremely sharp and very low.

TEST MADE BY Shelton/Hall

REPORT PREPARED BY D. F. Hall

IONIZER PELLET EVALUATION REPORT

PELLET TYPE Ir coated (chemically) TEST NO. 2b TE 9-65
 MADE BY Hughes Research Lab. PORES PER CM² _____
 AVERAGE PARTICLE SIZE 3.9μ AVERAGE PORE SIZE _____

PARTICLE SIZE DISTRIBUTION
 MICRON DIAMETER PERCENT

> 7.5 _____
 7.5 - 5.0 _____
 5.0 - 3.3 _____
 3.3 - 2.25 Std. deviation 0.7μ
 1.5 - 1.0 _____
 < 1.0 _____

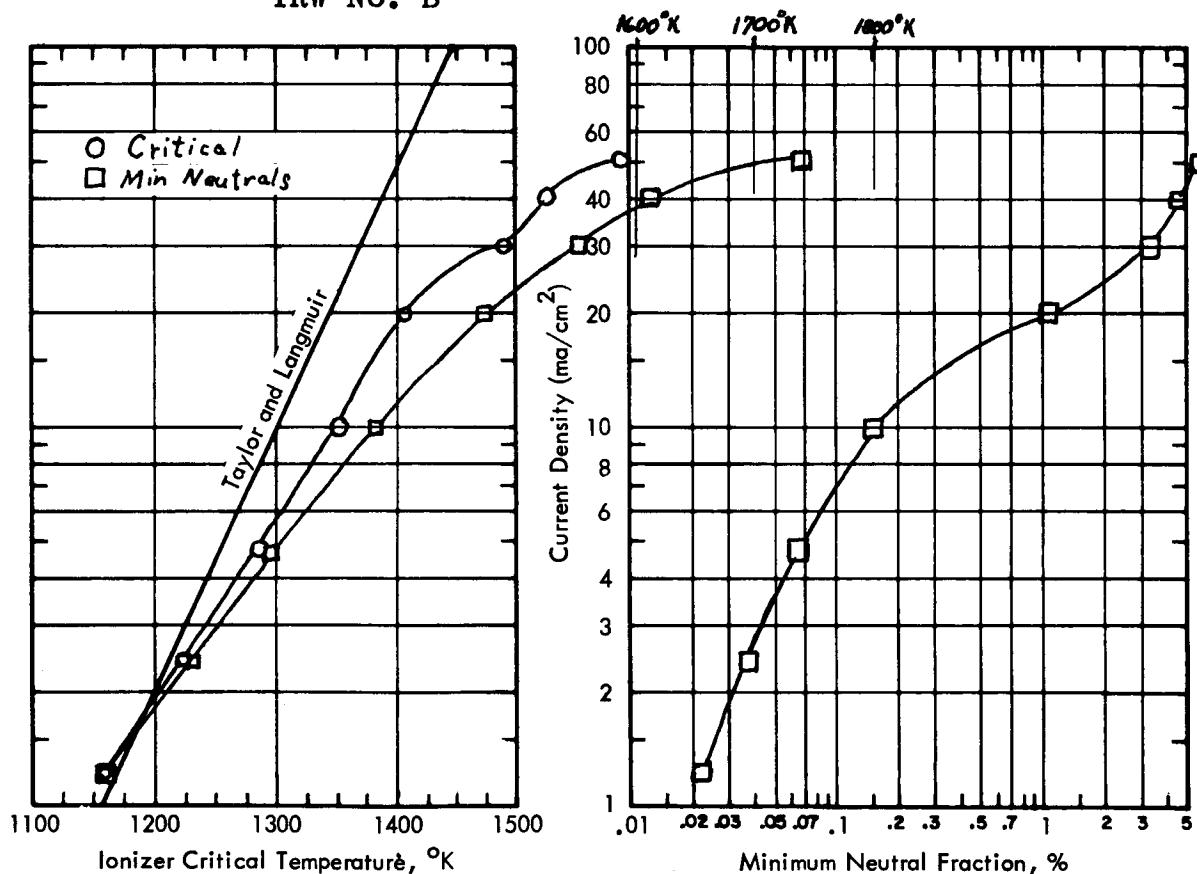
PORE SIZE DISTRIBUTION
 MICRON DIAMETER PERCENT

> 1.6 _____
 1.2 - 1.6 _____
 0.8 - 1.2 _____
 0.4 - 0.8 _____
 < 0.4 _____

PELLET DIAMETER (EFFECTIVE) 0.18
 TRANSMISSION COEFFICIENT 8×10^{-5} BY
 PRESSURE 10 (air) TORR
 CALCULATED TRUE DENSITY 79.2%
 SURFACE TREATMENT 0.5-1μ Ir coating
 SAMPLE INFORMATION Hughes No. 324-S
TRW No. B

AVERAGE DISTANCE BETWEEN PORES _____ μ
 THICKNESS 5×10^{-2} CM, DENSITY _____ %
 Δp/Δt _____ TORR/SEC
 WORK FUNCTION 4.85 *, eV

* SAHA-L. EQ. - % NEUTRALS AT 1 Ma/cm



CONCLUSIONS These tests subsequent to the initial exposure to O₂.
Performance similar to high quality clean porous W. Criticals
unchanged from early data but min. neutrals 2 to 3 times higher.
Curves more rounded.

TEST MADE BY Shelton/Hall REPORT PREPARED BY D. F. Hall

IONIZER PELLET EVALUATION REPORT

PELLET TYPE Ir coated (chemically) TEST NO. 3 rev. DATE 9-65
 MADE BY Hughes Research Lab. PORES PER CM² 7.6×10^6
 AVERAGE PARTICLE SIZE 3.9μ AVERAGE PORE SIZE 2.0μ

PARTICLE SIZE DISTRIBUTION
MICRON DIAMETER PERCENT

> 7.5	—
7.5 - 5.0	—
5.0 - 3.3	—
3.3 - 2.25	—
1.5 - 1.0	—
< 1.0	—

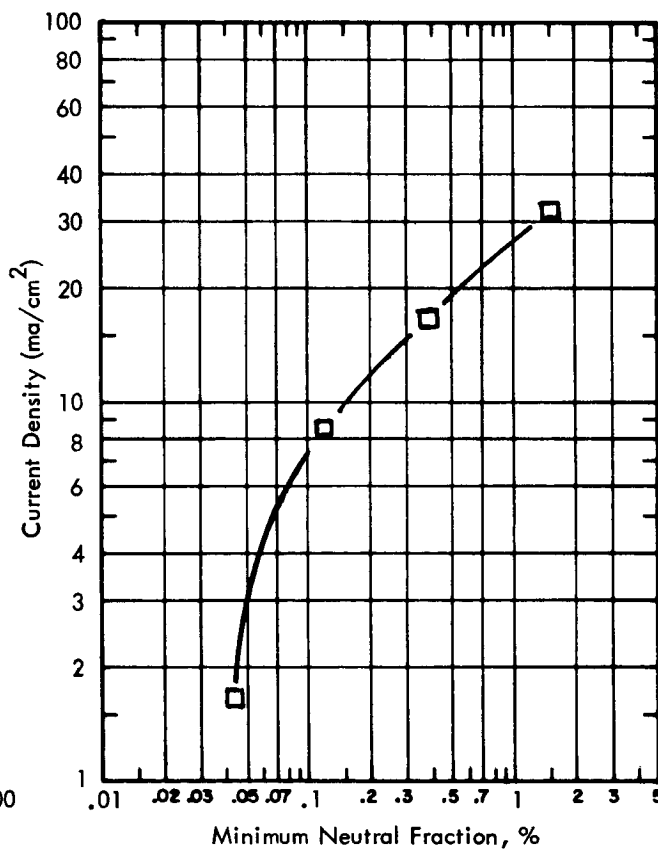
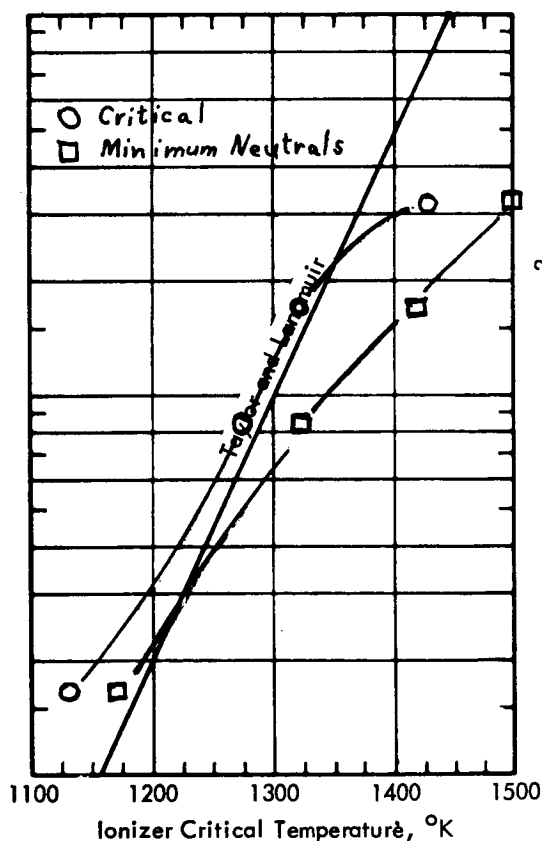
Std. deviation 0.7μ

PORE SIZE DISTRIBUTION
MICRON DIAMETER PERCENT

> 1.6	78
1.2 - 1.6	17
0.8 - 1.2	5
0.4 - 0.8	—
< 0.4	—

PELLET DIAMETER (EFFECTIVE) 0.18
 TRANSMISSION COEFFICIENT 4.7×10^{-5} BY
 PRESSURE 10 (air) TORR
 CALCULATED TRUE DENSITY 79.2%
 SURFACE TREATMENT 1-2 μ Ir coating
 SAMPLE INFORMATION Hughes No. 324-S
TRW No. A

AVERAGE DISTANCE BETWEEN PORES _____ μ
 THICKNESS 5×10^{-2} CM, DENSITY _____ %
 $\Delta p/\Delta t$ _____ TORR/SEC
 WORK FUNCTION 4.8 at 1.7 ma/cm^2 *, eV
 *SAHA-L. EQ. - % NEUTRALS AT 1 Ma/cm



CONCLUSIONS Initial tests. Data revised to reflect 40% reduction
from normal eff. ionizer area. Very superior performance.
Below 15 ma/cm^2 , Min. neutral similar to later sample B; above
 15 ma/cm^2 , Min. neutrals similar to early sample B. Criticals low.
Min. neutrals at 20 ma/cm^2 .55%; crit. 1425°K .
 TEST MADE BY Shelton/Hall REPORT PREPARED BY D. F. Hall

IONIZER PELLET EVALUATION REPORT

PELLET TYPE 4848-82-1
 MADE BY Union Carbide
 AVERAGE PARTICLE SIZE 3.6-8.2 μ

PARTICLE SIZE DISTRIBUTION
 MICRON DIAMETER PERCENT

> 7.5	—
7.5 - 5.0	—
5.0 - 3.3	—
3.3 - 2.25	—
1.5 - 1.0	—
< 1.0	—

PELLET DIAMETER (EFFECTIVE) 0.18
 TRANSMISSION COEFFICIENT 7.3×10^{-5} BY
 PRESSURE 10 (air) TORR
 CALCULATED TRUE DENSITY 79.4%
 SURFACE TREATMENT Etch & Sputter
 SAMPLE INFORMATION _____

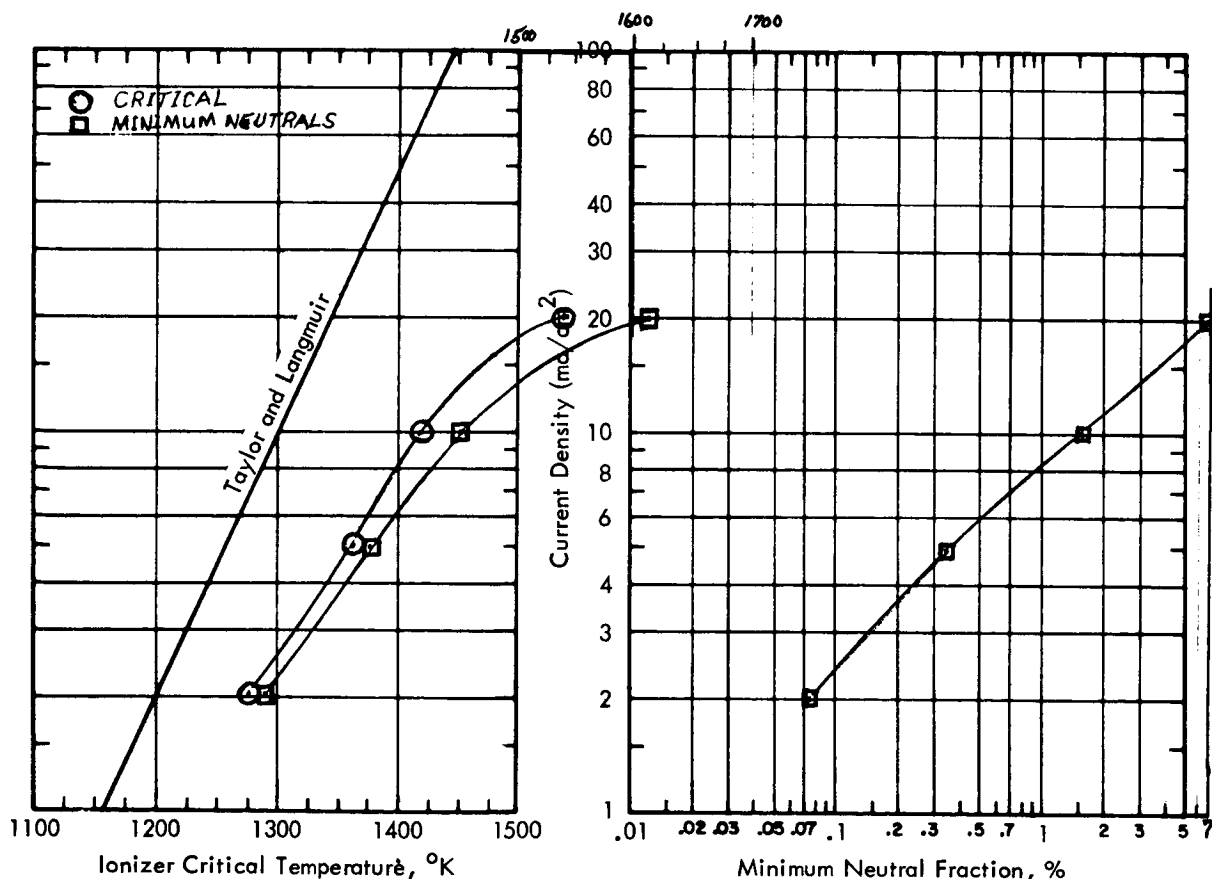
TEST NO. 4 DATE 10-65
 PORES PER CM² 4.9×10^6
 AVERAGE PORE SIZE 2.3 μ

PORE SIZE DISTRIBUTION
 MICRON DIAMETER PERCENT

> 1.6	93
1.2 - 1.6	6
0.8 - 1.2	1
0.4 - 0.8	—
< 0.4	—

AVERAGE DISTANCE BETWEEN PORES _____ μ
 THICKNESS 5×10^{-2} CM, DENSITY _____ %
 $\Delta p / \Delta t$ _____ TORR/SEC
 WORK FUNCTION ~ 4.75 at 2 ma/cm²*, eV

*SAHA-L. EQ. - % NEUTRALS AT 1 Ma/cm



CONCLUSIONS Fair results for clean porous W. Min. neutrals 6.5% at 20 ma/cm²; Critical temperature 1535°K.

TEST MADE BY Shelton/Hall REPORT PREPARED BY D. F. Hall

IONIZER PELLET EVALUATION REPORT

PELLET TYPE 324-S Sample F
 MADE BY Hughes Research Lab.
 AVERAGE PARTICLE SIZE 3.9 μ

TEST NO. 5 DATE Dec. 65
 PORES PER CM² 7.6 x 10⁶
 AVERAGE PORE SIZE 2.0 μ

PARTICLE SIZE DISTRIBUTION
 MICRON DIAMETER PERCENT

>7.5 _____
 7.5 - 5.0 _____
 5.0 - 3.3 _____
 3.3 - 2.25 _____
 1.5 - 1.0 _____
 <1.0 _____
 Std. deviation 0.7 μ

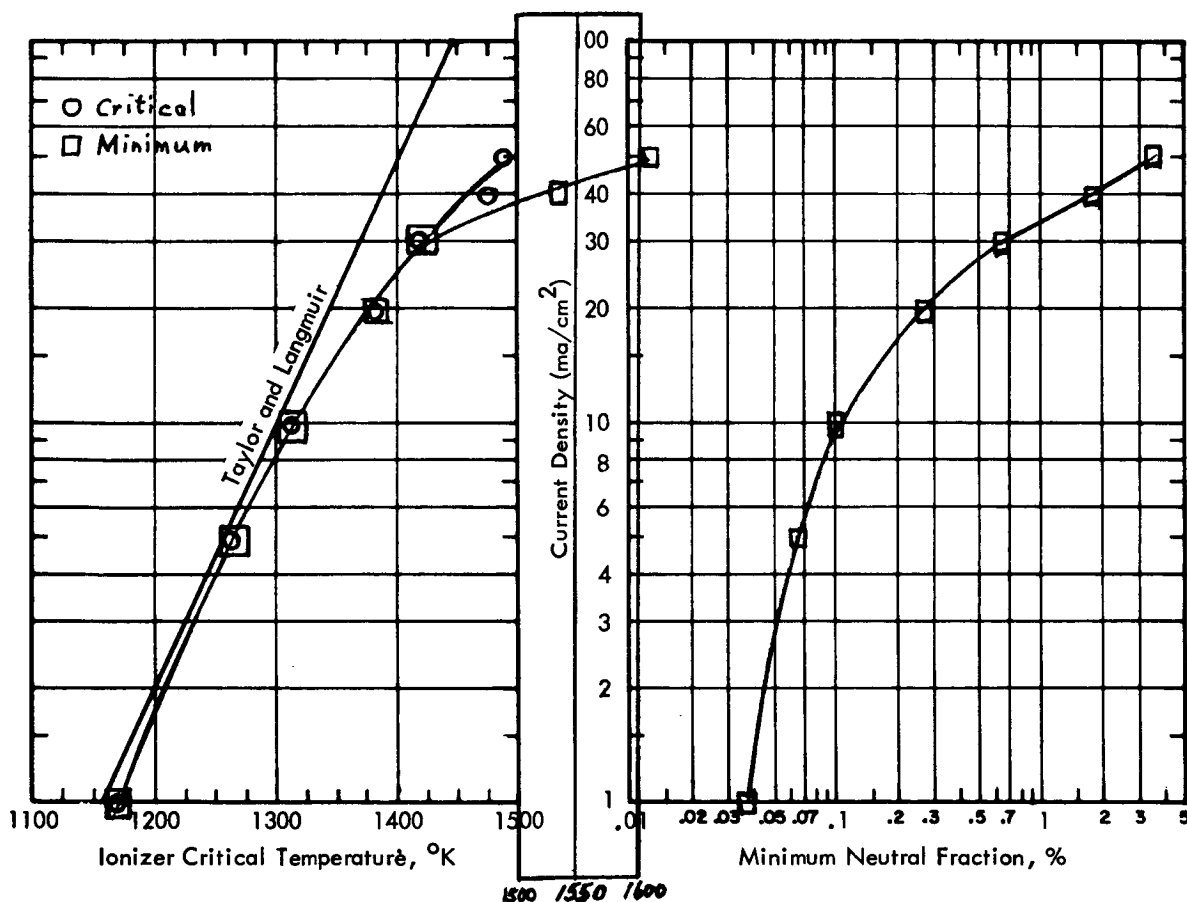
PORE SIZE DISTRIBUTION
 MICRON DIAMETER PERCENT

>1.6 _____
 1.2 - 1.6 _____
 0.8 - 1.2 _____
 0.4 - 0.8 _____
 <0.4 _____

PELLET DIAMETER (EFFECTIVE) 0.18
 TRANSMISSION COEFFICIENT 1.5x10⁻⁴ BY
 PRESSURE 10 (air) TORR
 CALCULATED TRUE DENSITY 79.2%
 SURFACE TREATMENT polished
 SAMPLE INFORMATION _____

AVERAGE DISTANCE BETWEEN PORES _____ μ
 THICKNESS 5 x 10⁻² CM, DENSITY _____%
 $\Delta p/\Delta t$ _____ TORR/SEC
 WORK FUNCTION 4.8 *, eV

*SAHA-L. EQ. - % NEUTRALS AT 1 Ma/cm



CONCLUSIONS Very superior performance. Slightly better than best data from Ir coated samples of Hughes 324-S at 15 ma/cm² and above. Unlike Ir coated samples, performance stable with time and not permanently effected by O₂. Min neutrals at 20 ma/cm² 0.3%, crit 1380°K.

TEST MADE BY Shelton/Hall

REPORT PREPARED BY D. F. Hall

IONIZER PELLET EVALUATION REPORT

PELLET TYPE W-5% Re No. 2
 MADE BY TRW
 AVERAGE PARTICLE SIZE 4.1 μ

PARTICLE SIZE DISTRIBUTION MICRON DIAMETER	PERCENT
> 7.5	100%
7.5 - 5.0	—
5.0 - 3.3	—
3.3 - 2.25	range <u>2-5μ</u>
1.5 - 1.0	—
< 1.0	—

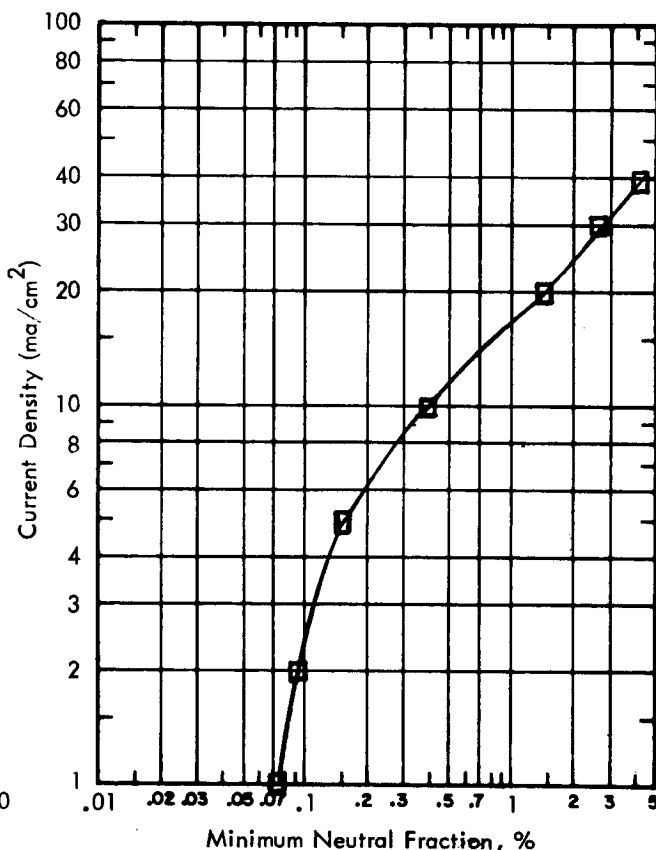
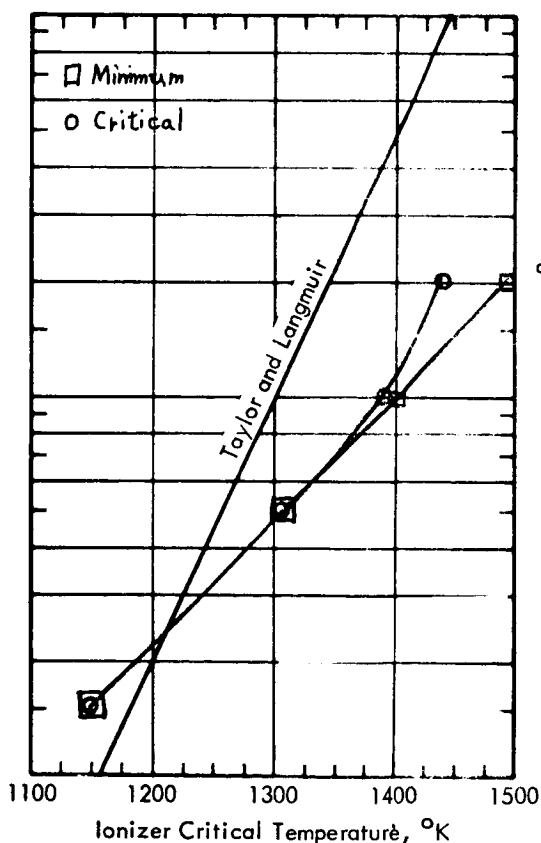
PELLET DIAMETER (EFFECTIVE) 0.18
 TRANSMISSION COEFFICIENT 6.9×10^{-5} BY
 PRESSURE 10 (air) TORR
 CALCULATED TRUE DENSITY _____
 SURFACE TREATMENT etched & Sputtered
 SAMPLE INFORMATION pre-alloyed powder

TEST NO. 6 DATE Dec. 65
 PORES PER CM² 7.2×10^6
 AVERAGE PORE SIZE 2.0 μ

PORE SIZE DISTRIBUTION MICRON DIAMETER	PERCENT
> 1.6	—
1.2 - 1.6	—
0.8 - 1.2	—
0.4 - 0.8	—
< 0.4	—

AVERAGE DISTANCE BETWEEN PORES _____ μ
 THICKNESS 5×10^{-2} CM, DENSITY _____ %
 $\Delta p / \Delta t$ _____ TORR/SEC
 WORK FUNCTION 4.75 *, eV

* SAHA-L. EQ. - % NEUTRALS AT 1 Ma/cm



CONCLUSIONS Results compare with good clean porous W, except
critical temperatures increase too rapidly with current density.
Min. neutrals at 20 ma/cm² 1.2% at 1490°K.

TEST MADE BY Shelton/Hall

REPORT PREPARED BY D. F. Hall

IONIZER PELLET EVALUATION REPORT

PELLET TYPE W-50% Ir Prealloy
 MADE BY Hughes
 AVERAGE PARTICLE SIZE 2-5 μ

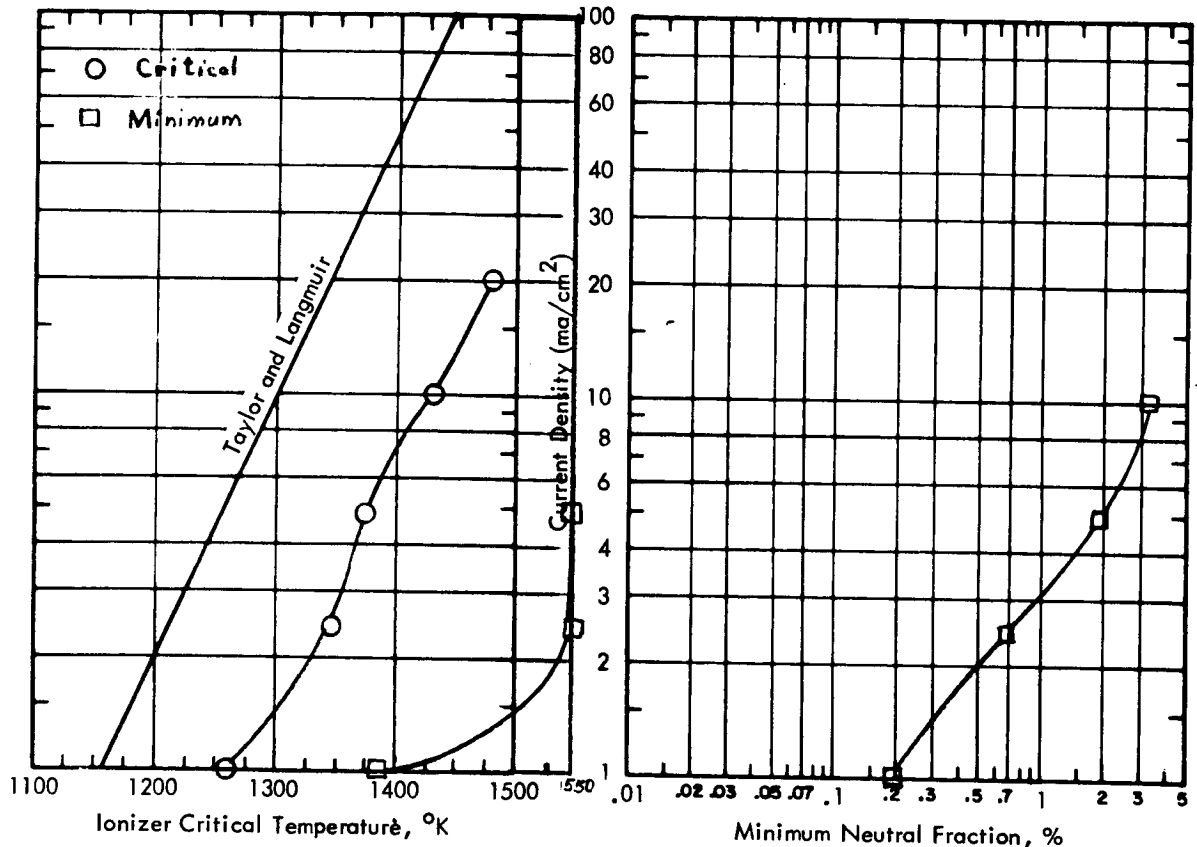
TEST NO. 7 DATE Jan. 1966
 PORES PER CM² -
 AVERAGE PORE SIZE -

PARTICLE SIZE DISTRIBUTION	
MICRON DIAMETER	PERCENT
> 7.5	—
7.5 - 5.0	—
5.0 - 3.3	—
3.3 - 2.25	—
2.25 - 1.5	—
1.5 - 1.0	—
< 1.0	—

PORE SIZE DISTRIBUTION	
MICRON DIAMETER	PERCENT
> 1.6	—
1.6 - 1.2	—
1.2 - 0.8	—
0.8 - 0.4	—
0.4 - 0.2	—
< 0.2	—

PELLET DIAMETER (EFFECTIVE) 0.18
 TRANSMISSION COEFFICIENT 6.9×10^{-4} BY
 PRESSURE 10 (air) TORR
 CALCULATED TRUE DENSITY 58.8
 SURFACE TREATMENT Sputtered
 SAMPLE INFORMATION Hughes No. 276

AVERAGE DISTANCE BETWEEN PORES — μ
 THICKNESS 5×10^{-2} CM, DENSITY — %
 $\Delta p / \Delta t$ — TORR/SEC
 WORK FUNCTION — eV
 *SAHA-L. EQ. - % NEUTRALS AT 1 Ma/cm



CONCLUSIONS Very poor performance, especially above 1 ma/cm². Neutrals increase rapidly with ion current density. Criticals high, curve shape poor. Sputtered surface probably has trace oxygen from bulk contamination. At 20 ma/cm², ~ 7% neutrals at 1550°K. Poor mechanical properties.
 TEST MADE BY Shelton/Hall REPORT PREPARED BY D. F. Hall

IONIZER PELLET EVALUATION REPORT

PELLET TYPE W-50% Ir Mixture

TEST NO. 8 DATE Jan. 1966

MADE BY Hughes

PORES PER CM² 3.5×10^6 (?)

AVERAGE PARTICLE SIZE W:3-6 μ ; Ir: 2-6 μ

AVERAGE PORE SIZE 3.5 μ (?)

PARTICLE SIZE DISTRIBUTION angular
MICRON DIAMETER PERCENT

PORE SIZE DISTRIBUTION
MICRON DIAMETER PERCENT

> 7.5
7.5 - 5.0
5.0 - 3.3
3.3 - 2.25
1.5 - 1.0
< 1.0

> 1.6
1.2 - 1.6
0.8 - 1.2
0.4 - 0.8
< 0.4

PELLET DIAMETER (EFFECTIVE) 0.18

AVERAGE DISTANCE BETWEEN PORES μ

TRANSMISSION COEFFICIENT 8.5×10^{-4} BY

THICKNESS 5×10^{-2} CM, DENSITY %

PRESSURE 10 (air) TORR

$\Delta p / \Delta t$ TORR/SEC

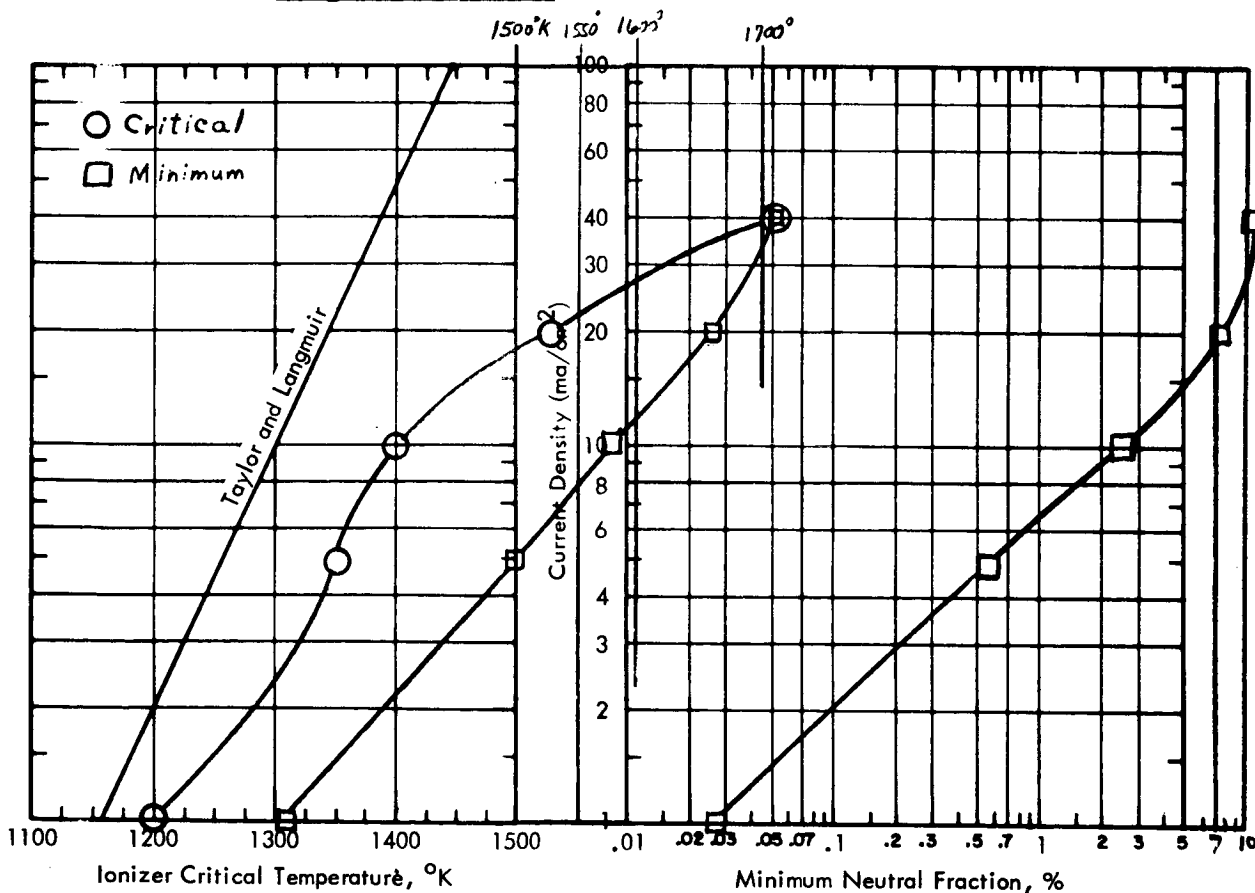
CALCULATED TRUE DENSITY 70.9

WORK FUNCTION 5.0 *, eV

SURFACE TREATMENT Sputtered

*SAHA-L. EQ. - % NEUTRALS AT 1 Ma/cm

SAMPLE INFORMATION Hughes No. 225



CONCLUSIONS Rather poor performance. Neutrals increase rapidly with current density. Criticals high; knees quite rounded. Sputtered surface probably has trace oxygen from bulk contaminate. At 20 ma/cm² ~7% neutrals at 1625°K. Poor mechanical properties.

TEST MADE BY Shelton/Hall

REPORT PREPARED BY D. F. Hall

IONIZER PELLET EVALUATION REPORT

PELLET TYPE 100% Ir
 MADE BY Hughes
 AVERAGE PARTICLE SIZE _____

TEST NO. 9 DATE February, 1966
 PORES PER CM² _____
 AVERAGE PORE SIZE _____

PARTICLE SIZE DISTRIBUTION
 MICRON DIAMETER PERCENT

> 7.5	_____
7.5 - 5.0	_____
5.0 - 3.3	_____
3.3 - 2.25	_____
1.5 - 1.0	_____
< 1.0	_____

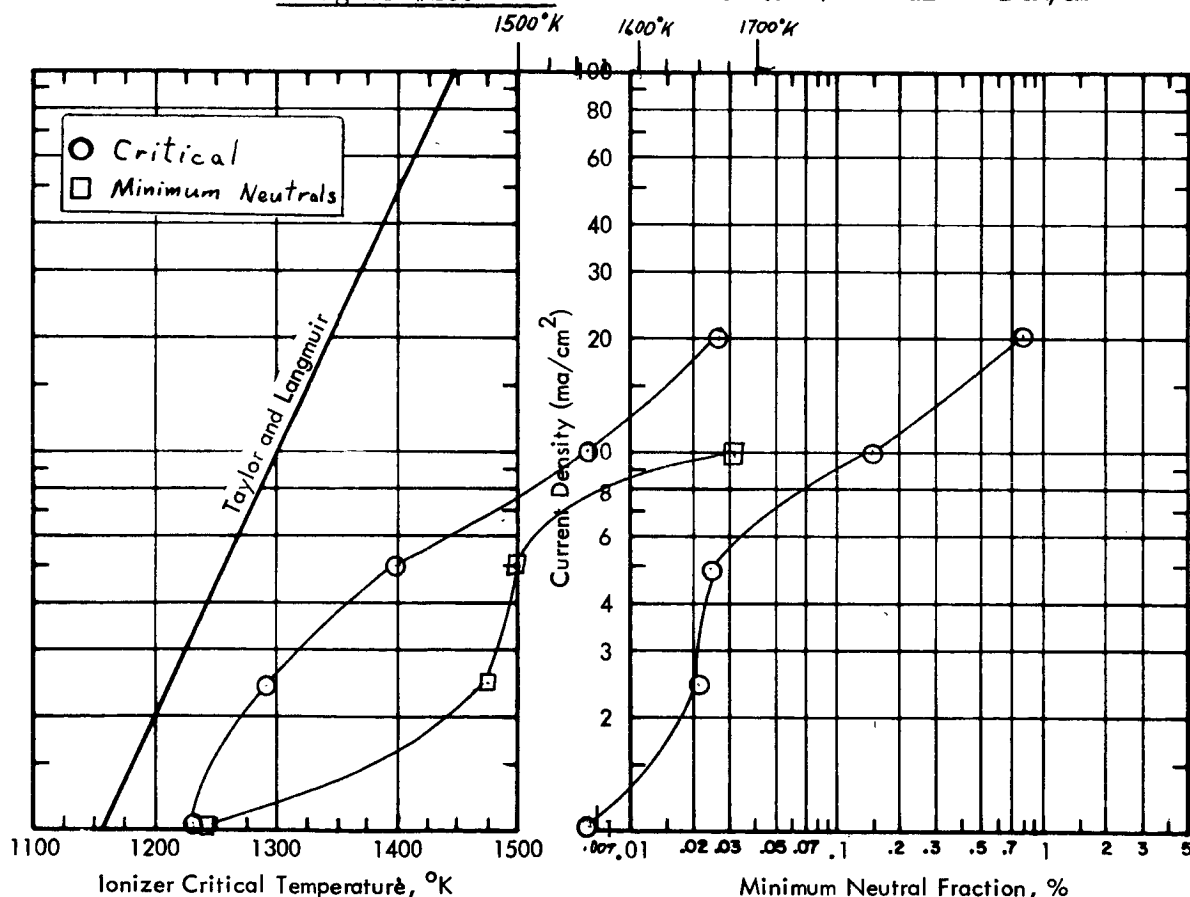
PORE SIZE DISTRIBUTION
 MICRON DIAMETER PERCENT

> 1.6	_____
1.2 - 1.6	_____
0.8 - 1.2	_____
0.4 - 0.8	_____
< 0.4	_____

PELLET DIAMETER (EFFECTIVE) 0.18
 TRANSMISSION COEFFICIENT 1.6×10^{-4} BY
 PRESSURE 10 (air) TORR
 CALCULATED TRUE DENSITY _____
 SURFACE TREATMENT Sputtered
 SAMPLE INFORMATION Hughes #280

AVERAGE DISTANCE BETWEEN PORES _____ μ
 THICKNESS 5×10^{-2} CM, DENSITY _____ %
 $\Delta p / \Delta t$ _____ TORR/SEC
 WORK FUNCTION 5.15 eV

*SAHA-L. EQ. - % NEUTRALS AT 1 Ma/cm



CONCLUSIONS Impressive neutral fraction at low current densities
degrading rapidly with increasing current density, probably due to pore
structure. Criticals high compared to W. Oxygen continuously diffused
to surface. Sample sintered closed during test.

TEST MADE BY Shelton/Hall

REPORT PREPARED BY D. F. Hall

IONIZER PELLET EVALUATION REPORT

PELLET TYPE Graded Spherical W
 MADE BY TRW Systems
 AVERAGE PARTICLE SIZE 3.9 μ

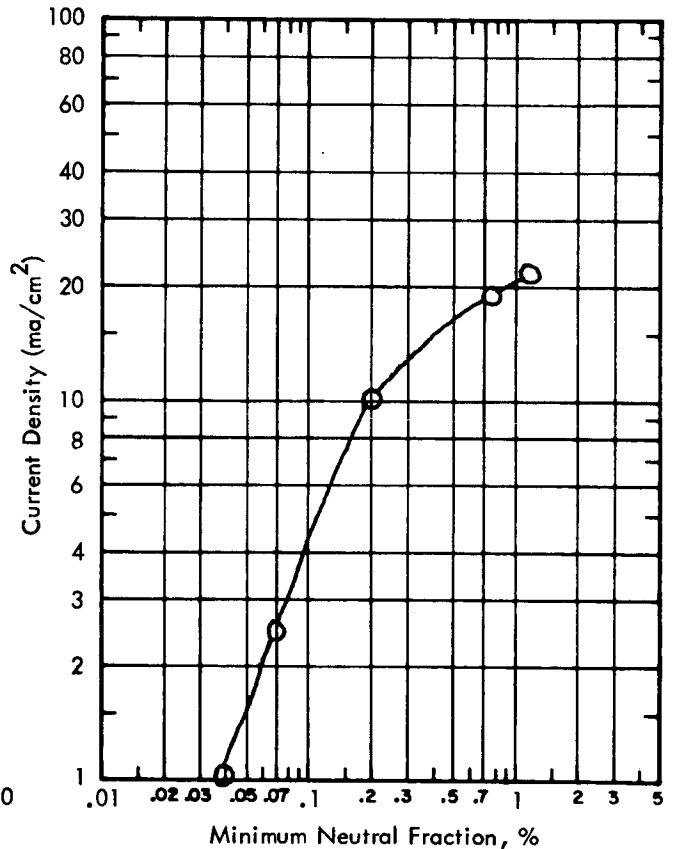
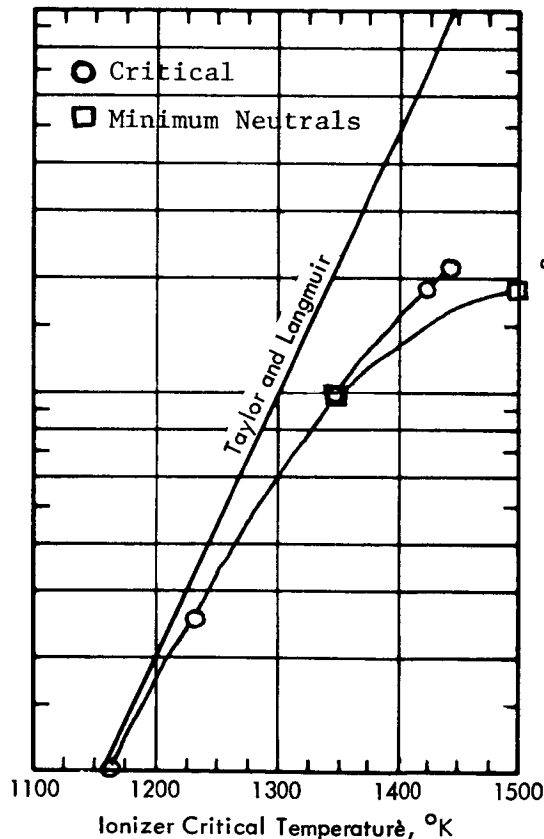
TEST NO. 10 DATE April, 1966
 PORES PER CM² 5.9×10^6
 AVERAGE PORE SIZE 2.0 μ

PARTICLE SIZE DISTRIBUTION
 MICRON DIAMETER PERCENT
 > 7.5 _____
 7.5 - 5.0 _____
 5.0 - 3.3 _____
 3.3 - 2.25 Std. deviation 1.0
 1.5 - 1.0 _____
 < 1.0 _____

PORE SIZE DISTRIBUTION
 MICRON DIAMETER PERCENT
 > 1.6 _____
 1.2 - 1.6 _____
 0.8 - 1.2 _____
 0.4 - 0.8 _____
 < 0.4 _____

PELLET DIAMETER (EFFECTIVE) 0.18
 TRANSMISSION COEFFICIENT 1.6×10^{-4} BY
 PRESSURE 10 (air) TORR
 CALCULATED TRUE DENSITY _____
 SURFACE TREATMENT Polished & Sputtered
 SAMPLE INFORMATION TRW ST 1-9

AVERAGE DISTANCE BETWEEN PORES _____ μ
 THICKNESS 5×10^{-2} CM, DENSITY _____ %
 $\Delta p / \Delta t$ _____ TORR/SEC
 WORK FUNCTION 4.77 *, eV
 *SAHA-L. EQ. - % NEUTRALS AT 1 Ma/cm



CONCLUSIONS Excellent neutral fraction and critical temperature through
10 ma/cm², but degrading rapidly with current density by 20 ma/cm².
Min neutrals at 20 ma/cm² 1% at 1500°K.

TEST MADE BY Shelton/Hall REPORT PREPARED BY D. F. Hall

IONIZER PELLET EVALUATION REPORT

PELLET TYPE Two-Phase W - Re
 MADE BY TRW Systems
 AVERAGE PARTICLE SIZE _____

TEST NO. 11 DATE May, 1966
 PORES PER CM² _____
 AVERAGE PORE SIZE _____

PARTICLE SIZE DISTRIBUTION
 MICRON DIAMETER PERCENT

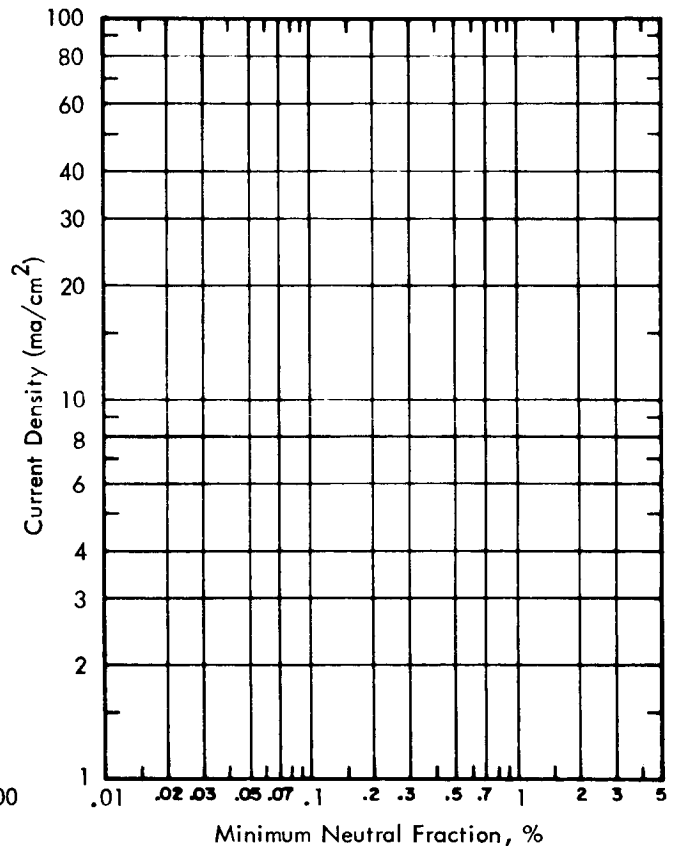
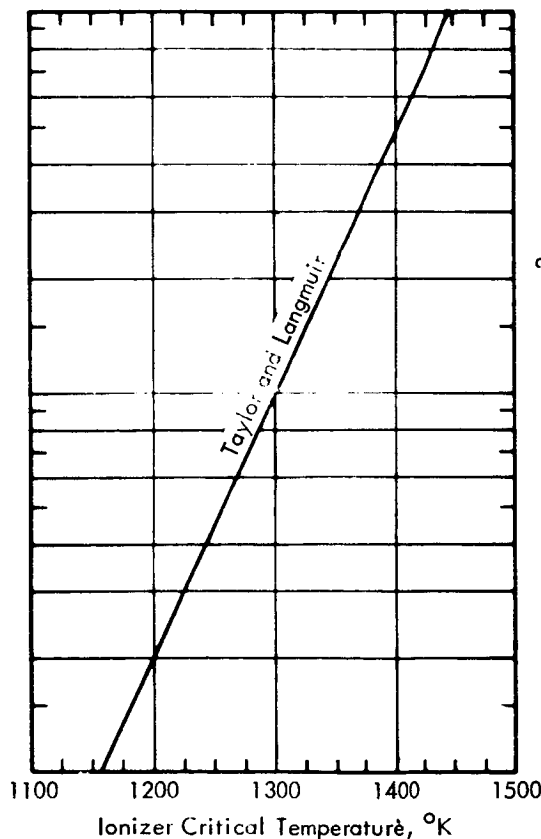
> 7.5 _____
 7.5 - 5.0 _____
 5.0 - 3.3 _____
 3.3 - 2.25 _____
 1.5 - 1.0 _____
 < 1.0 _____

PORE SIZE DISTRIBUTION
 MICRON DIAMETER PERCENT

> 1.6 _____
 1.2 - 1.6 _____
 0.8 - 1.2 _____
 0.4 - 0.8 _____
 < 0.4 _____

PELLET DIAMETER (EFFECTIVE) 0.18
 TRANSMISSION COEFFICIENT Very low BY
 PRESSURE 10 (air) TORR
 CALCULATED TRUE DENSITY _____
 SURFACE TREATMENT Etched & Sputtered
 SAMPLE INFORMATION TRW 57-3

AVERAGE DISTANCE BETWEEN PORES _____ μ
 THICKNESS 5 x 10⁻² CM, DENSITY _____ %
 $\Delta p / \Delta t$ _____ TORR/SEC
 WORK FUNCTION _____ *, eV
 *SAHA-L. EQ. - % NEUTRALS AT 1 Ma/cm



CONCLUSIONS Incomplete removal of the sigma phase during manufacture resulted
in very few passageways connecting the sample sides. These pores were
badly over-fed at nominally low current densities, producing very
high neutral fractions.

TEST MADE BY Shelton/Hall REPORT PREPARED BY D. F. Hall

IONIZER PELLET EVALUATION REPORT

PELLET TYPE Low Density, Shaped Pore W
MADE BY EOS
AVERAGE PARTICLE SIZE

TEST NO. 12 DATE May, 1966
PORES PER CM²
AVERAGE PORE SIZE

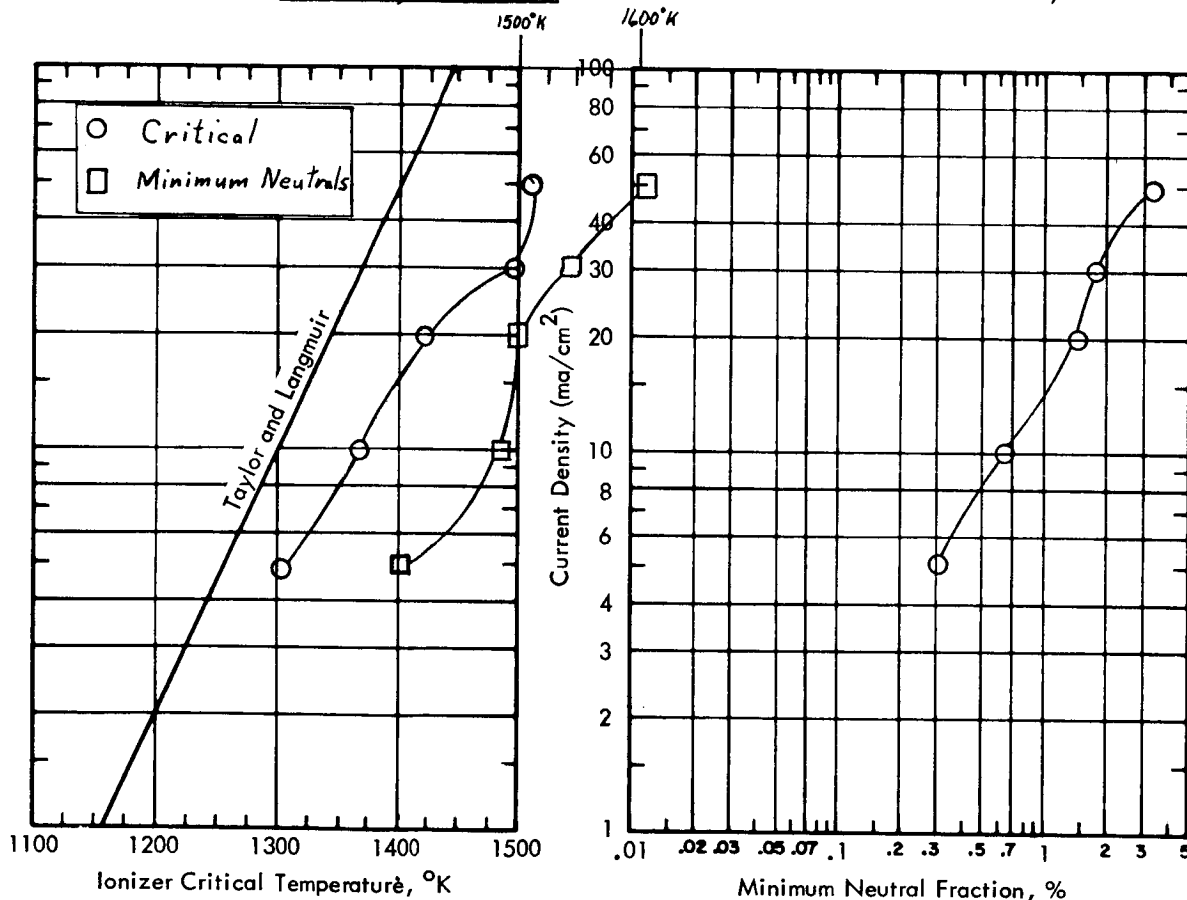
PARTICLE SIZE DISTRIBUTION MICRON DIAMETER	PERCENT
> 7.5	—
7.5 - 5.0	—
5.0 - 3.3	—
3.3 - 2.25	—
1.5 - 1.0	—
< 1.0	92

PORE SIZE DISTRIBUTION MICRON DIAMETER	PERCENT
> 1.6	—
1.2 - 1.6	—
0.8 - 1.2	—
0.4 - 0.8	—
< 0.4	—

PELLET DIAMETER (EFFECTIVE) 0.18
TRANSMISSION COEFFICIENT 6.5×10^{-4} BY
PRESSURE 10 (air) TORR
CALCULATED TRUE DENSITY 68%
SURFACE TREATMENT Polished & Sputtered
SAMPLE INFORMATION EOS 788, bar 1

AVERAGE DISTANCE BETWEEN PORES μ
THICKNESS 5×10^{-2} CM, DENSITY %
 $\Delta p / \Delta t$ TORR/SEC
WORK FUNCTION 4.7 @ 5 m/cm² *, eV

* SAHA-L. EQ. - % NEUTRALS AT 1 Ma/cm



CONCLUSIONS Results at low current density were poorer than usually observed, but high current density performance was as good or better than that of any other material tested. High propensity to further sinter; difficult to deinfiltate and braze.

TEST MADE BY Shelton/Hall

REPORT PREPARED BY D. F. Hall

METALLURGICAL STUDIES

Enhanced sintering by rhodium diffusion from the braze. - Many pictures have been taken of the tungsten in the vicinity of the braze. Invariably a region about 0.010 inch from the braze has been found to be more densely sintered. We are convinced that this area is untouched by the actual penetration of the braze but that this effect is related to the length and temperature of operation. Close examination of Figure 64 shows this densification as well as the eutectic nature of moly-rhodium braze. Pure rhodium powder is used but molybdenum from the plenum chamber dissolves. Figures 65 and 66 are enlargements of the porous material showing densification near the braze.

Evidence of enhanced sintering related to vacuum environment or hot molten copper. - During an experiment to investigate the influence of the potting compound and its possible effect on our interpretation of the microphotographs of mounted and polished samples, we tried to deinfiltate the copper out of a sample -- expending less care than usual as to the time and temperature schedule and possibly the degree of vacuum. Despite the facts that the sample remained for a long time at high temperature and the copper removal rate was reduced to zero, copper was found in the sample. Figure 67 shows that a section surrounding the copper has become solid, thereby encapsulating the copper. The two most plausible explanations of this result that have occurred to us are either a slight amount of tungsten is soluble in liquid copper at very high temperatures or that some gas in the vacuum system caused the sintering. Either of these two explanations seems sufficiently important that we believed this observation should be reported.

CONCLUSIONS

To summarize the work of this program, 12 porous samples were tested as cesium ion emitters operating at high current density, the work including measurement of the neutrals as a function of angle. Tests of many foreign elements adsorbed on or alloyed with the tungsten were also made. As a result of these studies, the following conclusions can be drawn:

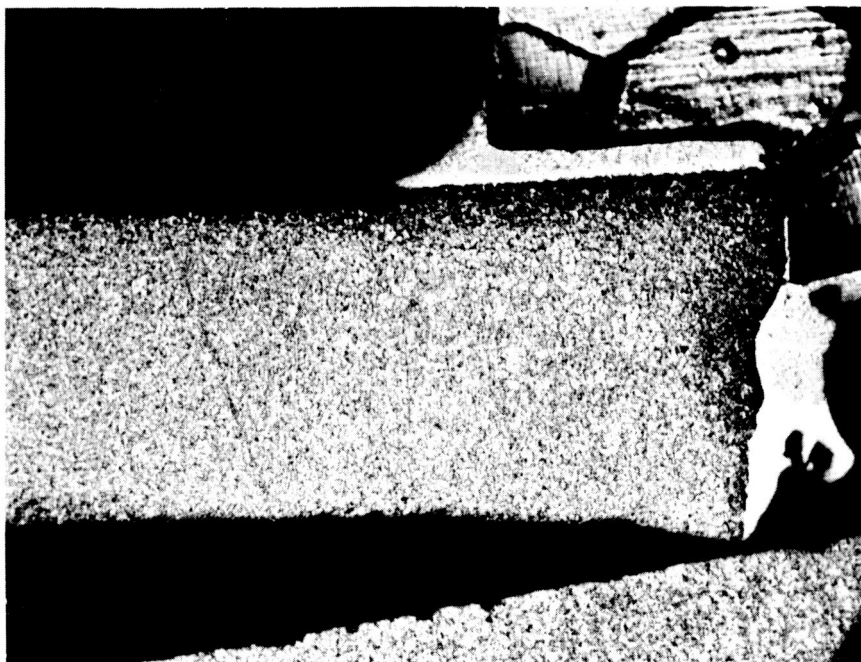


Figure 64. Cross section of Hughes 324-S Sample C, showing end of porous W, braze, and Mo plenum. 100X.

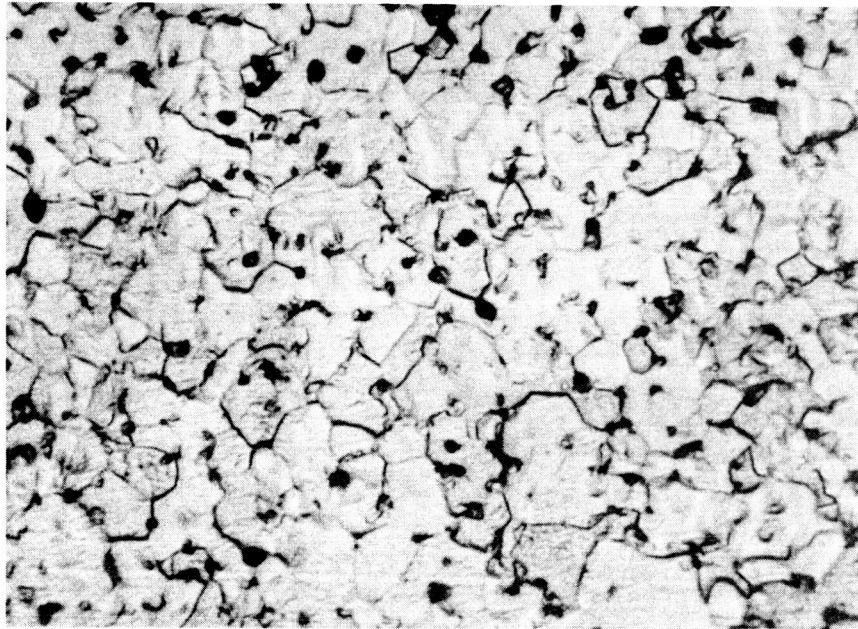


Figure 65. Cross section of Hughes 324-S Sample C, taken near braze material. 1000X.

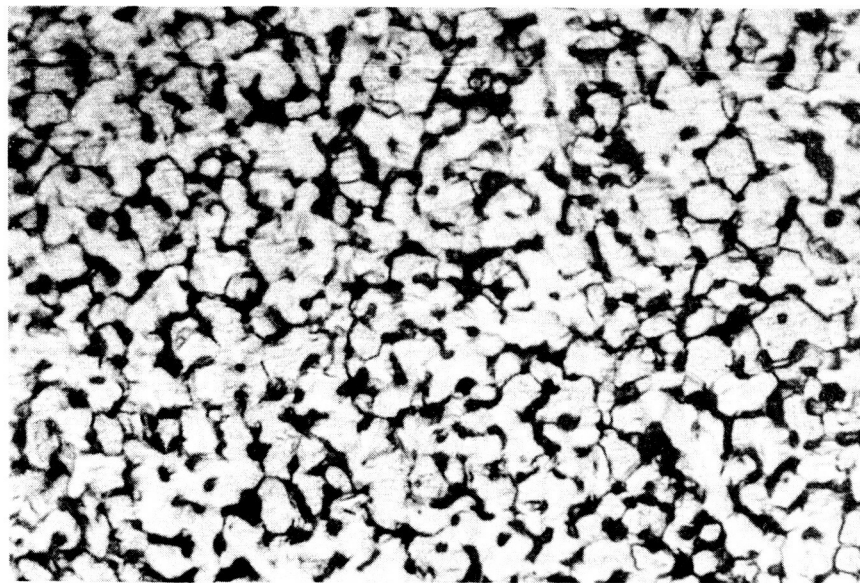


Figure 66. Cross section of Hughes 324-S Sample C, taken at ionizer center. 1000X.

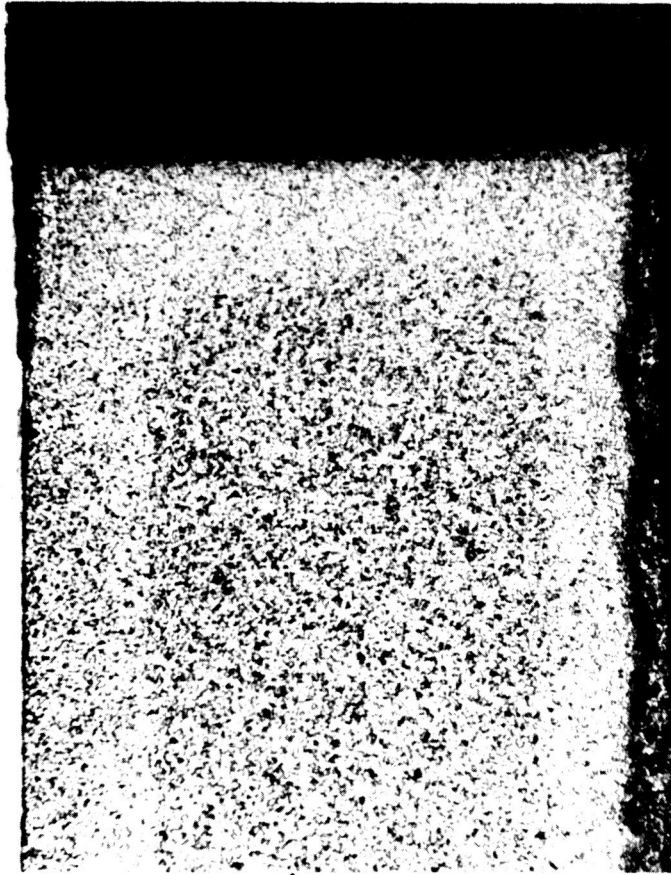


Figure 67. Photomicrograph at 100X of cross-section of ~ 35 mil thick Hughes 324-S sample after de-infiltration showing dense border surrounding copper containing center.

- 1) There are ion-emitting surfaces that are superior to tungsten (such as iridium, iridium-tungsten alloys, tungsten carbide, and tungsten silicide), but these materials are not as stable in porous form as is tungsten.
- 2) The neutral emission is not distributed as the cosine of the angle from normal but as a linearly decreasing function of the angle. This observation means that a correction to the neutral fraction as usually measured is required, and also indicates a cesium coverage that is small outside the pores, increases with depth into the pores, and remains quite constant with changes of temperature, feed rate, and electric field.
- 3) Clean porous tungsten surfaces at low current density have neutrals as predicted by the Saha-Langmuir equation for a constant work function usually between 4.7 and 4.8 volts to within a few degrees of a sharp critical temperature. Neutrals from superior porous material depart less rapidly from this line than those from poor, nonuniform materials, which at current densities above 5 ma/cm² depart rapidly from this line and begin to exhibit a monotonic increase as temperature is lowered and exhibit no sharp critical temperature.
- 4) Metallographic polishing the surface before removing the copper impregnate leaves the surface in a stable, open, and low-emissivity condition. After deinfiltration such surfaces show excellent ion emission characteristics. Sputtering opens a surface and removes surface impurities, but also increases the emissivity and alters critical geometrical surfaces.
- 5) Residual oxygen can be the sole offender in producing high neutrals increasing with decreasing temperature and a high indefinite critical temperature. This oxygen might disappear with time and high cesium throughput but can be more effectively removed by the controlled cracking of hydrocarbons on the surface.
- 6) Rhodium brazing is to be avoided because of enhanced sintering of the porous tungsten in the vicinity of the braze.
- 7) Aluminum degrades the performance of tungsten emitters if continuously incident on the ionizer. The adsorption lifetime is 170 seconds at 1500°K from clean tungsten, 10 seconds from a monolayer on clean tungsten, 0.3 seconds from tungsten carbide, and 0.01 second from bulk aluminum.
- 8) Small amounts of Ir and Re on tungsten improve performance, while small amounts of Ta, Ni, Mo, Rh, and Pt on tungsten have negative effects. Small amounts of C and Si are good for performance but larger amounts are bad.

REFERENCES

1. Cho, A. Y., D. F. Hall, and H. Shelton, "Program of Analytical and Experimental Study of Porous Metal Ionizers," NASA CR-54325, July 1965
2. Loeb, Leonard B., The Kinetic Theory of Gases, (McGraw-Hill Book Co., Inc., New York, 1934) pp. 306-309
3. Cho, A. Y., and H. Shelton, "Cesium Neutral and Ion Emission from Carburized and Oxygenated Porous Tungsten," AIAA J. 2, 2135-2137 (1964)
4. Shelton, H., and A. Y. H. Cho., "Evaporative Lifetimes of Copper, Chromium, Beryllium, Nickel, Iron, and Titanium on Tungsten and Oxygenated Tungsten," submitted to J. Appl. Phys. on 17 January 1966

DISTRIBUTION LIST

NASA Headquarters
FOB - 10B
600 Independence Ave., S.W.
Washington, D.C. 20546
Attn: RNT/James Lazar (1)

NASA-Lewis Research Center
21000 Brookpark Road
Cleveland, Ohio 44135

Attn: Spacecraft Technology Procurement
Section (M.S. 54-2) (1)

Attn: Technology Utilization Office (M.S. 3-19) (1)

Attn: Technical Information Division (M.S. 5-5) (1)

Attn: Library (M.S. 60-3) (1)

Attn: Spacecraft Technology Divn. (M.S. 54-1)

a. C. C. Conger (1)

b. R. Shattuck (2)

c. F. E. Kavanagh (3)

Attn: Electric Propulsion Laboratory (M.S. 301-1)

a. W. Moeckel (1)

b. E. Richley (1)

Attn: Report Control Office (M.S. 5-5) (1)

Attn: W. Klopp (M.S. 105-1) (1)

NASA Scientific & Technical Information Facility
P.O. Box 33

College Park, Maryland 20740

Attn: NASA Representative RWT-2448 (6)

NASA-Marshall Space Flight Center

Huntsville, Alabama 35812

Attn: Ernest Stuhlinger (M-RP-DIR) (1)

Research & Technology Division

Wright-Patterson AFB, Ohio 45433

Attn: AFAPL (APIE-2)/R.F. Cooper (1)

AFWL

Kirtland AFB, New Mexico 87417

Attn: WLPC/Capt. C. F. Ellis (1)

Aerospace Corporation

P.O. Box 95085

Los Angeles, California 90045

Attn: Library Technical Documents Group (1)

Jet Propulsion Laboratory

4800 Oak Grove Drive

Pasadena, California 91103

Attn: J.J. Paulson (1)

Hughes Research Laboratories
3011 Malibu Canyon Road
Malibu, California 90265
Attn: R. G. Brewer (1)
R. Turk (1)

Electro-Optical Systems, Inc.
300 North Halstead St.
Pasadena, California 91107
Attn: M. Ernstene (1)
H. Todd (1)

Ion Physics Corporation
South Bedford Street
Burlington, Mass. 02103 (1)

General Electric Space Flight
Propulsion Laboratory
Cincinnati, Ohio 45215
Attn: M. L. Bromberg (1)

Hiram College
Department of Physics
Hiram, Ohio 44234
Attn: Professor L. Shaffer (1)

Field Emission Corporation
611 Third Street
McMinnville, Oregon 97128
Attn: L. W. Swanson (1)

Litton Precision Products
San Carlos, California 94070
Attn: G. K. Wehner (1)

Varian Associates
611 Hansen Way
Palo Alto, California 94304
Attn: Technical Library (1)

Battelle Memorial Institute
505 King Avenue
Columbus, Ohio 43201
Attn: J. Anno (1)
E. Foster (1)
Defense Materials Information
Center (1)

NASA-Ames Research Center
Moffett Field, California 94035
Attn: T. W. Snouse (1)

University of California
Space Science Laboratory
Berkeley 4, California 94720
Attn: H. P. Smith (1)

NASA-Langley Research
Langley Field Station
Hampton, Virginia 23365
Attn: Technical Library (1)

Colorado State University
Fort Collins, Colorado 80521
Attn: L. Baldwin (1)

MSA Research Corporation
Callery, Pennsylvania 16024
Attn: R. C. Werner (1)

Massachusetts Institute of Technology
Naval Supersonic Laboratory
Cambridge 39, Mass. 02139
Attn: E. E. Covert (1)

Radio Corporation of America
Astro Electrical Division
Princeton, New Jersey 08540
Attn: W. H. Hendel (1)

Cornell University
Graduate School of Aeronautical Engineering
Ithaca, New York 14851
Attn: E. L. Resler, Jr. (1)

University of Illinois
Department of Electrical Engineering
Urbana, Illinois 61801
Attn: L. Goldstein (1)
A. Cho (1)

Aerospace Power Division
Wright Patterson AFB, Ohio 45433
Attn: Jack W. Geis-AFAPL/APIT (1)

Oak Ridge Gaseous Diffusion Plant
P.O. Box P
Oak Ridge, Tenn. 37830
Attn: R. Neal (1)
H. Trammel (1)

General Electric Co.
Cincinnati, Ohio 45215
Attn: L/ P. Jahnke (1)

TRW Inc.
New Product Research
23555 Euclid Avenue
Cleveland, Ohio 44117
Attn: R. T. Craig (1)

Clevite Corporation
Mechanical Research Division
540 E. 105th St.
Cleveland, Ohio 44108
Attn: Mr. Swope (1)

Wah-Chang Corporation
Albany, Oregon 97321
Attn: Sam Werster (1)

General Electric Company
Lamp Metals & Components Dept.
21800 Tungsten
Cleveland, Ohio 44117
Attn: Frank Adams (1)

Aerospace Corporation
P.O. Box 95085
Los Angeles, California 90045
Attn: Dr. E. G. Kendall (1)

National Research Corporation
70 Memorial Drive
Cambridge, Mass. 02142
Attn: Tech. Information Center (1)

Chase Brass & Copper Co.
Rhenium Division
28850 Aurora Road
Solon, Ohio 44139
Attn: Harvey Fisher (1)